Tract-based analysis in schizophrenia

Measuring structure and function along white matter tracts

Witte-stofbaan gebaseerde analyse in schizofrenie
het meten van structuur en functie langs witte-stofbanen

(met een samenvatting in het Nederlands)

Proefschrift

ter verkrijging van de graad van doctor aan de Universiteit Utrecht op gezag van de rector magnificus, prof.dr. J.C. Stoof, ingevolge het besluit van het college voor promoties in het openbaar te verdedigen op donderdag 26 februari 2009 des ochtends te 10.30 uur

door

René Christiaan William Mandl

geboren op 17 december 1964
te Amsterdam

Tract-based analysis in schizophrenia

Measuring structure and function along white matter tracts

René Christiaan William Mandl

2009

Table of Contents

voor Johanna Alderlieste

Chapter 1

Introduction

Chapter 1

Complex brain functions do not reside in only one particular gray matter region. Rather, they emerge from the dynamic flow of information between different (spatially distinct) gray matter regions (Catani and Ffytche, 2005; Mesulam, 2005). These regions are interconnected over long distances by white matter fiber bundles (**Figure 1a**) forming large-scale neural networks for which normal interregional communication is a prerequisite for proper functioning. These white matter fiber bundles can be considered the information highways of the brain. White matter fiber bundles consist of large numbers of axons running in parallel, each surrounded by a myelin sheath (Kandel, 2000). An axon is the part of a neuron that transports the outgoing signals from the cell body to other neurons (see **Figure 1b**). Myelin is a fatty insulating substance and the presence of the myelin sheath increases signal transport efficiency over the axon in terms of the energy needed as well as in speed. The myelin sheath is formed by oligodendrocytes (a type of glial cell) that wrap around the axon and it is the myelin that is responsible for the tissue's white color.
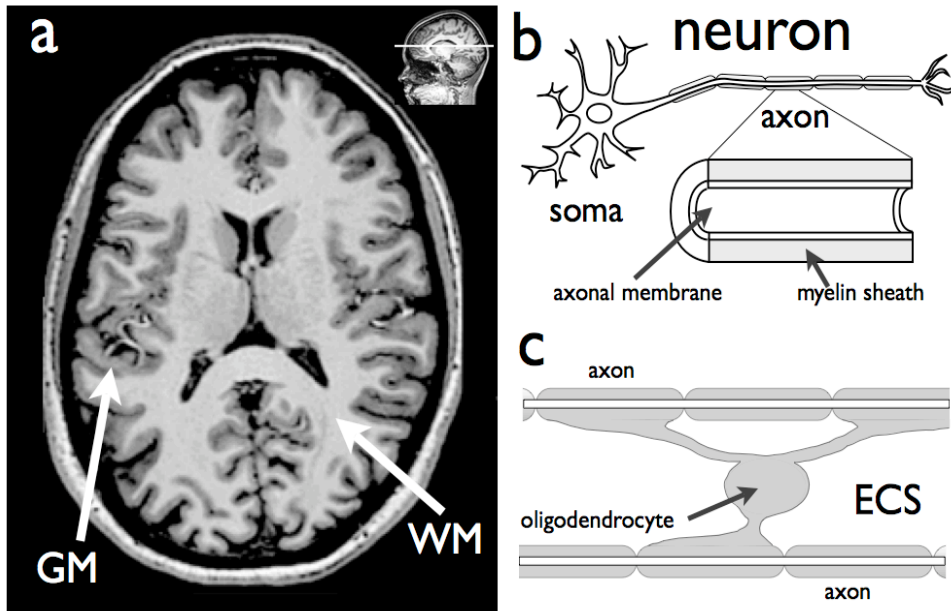
Figure 1. a) A typical MRI scan of the human brain showing locations of gray matter (GM) and white matter (WM). b) The gray matter predominantly consists of the soma of the neurons (b) while the white matter is formed by the myelinated axons of the neurons. c) In the central nervous system the insulating myelin sheath is created by oligodendrocytes. One oligodendrocyte may create more than one myelin sheath segment for several axons. Water molecules are present in the intracellular space (that is the space within the neurons and glial cells) as well as in the extra-cellular space (ECS)

Modern magnetic resonance imaging (MRI) methods such as diffusion weighted MRI (DWI) in combination with fiber tracking algorithms allow us to reconstruct these white matter fiber bundles and to study several aspects of these bundles in considerable detail (for an introduction see (Le Bihan et al., 2001; Mori and van Zijl, 2002; Skare, 2002; Jones, 2008)). In this thesis various structural aspects of white matter fiber bundles were studied in both healthy participants and in schizophrenia patients using a novel technique named tract-based analysis. With this type of analysis groups are compared at the level of complete fiber bundles. Furthermore, the intriguing possibility was explored to study functional aspects of these white matter fiber bundles with a new method that is based on tract-based analysis and that was dubbed functional diffusion tensor imaging (fDTI).

Diffusion weighted imaging

Diffusion weighted magnetic resonance imaging (DWI) (Le Bihan and Breton, 1985; Le Bihan et al., 2001) has become a standard tool that allows us to probe the diffusion profile of water molecules at the level of voxels. Voxels (volume elements) are the 3-dimensional equivalent of pixels (picture elements). Diffusion (also known as Brownian motion) is the process of thermally driven displacement of the water molecules due to collisions with their surrounding molecules. From the diffusion profile of the water molecules we can infer characteristics of the microstructure of the underlying tissue that cannot be measured in a direct way. DWI has proven to be in particular useful to study the human brain's white matter because in white matter the diffusion profile of the water molecules provides directional information of the underlying white matter fiber bundles (Chenevert et al., 1990; Doran et al., 1990). In white matter fiber bundles water molecules diffuse more easily in the direction parallel to the fiber bundle than in the perpendicular direction (**Figure 2b**). As a consequence the diffusion profile of the water molecules is anisotropic (that is, not the same in every direction). Information about the shape of the diffusion profile can be obtained by measuring the level of diffusion in different directions.

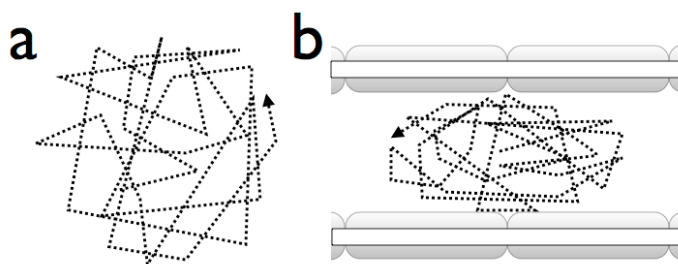**Figure 2.** *a) The diffusion path of a single water molecule in case of unrestricted diffusion. The diffusion profile of all the water molecules combined will be isotropic. b) The diffusion path of a single water molecule in white matter. The hindering of the diffusion of the water molecules by the axons results in an anisotropic diffusion profile, pointing in the direction of the fiber bundle.*
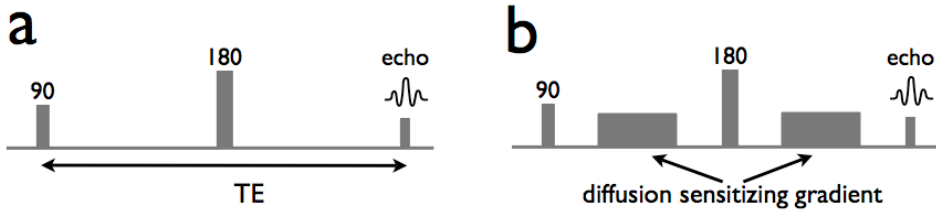
Figure 3. *a) A conventional spin-echo MRI scan sequence. The sequence starts with a 90 degrees radio frequency pulse to excite the water protons. After a time-period TE/2 a 180 degrees radio frequency pulse is applied leading to a measurable echo at time TE which is read out. b) In the Stejskal-Tanner scan sequence a diffusion gradient in a given direction is added to the conventional scan sequence (split up in two blocks positioned symmetrically around the 180 degrees radio frequency pulse). The amount of diffusion in the given direction is directly related to the reduction in measured signal strength of the Stejskal-Tanner sequence (b) compared to the signal strength of the conventional (diffusion unweighted) scan sequence (a).*

Measurement of the diffusion profile in a specific direction is done using a DWI scan sequence which includes a so-called diffusion sensitizing gradient that can be applied in any direction needed. A frequently used DWI scan sequence is the Stejskal-Tanner sequence (**Figure 3b**) (Stejskal and Tanner, 1965). In this scan-sequence the diffusion sensitizing gradient is added to a conventional MRI spin-echo sequence (**Figure 3a**) (Haacke et al., 1999). To measure the amount of diffusion in the direction of the applied diffusion gradient, two scans are acquired: one with the diffusion sensitizing gradient (the DWI scan) and one without such a diffusion sensitizing gradient (the conventional spin-echo scan). The signal of the DWI scan is compared to the signal of the unweighted scan. The difference in signal depends on the strength and duration of the applied diffusion gradient (which is known and given by the b-value) as well as the level of diffusion in the probed direction. The relation between the diffusion weighted and unweighted scan is described by:

$$\frac{M_d}{M_0} = e^{-bD}$$

(1)

where M_0 is the diffusion unweighted scan, M_d is the diffusion weighted scan, b is the b-value, and D is the diffusion coefficient.

From (1) it follows that the diffusion coefficient D can be computed using:

$$D = \frac{\ln(M_d / M_0)}{b} \tag{2}$$

Although the relation between the anisotropic shape of the diffusion profile and the direction of white matter is firmly established, the mechanism itself is not fully understood. For instance, it is not clear how much the intracellular water and extracellular water fractions contribute to the measured signal. However, the current belief is that for the DWI acquisitions as used in the experiments in this thesis (that is with diffusion-weighting b = 1000 s/mm^2 and echo time TE ~ 70-100 ms) the majority of the signal stems from water molecules in the extra-cellular space (Clark and Le Bihan, 2000). Another open question is to what extent the various structuring elements of the white matter tissue pose restrictions on the diffusion process leading to an anisotropic diffusion profile. It is now generally accepted that at least both axonal membranes and myelin sheath hinder the diffusion of water molecules leading to the characteristic anisotropic shape of the diffusion profile in white matter (Norris, 2001; Beaulieu, 2002). Note that the latter suggests that DWI can only provide limited information on the level of myelination because, in contrast to myelin sheaths, axonal membranes are always present leading to anisotropic diffusion. Changes in myelin content can therefore only moderate the - already anisotropic - diffusion profile in white matter fiber bundles.

Diffusion tensor imaging

Diffusion tensor imaging (DTI) is a DWI acquisition where a positive definite symmetric 2nd-order tensor is used as a model to describe the diffusion profile of water molecules. Mathematically this tensor can be represented by a 3×3 matrix. For the computation of the diffusion tensor **D** it is necessary that the diffusion profile is probed in at least 6 different non-collinear directions (because the tensor is symmetric around the main diagonal there are 6 unknown values instead of 9 unknown values). The relation between the diffusion tensor **D** and the diffusion profile D_i measured in direction given by diffusion gradient $\mathbf{q}_i = [q_{ix}, q_{iy}, q_{iz}]^T$ is given by:

$$D_i = \mathbf{q}_i^T \mathbf{D} \mathbf{q}_i \tag{3}$$

To compute the diffusion tensor **D** at least 6 ($1 < i \leq n; \ n \geq 6$) diffusion weighted (M_{id}) scans and one unweighted (M_0) scan must be acquired. Using (2) the corresponding D_i scans can be computed yielding at least 6 equations with 6 unknown values (the unknown elements of the diffusion tensor):

$$D_1 = \mathbf{q}_1^T \mathbf{D} \mathbf{q}_1$$
$$D_2 = \mathbf{q}_2^T \mathbf{D} \mathbf{q}_2$$
$$\bullet$$
$$\bullet$$
$$D_n = \mathbf{q}_n^T \mathbf{D} \mathbf{q}_n \qquad\qquad (4)$$

In a noise-free setting the values of the tensor elements can be analytically determined but in more realistic settings the presence of noise requires the use of error minimizing fitting routines. Because most DTI acquisitions have a low signal-to-noise ratio (SNR) the number of diffusion weighted scans (n) that are acquired is usually larger than six. It was shown that in those cases acquisition of scans with an increased number of different diffusion weighted directions is favorable because it leads to better noise distributions than simply collecting multiple sets of scans with only six different diffusion weighted directions (Jones et al., 1999; Skare et al., 2000). After diagonalization of the tensor, the major eigenvector of the tensor with eigenvalue λ_1 points in the direction of the largest diffusion coefficient (**Figure 4**). In white matter this is the direction of the fiber bundle.
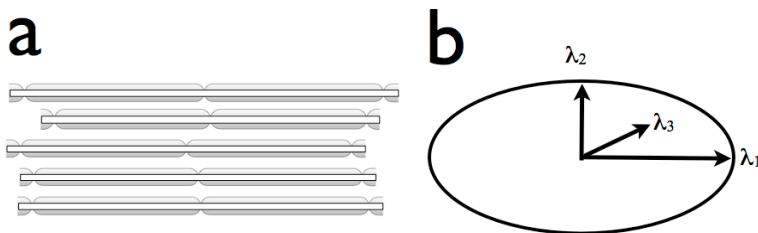
Figure 4. Because in white matter fiber bundles (a) the diffusion profile of water molecules is anisotropic, the diffusion tensor (usually graphically represented by an ellipsoid) which represents the diffusion profile is cigar-shaped (b) and points in the direction of the fiber bundle.

Fractional anisotropy

The fractional anisotropy (FA) (Basser and Pierpaoli, 1996) is a relative measure that is computed on the diffusion tensor and describes the variation between the levels of diffusion measured in the different directions. The FA is a scalar that assumes values between 0 and 1 and is defined by:

$$FA = \sqrt{\frac{3}{2}\left(\frac{(\lambda_1 - \overline{\lambda})^2 + (\lambda_2 - \overline{\lambda})^2 + (\lambda_3 - \overline{\lambda})^2}{\lambda_1^2 + \lambda_2^2 + \lambda_3^2}\right)},$$

(5)

$$\overline{\lambda} = \frac{\lambda_1 + \lambda_2 + \lambda_3}{3}$$

where the major eigenvector with eigenvalue λ_1 of the diffusion tensor represents the direction parallel to the fiber and both minor eigenvectors with eigenvalues λ_2 and λ_3 represent the radial directions (**Figure 4b**). The FA represents the level of directionality of the underlying white matter bundle and is believed to reflect (to some extent) fiber integrity. However, the FA values may vary considerably along one and the same fiber bundle for a number of reasons. For instance, at the crossing point of the two fiber bundles there is no longer one major fiber direction. Such a crossing cannot be adequately represented by a tensor and as a consequence the FA value will be low. The FA will also be lower in regions where the fiber bundle fans-out (i.e. near the cortex) than in regions where the same fiber bundle is more compact. Another possible source for reduced FA values is the presence of two or more tissue types in a single voxel (partial voluming). The diffusion profile of water molecules in gray matter and cerebral spinal fluid has no preferential direction and as a consequence the FA will be very low. Inclusion of gray matter tissue and/or cerebral spinal fluid in a white matter voxel will therefore result in a lowering of the FA value. Various studies have shown that axonal damage as well as reduction of myelin could lead to reduced FA values (Harsan et al., 2006; Kozlowski et al., 2008; Sun et al., 2008). However, the examples above show that a lowering of FA values cannot automatically be ascribed to axonal damage or reductions in myeline.

Fiber tracking

Fiber tracking algorithms combine the directional information of the fiber bundles provided by DWI at the level of voxels to reconstruct entire white matter fiber tracts.
Fiber tracking algorithms can roughly be divided into two classes, namely deterministic fiber tracking algorithms, which provide the actual paths between regions (if they are connected), and probabilistic fiber tracking algorithms, which merely provide the probability for two given regions of being connected (see (Jones, 2008) for a discussion of the possibilities and limitations of both classes). In this thesis a deterministic fiber tracking algorithm is used. Figure 5 shows an example of fiber tract reconstruction with the widely used deterministic fiber assignment by continuous tracking (FACT) algorithm (Mori et al., 1999), which only uses the major eigenvector λ_1 of the tensor to determine the direction of the tracts. For reasons of clarity we will use the term 'fiber bundle' for the actual

anatomical fiber bundle and 'tracts' for the results of the fiber tracking procedure. Note that DWI information is obtained at the level of voxels (typically $2.5 \times 2.5 \times 2.5$ mm), which contains millions of axons (with diameters ranging from 0.2 - 20 µm) (Kandel, 2000) and therefore only information of large fiber bundles and not of individual axons is obtained. Of further note, due to the symmetric nature of the process of diffusion it is not possible to distinguish between opposite directions (e.g up versus down, left versus right).
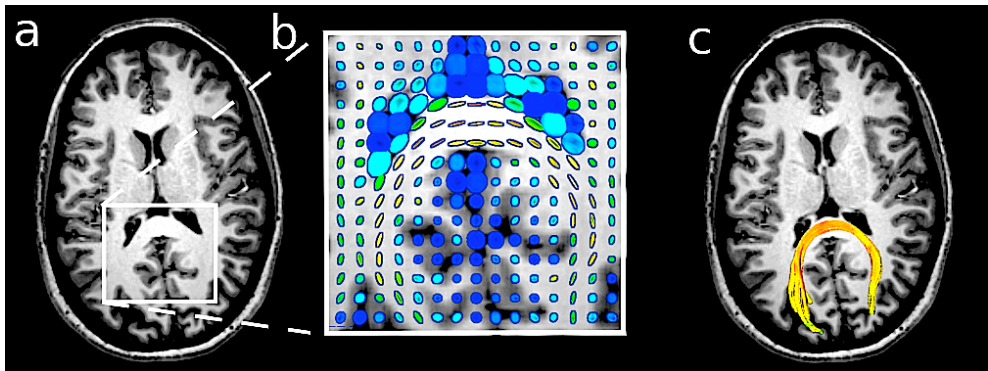

Figure 5. *Fiber tracking example using the deterministic FACT algorithm. a) Region for which the tensors are shown in b). b) For clarity only every second tensor is shown. The large size of tensors in the cerebral spinal fluid (blue) reflect high diffusivity. The tensors in white matter point in the direction of the fiber bundle (in this case the splenium of the corpus callosum). c) Using the directional information from the tensors b) the tracts from the splenium of the corpus callosum were reconstructed.*

Tract-based analysis

A basic question that can be answered using fiber tracking is whether two (or more) gray matter regions are connected by white matter fiber bundles. The existence of such a "high-speed" connection between spatially distinct gray matter regions may serve as supporting evidence in case it is not known whether these gray matter regions are actually part of the same neuronal network. In many cases, however, the existence of connecting white matter tracts is not an issue but the question is rather whether certain characteristics of fiber bundles differ between groups (for example, levels of myelination between schizophrenia patients and healthy participants). In those cases a novel technique named tract-based analysis (Gerig et al., 2004; Jones et al., 2005) comes into play. In tract-based analysis groups are compared at the level of fiber tracts. Such an analysis method is optimal for the detection of subtle diffuse group differences that occur over complete fiber tracts. This in contrast to a voxel-based analysis, which performs a point-by-point comparison and is optimal to detect focal group differences at the level of voxels. An example of differences that may go unnoticed with a standard voxel-based analysis but could be detected with tract-based analysis are differences due to altered expression levels of myelin-related genes in brains of patients with schizophrenia as was suggested by postmortem findings (Hakak et

al., 2001; Tkachev et al., 2003). If we assume that these differences in expression are likely to affect myelin levels along entire fiber tracts and are not confined to focal white matter regions (Barkovich, 2000), an analysis that examines complete fiber bundles should be the method of choice.

Tract selection

A key issue with tract-based analysis is the unequivocal definition of the tract(s) of interest because between subjects there exists no one-to-one correspondence at the level of individual tracts. A one-to-one correspondence can be obtained at the level of complete fiber bundles by selecting a group of reconstructed tracts that represent an anatomically distinct white matter fiber bundle. There are various ways to define these fiber bundles. Two frequently used methods start with the reconstruction of all tracts in the brain. Then, in a second step, all fibers are removed that do not meet the specific requirements for the tracts of interest. The two methods only differ in the way these requirements are defined.

Figure 6. Example of tract selection based on multiple white matter selection regions. Note that the selection regions are defined at positions where the fiber bundle is compact. The two different alternative selection regions given for region A and region B will yield identical results. This shows that the selection of the tracts is predominantly based on the relation between selection regions A and B and is fairly robust against variations in the sizes and positions of the regions used.
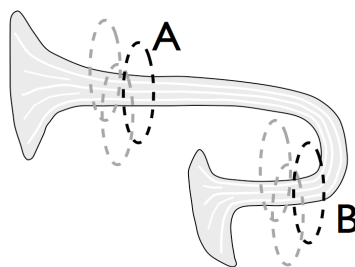
In the first method the requirements are based on whether or not tracts pass through a series of predefined white matter selection regions (Conturo et al., 1999; Wakana et al., 2004). In **Figure 6**, for example the tracts of interest are those tracts that pass trough region A *and* region B. This selection method is robust if the selection regions are placed at positions were the fiber bundle of interest is compact (usually away from the gray matter) and does not fan-out. In that case the definition of the fiber bundle is predominantly based on the relation between the different regions rather than on their exact sizes and positions (Zhang et al., 2008). This is shown in **Figure 6** were the alternative selection regions (the gray dashed regions) will lead to the selection of the same bundle. We can refine the selection process by simply adding more white matter regions or by more complex requirements (for example, all tracts that pass through A *and* B but *not* through C). In **Figure 7** it is shown how this method can be used to select the left uncinate fasciculus.

Because the method is fairly robust against variations in the sizes and positions of the white matter selection regions this method is well-suited to be applied in a fully

automatic scheme enabling the processing of large samples (Zhang et al., 2008). In such a scheme the white matter regions have to be defined only once on a model brain. Then, for each individual subject, a spatial transformation is computed between the subject's native space and the model space. These transformations are then used to place all tracts of each subject into model space where the actual selection of the tracts is carried out using the white matter selection regions. An advantage of mapping all tracts to model space instead of mapping the white matter regions to each native space is that tracts are geometric representations, which can be spatially transformed without resampling. This in contrast to the white matter regions, which are defined using voxels and transformation of voxels does require interpolation that introduces interpolation variations. In practice, however, the results will be identical.
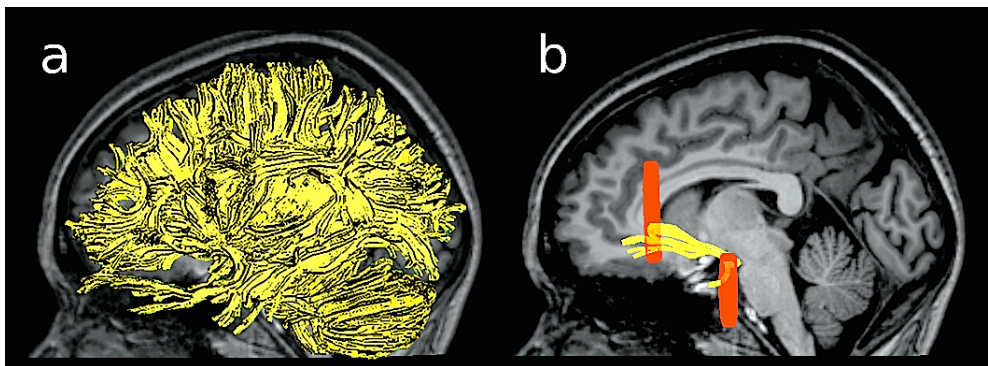
Figure 7. *Example of selection of the left uncinate fasciculus using two white matter selection regions. a) First all possible tracts in the brain are reconstructed and placed in model space. b) using two selection regions (one placed in the frontal lobe and one in the temporal lobe) the tracts that are part of the left uncinate fasciculus were selected.*

The second method differs from the first in that the selection regions are not defined in white matter but in gray matter. A major advantage of the latter method is that it can be combined with other imaging techniques such as functional magnetic resonance imaging (fMRI) (Ogawa et al., 1992) that can be used to define gray matter regions on an individual basis (Kim and Kim, 2005). For example, selection regions can be defined by gray matter regions that show activation during a given neurobehavioral task, or by different gray matter regions that show coherent signal fluctuations during rest; so-called resting-state fMRI (Fox and Raichle, 2007). In this case the method can be implemented in a fully automatic way with the difference that the selection regions are defined on an individual basis. However, a possible disadvantage of this method is that it is more sensitive to both position and size of the selection regions as the fiber bundle tends to be less compact (it tends to fan-out) when it reaches the cortex. Another possible complication is that fiber tracking in the vicinity of gray matter becomes increasingly difficult because of reduced directional information (e.g. due to partial voluming) although this problem can partly be circumvented by simply extending both ends of the tract in the last known

direction. In this thesis both methods are used. In Chapter 2 the first method is used while in Chapter 3 the fibers are selected with the second method using gray matter selection regions determined with resting-state fMRI. Once the fiber tracts are defined that represent a specific white matter fiber bundle it is possible to compute characteristics such as the average fractional anisotropy along the tracts for comparison between groups. The measures that can be averaged along the tracts are not limited to measures specific for DWI. Other types of MRI contrasts (or even signals from other imaging modalities such as PET or SPECT) can be averaged along these tracts as well, provided that registration between the data and reconstructed tracts is possible.

Magnetization Transfer Imaging

Magnetization transfer imaging (MTI) is an MRI technique that infers the amount of macromolecules including myelin (Wolff and Balaban, 1994). MTI is based on the fact that the frequency spectrum for the excitation of macromolecules is much broader than the frequency spectrum for excitation of water molecules in the free water pool (known as the Larmor frequency). With MTI a so-called magnetization prepulse is applied at the beginning of the acquisition with a certain offset from the Larmor frequency. This magnetization prepulse excites the macromolecules but not the water molecules. In turn, these macromolecules transfer their magnetization (hence the name) onto the water molecules in the free water pool. As a consequence the signal strength from the water pool that can be measured is reduced and this signal reduction is proportional to the amount of macromolecules (**Figure 8**). By collecting two MRI scans, one with - and one without magnetization transfer prepulse, it is possible to compute the reduction of the signal due to magnetization transfer and this is expressed by the magnetization transfer ratio MTR which is defined by: MTR $= (S_0 - S_{mt}) / S_0$, where S_{mt} is the scan with the magnetization transfer prepulse and S_0 is the scan without the magnetization transfer prepulse. MTR is therefore a scalar value, ranging between 0 to 1, where higher values represent the presence of more macromolecules. Thus, similar to DTI - where characteristics of the microstructure are inferred from the shape of the diffusion profile - with MTR one does not directly measure the presence of macromolecules but infers their presence by measuring their effect on the magnetization of the free water molecules. Hence, mechanisms that directly alter characteristics of the water molecules themselves and are not related to macromolecule content will also influence the resulting MTR value. One should always keep this in mind when interpreting differences in group results for these indirect measures (Barkovich, 2000; Laule et al., 2007).

Although FA and MTR can be measured along entire tracts to obtain structural information of the white matter fiber bundles, we think that the FA can also be used as contrast mechanism in an fMRI-like setting.
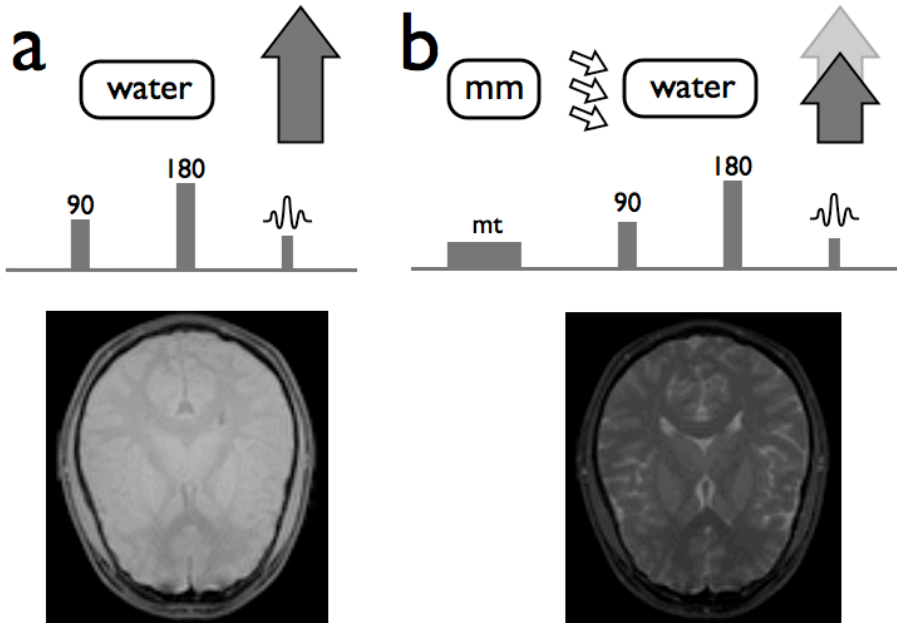
***Figure 8.** Magnetization transfer ratio is computed between two scans, one with and one without a magnetization transfer prepulse. a) In a standard MRI scan sequence a 90 degrees pulse excites the water molecules in the free water pool that results (after the 180 degrees pulse) in a measurable signal with a certain signal strength (here denoted by the size of the arrow). b) In a magnetization transfer prepulse MRI sequence, the magnetization transfer prepulse (mt) excites the macromolecules (mm) but not the water molecules. In turn the macromolecules transfer their magnetization onto the water molecules. The result of this transfer of magnetization is that the excitation of the 90 degrees pulse is reduced, resulting in a reduced signal strength. The reduction of the signal strength is proportional to the amount of macromolecules present in the sample.*

functional DTI

Activation of the human brain's gray matter regions have been extensively studied with neuroimaging techniques such as functional magnetic resonance imaging (fMRI), positron emission tomography (PET), single photon emission computed tomography (SPECT), electro-encephalography (EEG) and magneto-encephalography (MEG). However, these techniques do not provide information on the white matter pathways and their corresponding activity. In this thesis (Chapters 4 and 5) we explore the possibility to detect task-related changes in FA that may represent the activity of white matter tracts. Directly testing the white matter tracts for activation would provide us with a unique opportunity to study the connections of neural networks that become active during various cognitive

functions. The contrast mechanism of this new method is based on the assumption that repetitive axonal discharge results in an increase of potassium ions in the extra-cellular space (Kandel, 2000), will lead to morphological changes of the surrounding glial cells (Ransom et al., 1985; Svoboda and Sykova, 1991; Anderson et al., 1996; Ransom et al., 2000; Beshay et al., 2005). In turn, the morphological changes of the glial cells alter the extra-cellular space (Sykova, 2005; Stroman et al., 2008), something that can be measured because the DWI acquisitions used here are thought to be most sensitive to water in the extra-cellular space (Clark and Le Bihan, 2000). Considering previous work using DTI and intrinsic optical signal measurements (MacVicar et al., 2002; Sykova et al., 2003) we assume that these activity-related morphological changes of glial cells result in a narrowing of the extra-cellular space in the direction perpendicular to the fiber bundle and therefore a reduction of apparent diffusivity in that direction. Using an fMRI-like experimental design, DTI scans are acquired during an alternating series of active and rest conditions. According to our hypothesis the FA value for the active conditions is higher compared to the FA value for the rest conditions. However, these differences can be expected to be very small (Gulani et al., 1999) and a standard voxel-based analysis approach (which is the usual approach for the analysis of fMRI data) will not suffice. Tract-based analysis on the other hand is a very good option because it can be assumed that the effects occur along entire fiber tracts.

The role of tract-based analysis in schizophrenia

Schizophrenia is a severe psychiatric disorder that is characterized by hallucinations, delusions, thought disorder and impairments in cognitive functions. The etiology of schizophrenia is not known. Using standard anatomical magnetic resonance imaging (MRI) methods, numerous studies have revealed gray matter volume decreases in the brains of patients with schizophrenia, in particular in the fronto-temporal regions (Wright et al., 2000; Hulshoff Pol et al., 2001; Wright et al., 2001; Honea et al., 2005). From about the time of its definition (Bleuler, 1911; Kraepelin, 1919) it was suggested that schizophrenia is a connectivity disease. Recently, evidence is accumulating that the integrity of white matter fibers connecting the spatially distinct gray matter regions is compromised in schizophrenia and that impaired functioning of white matter is part of its pathophysiology (Davis et al., 2003). Indeed, earlier we found decreases in white matter density in the anterior corpus callosum using a voxel-based morphometry approach (Hulshoff Pol et al., 2004; Hulshoff Pol et al., 2006).

The introduction of diffusion weighted imaging (DWI) in combination with fiber tracking made it possible to non-invasively study the white matter fiber bundles and it opened the door to study the brain's connections *in vivo*. Moreover, the introduction of tract-based analysis provided us with a tool that is well suited to detect any subtle aberrations of these connections in schizophrenia. Both DTI and magnetization transfer ratio (MTR) imaging allow us to study different aspects of the connecting white matter fiber bundles that cannot be measured using standard T1- or T2-weighted MRI. Using DTI, decreases in fractional anisotropy (FA) have been found in several studies in schizophrenia

((Kanaan et al., 2005; Kubicki et al., 2007; Konrad and Winterer, 2008)). Most studies applied voxel-based analysis of DTI images (Kanaan et al., 2005; Kubicki et al., 2007; Konrad and Winterer, 2008). More recently fiber tracking techniques (Mori and van Zijl, 2002; Jones, 2008) are being used to infer fiber integrity along complete tracts (Jones et al., 2005; Kanaan et al., 2006). In the few studies that applied a tract-based analysis to measure FA in schizophrenia no differences in mean FA values between groups were found (Jones et al., 2005; Mori et al., 2007; Rosenberger et al., 2008). However, a significant correlation between higher age and lower mean FA was shown in schizophrenia patients and not in healthy participants (Mori et al., 2007; Rosenberger et al., 2008). This group-by-age interaction suggests that the deficits found in schizophrenia may be more prominent in patients with longer illness duration. Indeed, recently, reductions in FA were found in chronically ill and not in first-episode schizophrenia patients compared to healthy participants (Friedman et al., 2008).

A few MTR imaging studies of white matter have been completed in schizophrenia. In the first study, using an ROI approach, reduced mean MTR values were found in the left and right temporal regions, but not in frontal, parietal and occipital regions (Foong et al., 2000). Similarly, reductions in mean MTR values were found in the splenium but not in the genu of the corpus callosum (Foong et al., 2000). Bilaterally reduced MTR was found using a voxel-based analysis in the uncinate fasciculus (with left reductions greater than right reductions) in first episode schizophrenia patients (Bagary et al., 2003), although another voxel-based analysis study did not find significant reductions in MTR (Antosik-Biernacka et al., 2006). In the one combined DTI and MTR voxel-based analysis study in schizophrenia, decreased MTR was found in the posterior cingulum bundle, corpus callosum, fornix, right internal capsule, and superior occipito-frontal fasciculus bilaterally in schizophrenia patients compared to healthy participants (Kubicki et al., 2005).

Genetic and post-mortem findings suggest that oligodendrocytes play a role in schizophrenia (Hakak et al., 2001; Tkachev et al., 2003; Uranova et al., 2004; Harrison and Weinberger, 2005; Karoutzou et al., 2008; Mitkus et al., 2008). In the central nervous system oligodendrocytes are the glial cells responsible for the formation of myelin sheath around the axons. Changes in the number, size and/or shape of oligodendrocytes may be reflected in subtle changes of the extra-cellular space, which can be picked up with DWI. Therefore, measures such as the FA (computed on diffusion tensor imaging data) may provide valuable information when studying structural aspects of schizophrenia. Especially when they are combined with other contrast mechanisms such as MTR to study the possible role of myelin in the measured FA signal changes. Oligodendrocytes also play a key role in functional diffusion tensor imaging (fDTI) because we hypothesize that task-related morphological changes of oligodendrocytes form the basis of the functional contrast mechanism. This would make fDTI a valuable tool to study schizophrenia and future fDTI studies could help us to determine if aberrant oligodendrocytes may lead to impaired communication in schizophrenia.

Aim of this thesis

In this thesis we assess the possibilities of tract-based analysis to study structural and functional aspects of white matter fiber bundles in schizophrenia.

Outline of this thesis

In **Chapter 2** we used tract-based analysis to study the role of frontal and fronto-temporal connections in schizophrenia by comparing FA and MTR values between groups. We focus on the left and right uncinate fasciculus and the genu of the corpus callosum. The rationale behind this approach is that the combination of FA and MTR provides more information about the role of myelin in the previously reported group differences in FA. If these group differences are exclusively myelin-related then one could also expect to find similar group differences in MTR. In **Chapter 3** fMRI was combined with DTI to determine if there is a relation between the strength of correlation of fMRI signals from gray matter regions and the "strength" of the connecting fiber bundles. fMRI was used to determine correlations in gray matter regions during rest (resting-state fMRI) to identify the so-called default mode network. FA values were measured along the tracts (the cinguli) connecting these gray matter regions and correlated with the level of resting-state in the regions of the default mode network. Although the study presented in Chapter 3 successfully combines functional information of gray matter regions with structural information of white matter tracts, it does not provide information on the functioning of the white matter tracts themselves. This kind of information cannot be obtained with standard fMRI or standard DTI and therefore a new imaging method had to be developed. In **Chapter 4** we explored the possibility to study activation of white matter introducing a new method that was dubbed functional DTI. Tactile and visual stimuli were presented to eight healthy participants that were scanned using a 1.5 Tesla scanner. Activation was found in the expected fiber tracts (the contra-lateral thalamocortical sensory tract and optic radiations, respectively). The results of this study did not only suggest that detection of white matter activation using fDTI is feasible, they also suggest that different types of stimuli have different types of slow varying response functions. This information was incorporated into the experimental-setup of a second fDTI study. In this second fDTI study, described in **Chapter 5**, we not only replicated our findings presented in Chapter 4 but also ruled out a number of possible confounding factors. Twelve subjects were scanned on a 3 Tesla scanner using the same type of stimuli as were used in the first fDTI experiment. Finally, in **Chapter 6** we discuss the results of the studies presented in chapters 2,3,4 and 5.

References

Anderson AW, Zhong J, Petroff OA, Szafer A, Ransom BR, Prichard JW, Gore JC (1996) Effects of osmotically driven cell volume changes on diffusion-weighted imaging of the rat optic nerve. Magn Reson Med 35:162-167.

Antosik-Biernacka A, Peuskens H, De Hert M, Peuskens J, Sunaert S, Van Hecke P, Goraj B (2006) Magnetization transfer imaging in chronic schizophrenia. Med Sci Monit 12:MT17-21.

Bagary MS, Symms MR, Barker GJ, Mutsatsa SH, Joyce EM, Ron MA (2003) Gray and white matter brain abnormalities in first-episode schizophrenia inferred from magnetization transfer imaging. Arch Gen Psychiatry 60:779-788.

Barkovich AJ (2000) Concepts of myelin and myelination in neuroradiology. AJNR Am J Neuroradiol 21:1099-1109.

Basser PJ, Pierpaoli C (1996) Microstructural and physiological features of tissues elucidated by quantitative-diffusion-tensor MRI. J Magn Reson B 111:209-219.

Beaulieu C (2002) The basis of anisotropic water diffusion in the nervous system - a technical review. NMR Biomed 15:435-455.

Beshay JE, Hahn P, Beshay VE, Hargittai PT, Lieberman EM (2005) Activity-dependent change in morphology of the glial tubular lattice of the crayfish medial giant nerve fiber. Glia 51:121-131.

Bleuler E (1911) Dementia Praecox or the Group of Schizophrenias. New York: International Universities Press.

Catani M, Ffytche DH (2005) The rises and falls of disconnection syndromes. Brain 128:2224-2239.

Chenevert TL, Brunberg JA, Pipe JG (1990) Anisotropic diffusion in human white matter: demonstration with MR techniques in vivo. Radiology 177:401-405.

Clark CA, Le Bihan D (2000) Water diffusion compartmentation and anisotropy at high b values in the human brain. Magn Reson Med 44:852-859.

Conturo TE, Lori NF, Cull TS, Akbudak E, Snyder AZ, Shimony JS, McKinstry RC, Burton H, Raichle ME (1999) Tracking neuronal fiber pathways in the living human brain. Proc Natl Acad Sci U S A 96:10422-10427.

Davis KL, Stewart DG, Friedman JI, Buchsbaum M, Harvey PD, Hof PR, Buxbaum J, Haroutunian V (2003) White matter changes in schizophrenia - Evidence for myelin-related dysfunction. Archives of General Psychiatry 60:443-456.

Doran M, Hajnal JV, Van Bruggen N, King MD, Young IR, Bydder GM (1990) Normal and abnormal white matter tracts shown by MR imaging using directional diffusion weighted sequences. J Comput Assist Tomogr 14:865-873.

Foong J, Maier M, Barker GJ, Brocklehurst S, Miller DH, Ron MA (2000) In vivo investigation of white matter pathology in schizophrenia with magnetisation transfer imaging. J Neurol Neurosurg Psychiatry 68:70-74.

Fox MD, Raichle ME (2007) Spontaneous fluctuations in brain activity observed with functional magnetic resonance imaging. Nat Rev Neurosci 8:700-711.

Friedman JI, Tang C, Carpenter D, Buchsbaum M, Schmeidler J, Flanagan L, Golembo S, Kanellopoulou I, Ng J, Hof PR, Harvey PD, Tsopelas ND, Stewart D, Davis KL (2008) Diffusion Tensor Imaging Findings in First-Episode and Chronic Schizophrenia Patients. Am J Psychiatry. 165:1024-1032.

Gerig G, Gouttard S, Corouge I (2004) Analysis of brain white matter via fiber tract modeling. Conf Proc IEEE Eng Med Biol Soc 6:4421-4424.

Gulani V, Iwamoto GA, Lauterbur PC (1999) Apparent water diffusion measurements in electrically stimulated neural tissue. Magn Reson Med 41:241-246.

Haacke EM, Brown RW, Thompson MR, Venkatesan R (1999) Magnetic Resonance Imaging: Physical Principles and Sequence Design. New York: John Wiley & Sons, Inc.

Hakak Y, Walker JR, Li C, Wong WH, Davis KL, Buxbaum JD, Haroutunian V, Fienberg AA (2001) Genome-wide expression analysis reveals dysregulation of myelination-related genes in chronic schizophrenia. Proc Natl Acad Sci U S A 98:4746-4751.

Harrison PJ, Weinberger DR (2005) Schizophrenia genes, gene expression, and neuropathology: on the matter of their convergence. Mol Psychiatry 10:40-68; image 45.

Harsan LA, Poulet P, Guignard B, Steibel J, Parizel N, de Sousa PL, Boehm N, Grucker D, Ghandour MS (2006) Brain dysmyelination and recovery assessment by noninvasive in vivo diffusion tensor magnetic resonance imaging. J Neurosci Res 83:392-402.

Honea R, Crow TJ, Passingham D, Mackay CE (2005) Regional deficits in brain volume in schizophrenia: a meta-analysis of voxel-based morphometry studies. Am J Psychiatry 162:2233-2245.

Hulshoff Pol HE, Schnack HG, Mandl RC, Cahn W, Collins DL, Evans AC, Kahn RS (2004) Focal white matter density changes in schizophrenia: reduced inter-hemispheric connectivity. Neuroimage 21:27-35.

Hulshoff Pol HE, Schnack HG, Mandl RC, van Haren NE, Koning H, Collins DL, Evans AC, Kahn RS (2001) Focal gray matter density changes in schizophrenia. Arch Gen Psychiatry 58:1118-1125.

Hulshoff Pol HE, Schnack HG, Mandl RC, Brans RG, van Haren NE, Baare WF, van Oel CJ, Collins DL, Evans AC, Kahn RS (2006) Gray and white matter density changes in monozygotic and same-sex dizygotic twins discordant for schizophrenia using voxel-based morphometry. Neuroimage 31:482-488.

Jones DK (2008) Studying connections in the living human brain with diffusion MRI. Cortex 44:936-952.

Jones DK, Horsfield MA, Simmons A (1999) Optimal strategies for measuring diffusion in anisotropic systems by magnetic resonance imaging. Magn Reson Med 42:515-525.

Jones DK, Catani M, Pierpaoli C, Reeves SJ, Shergill SS, O'Sullivan M, Maguire P, Horsfield MA, Simmons A, Williams SC, Howard RJ (2005) A diffusion tensor magnetic resonance imaging study of frontal cortex connections in very-late-onset schizophrenia-like psychosis. Am J Geriatr Psychiatry 13:1092-1099.

Kanaan RA, Kim JS, Kaufmann WE, Pearlson GD, Barker GJ, McGuire PK (2005) Diffusion tensor imaging in schizophrenia. Biol Psychiatry 58:921-929.

Kanaan RA, Shergill SS, Barker GJ, Catani M, Ng VW, Howard R, McGuire PK, Jones DK (2006) Tract-specific anisotropy measurements in diffusion tensor imaging. Psychiatry Res 146:73-82.

Kandel ER, Schwartz, J.H., and Jessell, T.M. (2000) Principles of Neural Science, 4th Edition: McGraw-Hill Inc.

Karoutzou G, Emrich HM, Dietrich DE (2008) The myelin-pathogenesis puzzle in schizophrenia: a literature review. Molecular Psychiatry 13:245-260.

Kim DS, Kim M (2005) Combining functional and diffusion tensor MRI. Ann N Y Acad Sci 1064:1-15.

Konrad A, Winterer G (2008) Disturbed structural connectivity in schizophrenia - Primary factor in pathology or epiphenomenon? Schizophrenia Bulletin 34:72-92.

Kozlowski P, Raj D, Liu J, Lam C, Yung AC, Tetzlaff W (2008) Characterizing white matter damage in rat spinal cord with quantitative MRI and histology. J Neurotrauma 25:653-676.

Kraepelin E (1919) Dementia Praecox and Paraphrenia., 8 Edition. Edinburgh, Livingstone.

Kubicki M, McCarley R, Westin CF, Park HJ, Maier S, Kikinis R, Jolesz FA, Shenton ME (2007) A review of diffusion tensor imaging studies in schizophrenia. J Psychiatr Res 41:15-30.

Kubicki M, Park H, Westin CF, Nestor PG, Mulkern RV, Maier SE, Niznikiewicz M, Connor EE, Levitt JJ, Frumin M, Kikinis R, Jolesz FA, McCarley RW, Shenton ME (2005) DTI and MTR abnormalities in schizophrenia: analysis of white matter integrity. Neuroimage 26:1109-1118.

Laule C, Vavasour IM, Kolind SH, Li DKB, Traboulsee TL, Moore GRW, MacKay AL (2007) Magnetic resonance imaging of myelin. Neurotherapeutics 4:460-484.

Le Bihan D, Breton E (1985) Imagerie de diffusion in vivo par résonance magnétique nucléaire. Compte Rendus de l'Académie de Sciences Paris 301:1109-1112.

Le Bihan D, Mangin JF, Poupon C, Clark CA, Pappata S, Molko N, Chabriat H (2001) Diffusion tensor imaging: concepts and applications. J Magn Reson Imaging 13:534-546.

MacVicar BA, Feighan D, Brown A, Ransom B (2002) Intrinsic optical signals in the rat optic nerve: Role for K+ uptake via NKCC1 and swelling of astrocytes. Glia 37:114-123.

Mesulam M (2005) Imaging connectivity in the human cerebral cortex: the next frontier? Ann Neurol 57:5-7.

Mitkus SN, Hyde TM, Vakkalanka R, Kolachana B, Weinberger DR, Kleinman JE, Lipska BK (2008) Expression of oligodendrocyte-associated genes in dorsolateral prefrontal cortex of patients with schizophrenia. Schizophrenia Research 98:129-138.

Mori S, van Zijl PC (2002) Fiber tracking: principles and strategies - a technical review. NMR Biomed 15:468-480.

Mori S, Crain BJ, Chacko VP, van Zijl PC (1999) Three-dimensional tracking of axonal projections in the brain by magnetic resonance imaging. Ann Neurol 45:265-269.

Mori T, Ohnishi T, Hashimoto R, Nemoto K, Moriguchi Y, Noguchi H, Nakabayashi T, Hori H, Harada S, Saitoh O, Matsuda H, Kunugi H (2007) Progressive changes of white matter integrity in schizophrenia revealed by diffusion tensor imaging. Psychiatry Res 154:133-145.

Norris DG (2001) The effects of microscopic tissue parameters on the diffusion weighted magnetic resonance imaging experiment. NMR Biomed 14:77-93.

Ogawa S, Tank DW, Menon R, Ellermann JM, Kim SG, Merkle H, Ugurbil K (1992) Intrinsic signal changes accompanying sensory stimulation: functional brain mapping with magnetic resonance imaging. Proc Natl Acad Sci USA 89:5951-5955.

Ransom BR, Yamate CL, Connors BW (1985) Activity-dependent shrinkage of extracellular space in rat optic nerve: a developmental study. J Neurosci 5:532-535.

Ransom CB, Ransom BR, Sontheimer H (2000) Activity-dependent extracellular K+ accumulation in rat optic nerve: the role of glial and axonal Na+ pumps. J Physiol 522 Pt 3:427-442.

Rosenberger G, Kubicki M, Nestor PG, Connor E, Bushell GB, Markant D, Niznikiewicz M, Westin CF, Kikinis R, A JS, McCarley RW, Shenton ME (2008) Age-related deficits in fronto-temporal connections in schizophrenia: A diffusion tensor imaging study. Schizophr Res. 102:181-188.

Skare S (2002) Optimisation Strategies in Diffusion Tensor MR Imaging. PhD Thesis, Department of Clinical Neuroscience. Stockholm: Karolinska Institutet.

Skare S, Hedehus M, Moseley ME, Li TQ (2000) Condition number as a measure of noise performance of diffusion tensor data acquisition schemes with MRI. J Magn Reson 147:340-352.

Stejskal EO, Tanner JE (1965) Spin diffusion measurements: spin echoes in the presence of a time-dependent field gradient. Journal of Chemical Physics 42:288-292.

Stroman PW, Lee AS, Pitchers KK, Andrew RD (2008) Magnetic Resonance Imaging of Neuronal and Glial Swelling as an Indicatior of Function in Cerebral Tissue Slices. Magnetic Resonance in Medicine 59:700-706.

Sun SW, Liang HF, Cross AH, Song SK (2008) Evolving Wallerian degeneration after transient retinal ischemia in mice characterized by diffusion tensor imaging. Neuroimage 40:1-10.

Svoboda J, Sykova E (1991) Extracellular space volume changes in the rat spinal cord produced by nerve stimulation and peripheral injury. Brain Res 560:216-224.

Sykova E (2005) Glia and volume transmission during physiological and pathological states. J Neural Transm 112:137-147.

Sykova E, Vargova L, Kubinova S, Jendelova P, Chvatal A (2003) The relationship between changes in intrinsic optical signals and cell swelling in rat spinal cord slices. Neuroimage 18:214-230.

Tkachev D, Mimmack ML, Ryan MM, Wayland M, Freeman T, Jones PB, Starkey M, Webster MJ, Yolken RH, Bahn S (2003) Oligodendrocyte dysfunction in schizophrenia and bipolar disorder. Lancet 362:798-805.

Uranova NA, Vostrikov VM, Orlovskaya DD, Rachmanova VI (2004) Oligodendroglial density in the prefrontal cortex in schizophrenia and mood disorders: a study from the Stanley Neuropathology Consortium. Schizophrenia Research 67:269-275.

Wakana S, Jiang HY, Nagae-Poetscher LM, van Zijl PCM, Mori S (2004) Fiber tract-based atlas of human white matter anatomy. Radiology 230:77-87.

Wolff SD, Balaban RS (1994) Magnetization transfer imaging: practical aspects and clinical applications. Radiology 192:593-599.

Wright IC, Rabe-Hesketh S, Woodruff PWR, David AS, Murray RM, Bullmore ET (2000) Meta-analysis of regional brain volumes in schizophrenia. American Journal of Psychiatry 157:16-25.

Wright P, Nimgaonkar VL, Donaldson PT, Murray RM (2001) Schizophrenia and HLA: a review. Schizophr Res 47:1-12.

Zhang W, Olivi A, Hertig SJ, van Zijl P, Mori S (2008) Automated fiber tracking of human brain white matter using diffusion tensor imaging. Neuroimage 42:771-778.

Chapter 2

Tract-based analysis of magnetization transfer ratio and diffusion tensor imaging of the frontal and fronto-temporal connections in schizophrenia

René C.W. Mandl, Hugo G. Schnack, Judy Luigjes, Martijn P. van den Heuvel, Wiepke Cahn, René S. Kahn and Hilleke E. Hulshoff Pol

Abstract

In the pathophysiology of schizophrenia aberrant connectivity between brain regions may be a central feature. Diffusion tensor imaging (DTI) studies have shown altered fractional anisotropy (FA) in white brain matter in schizophrenia. Focal reductions in myelin have been suggested in patients using magnetization transfer ratio (MTR) imaging but to what extent schizophrenia may be related to changes in MTR measured along entire fiber bundles is still unknown. DTI and MTR images were acquired with a 1.5 Tesla scanner in 40 schizophrenia patients and compared to those of 40 healthy participants. The mean FA and mean MTR were measured along the genu of the corpus callosum and left and right uncinate fasciculus. A higher mean MTR of 1% was found in the right uncinate fasciculus in patients compared to healthy participants. A significant negative correlation between age and mean FA in the left uncinate fasciculus was found in schizophrenia patients but not in healthy participants. Decreased FA in the left uncinate fasciculus may be more prominent in patients with longer illness duration. The increased mean MTR in the right uncinate fasciculus could reflect a compensatory role for myelin in these fibers or possibly represent aberrant fronto-temporal connectivity.

Using standard anatomical magnetic resonance imaging (MRI) methods, numerous studies have revealed gray matter volume decreases in the brains of patients with schizophrenia, in particular in the fronto-temporal regions (Wright et al., 2001). These regions do not operate in isolation but form large-scale neural networks for which normal interregional communication is a prerequisite for proper functioning. Indeed, from about the time schizophrenia was defined it was suggested that aberrant connectivity between these brain regions is a central feature of the disease (Bleuler, 1911; Kraepelin, 1919). Recently, evidence is accumulating that the integrity of white matter fibers connecting the spatially distinct gray matter regions is compromised in schizophrenia and that impaired functioning of white matter is part of its pathophysiology (Davis et al., 2003).

Diffusion tensor imaging (DTI) and magnetization transfer ratio (MTR) imaging are MRI methods that allow us to study different aspects of the connecting white matter fiber bundles *in vivo* that cannot be measured using standard T1- or T2-weighted MRI. Using DTI, decreases in fractional anisotropy (FA) - which is believed to reflect microstructural directionality (Beaulieu, 2002) and to a certain extent fiber integrity - have been found in several studies in schizophrenia (for reviews see Kanaan et al, Kubicki et al, Konrad et al (Kanaan et al., 2005; Kubicki et al., 2007; Konrad and Winterer, 2008)). Most studies applied voxel-based analysis of DTI images (Kanaan et al., 2005; Kubicki et al., 2007; Konrad and Winterer, 2008). More recently fiber tracking techniques (Mori and van Zijl, 2002; Jones, 2008) are being used to infer fiber integrity along complete tracts (Jones et al., 2005; Kanaan et al., 2006; van den Heuvel et al., 2008). Using such tract-based analysis methods characteristic values such as FA can be measured along fiber tracts and subsequently their average values between groups can be compared. As such, tract-based analysis methods are optimal to detect subtle group-related changes that may occur along entire fiber tracts. This in contrast to voxel-based analyses, which are optimized to detect focal differences in white matter.

In the few studies that applied a tract-based analysis to measure FA in schizophrenia no differences in mean FA values between groups were found in the uncinate fasciculi (Jones et al., 2006; Rosenberger et al., 2008). However, a significant correlation between higher age and lower mean FA was shown in schizophrenia patients and not in healthy participants (Mori et al., 2007; Rosenberger et al., 2008). This group-by-age interaction suggests that the deficits found in schizophrenia may be more prominent in patients with longer illness duration. Indeed, recently, reductions in FA were found in chronically ill and not in first-episode schizophrenia patients compared to healthy participants (Friedman et al., 2008).

MTR imaging infers the presence of macro-molecules in tissue, including myelin, and thus may provide additional information to DTI on white matter integrity (Wolff and Balaban, 1994; van Buchem et al., 1999; Barkovich, 2000; Henkelman et al., 2001). A few MTR imaging studies of white matter have been completed in schizophrenia. In the first study, using an ROI approach, reduced mean MTR values were found in the left and right temporal regions, but not in frontal, parietal and occipital regions (Foong et al., 2000b). Similarly, reductions in mean MTR values were found in the splenium but not in the genu of the corpus callosum (Foong et al., 2000a). Bilaterally reduced MTR was found using a

voxel-based analysis in the uncinate fasciculus (with left reductions greater than right reductions) in first episode schizophrenia patients (Bagary et al., 2003), although another voxel-based analysis study did not find significant reductions in MTR (Antosik-Biernacka et al., 2006). In the one combined DTI and MTR voxel-based analysis study in schizophrenia, decreased MTR was found in the posterior cingulum bundle, corpus callosum, fornix, right internal capsule, and superior occipito-frontal fasciculus bilaterally in schizophrenia patients compared to healthy participants (Kubicki et al., 2005). Tract-based analysis of FA in combination with MTR (Lin, et al. 2008) may provide more information about to what extent possible group differences in FA can be attributed to differences in myelination. To our knowledge no tract-based analysis has been done for MTR in schizophrenia and its associations with age.

In this study we measured fiber integrity and myelin concentration over entire fiber tracts in schizophrenia. We compared both FA and MTR along averaged white matter tracts (Gerig et al., 2004) computed for the uncinate fasciculi which connect the temporal and frontal lobes, and the genu of the corpus callosum (genu) which connects the frontal lobes of both hemispheres. We selected fibers connecting the frontal lobes of the left and right hemispheres, and fibers connecting the frontal and temporal lobes, because these brain areas are known to be involved in the pathophysiology of schizophrenia. Indeed, numerous studies have reported decreases in frontal and temporal gray matter volumes and densities (Wright et al., 2000; Hulshoff Pol et al., 2001; Honea et al., 2005). Moreover, earlier we found decreases in white matter density in the anterior corpus callosum using a voxel-based morphometry approach. Therefore, we hypothesized that fibers integrity as measured using DTI and MTR along the uncinate fasciculi and anterior corpus callosum would be compromised in patients with schizophrenia as compared to healthy participants. In addition, we investigated associations of FA and MTR with age, severity of positive and negative symptoms, outcome, age at onset, duration of illness, and antipsychotic medication intake.

Materials and methods

Subjects

Forty patients with schizophrenia and 40 healthy participants, matched for age, gender, handedness and parental education participated in this study. The healthy participants were recruited by means of local newspaper advertisements. All subjects participated after written informed consent was obtained. The study was approved by the medical ethics committee for research in humans (METC) of the University Medical Center Utrecht, the Netherlands. All participants underwent extensive psychiatric assessment procedures using the Comprehensive Assessment of Symptoms and History (CASH). Patients met DSM-IV criteria for schizophrenia.

Table 1. Demographic data

	Patients with schizophrenia (N=40)	Healthy participants (N=40)
Male/female, no	30/10	29/11
Age, yr [†]	26.8 (5.8)	28.0 (7.7)
Age, yr range	20-41	18-45
Height, cm [†]	179.3 (9.2)	182.5 (9.0)
Height, cm range	163-198	167-204
Weight, kg[†]	76.3 (13.3)	74.3 (9.1)
Weight, kg range	55-110	57-92
Handedness – right /left /ambidexter, no	37/3/0	35/5/0
Level of education, yr [†]	10.4 (2.5)*	13.8 (2.2)
Parental level of education, yr [†]	13.6 (2.7)	13.6 (3.2)
Age at first symptoms, yr [†]	24.7 (5.6)	
Age at first symptoms yr range	16.9-38.4	
Duration of illness, mean (sd), months	25.1 (17.4)	
Medication at time of the scan [‡¶]		
Typical antipsychotics, no	4	
– median (range) Haldol eq.	3.5 (4.7)	
Atypical antipsychotics, no	29	
– median (range) Haldol eq.	7.1 (12)	
No medication at time of scan, no	0	
Cumulative medication[†§]		
Typical antipsychotics no	1	
– mean	106.5	
Atypical antipsychotics no	22	
– mean	6208.4 (6830.9)	
Typical+Atypical antipsychotics no	13	
– mean	10956.2 (9640.3)	
PANSS positive symptoms	15.7 (5.6)	
PANSS negative symptoms	15.6 (5.7)	
PANSS general symptoms	31.0 (7.2)	
PANSS total score	62.3 (15.8)	
CAN total score	14.4 (7.9)	

p<0.01

† values are mean ± SD

‡ in 7 patients medication information was unavailable

¶ haloperidol, broomperidol, pipamperon, thioridazine, flufenazine, perfenazine, zuclopentixol, penfluridol, pimozide, fluspirilen, largactil and flufenazine were considered typical antipsychotic drugs; clozapine, risperidone, olanzapine, and sertindole were considered atypical antipsychotic drugs.

§ in 4 patients cumulative medication use was unavailable.

"Age of onset of illness" was defined as the age at which the patients experienced psychotic symptoms for the first time, as obtained from the CASH interview, and Schedule for Affective Disorder and Schizophrenia Lifetime version (SADS-L) assessed by two independent raters. Diagnostic consensus was achieved in the presence of a psychiatrist. "Duration of illness", was defined as time between age of onset of illness and age at the time of the MRI scan. All healthy participants met Research Diagnostic Criteria for "never mentally ill" and had no first-degree family member with a mental illness or second-degree relatives with a psychotic disorder.

      All patients were receiving typical, or atypical, antipsychotic medication at the time of the scan. A table from the Dutch National Health Service (Commissie Farmaceutische Hulp van het College voor Zorgverzekeringen, 2002) was used to calculate the cumulative dosage of typical antipsychotics during the scan interval and to derive the haloperidol equivalents. For atypical antipsychotics, the respective pharmaceutical companies suggested how to convert dosage into haloperidol equivalents (clozapine, 40:1; olanzapine, 2.5:1; risperidone, 1:1, sulpiride, 170:1; quetiapine, 50:1; and sertindole, 2:1). Drug use was assessed with the Composite International Diagnostic Interview (CIDI). Four patients and one healthy participant met criteria for drug abuse, one patient met criteria for drug dependency. Drugs used included cannabis (in all 6 subjects) and others (3). For demographics see **Table 1**.

Image acquisition

Magnetic resonance imaging (MRI) scans of the whole brain were made on a 1.5 Tesla Intera Achieva Philips System at the University Medical Center Utrecht using a six-element SENSE receiver head-coil. For each subject DTI scans, an MTR scan and a high-resolution T1-weighted scan (used for anatomical reference) were collected. First, a three-dimensional T1-weighted coronal (spoiled-gradient) echo scan of the whole head was acquired (256×256 matrix; TE = 4.6 ms; TR = 30 ms; flip angle = 30 degrees; 160-180 contiguous slices; total scan duration 405-456 s; $1 \times 1 \times 1.2$ mm^3 voxels; FOV = 256 mm / 70%; parallel imaging applied in both phase-encoding directions with SENSE-factor = 1.5). For white matter fiber tract reconstruction and computation of the FA value two transverse DTI scans were acquired (32 diffusion weighted volumes with different non-collinear diffusion directions with b-factor = 1000 s/mm^2 and 8 diffusion unweighted volumes with b-factor = 0 s/mm^2; parallel imaging SENSE factor 2.5; flip angle 90 degrees; 60 slices of 2.5 mm; no slice gap; 96×96 acquisition matrix; reconstruction matrix 128×128; FOV 240 mm; TE = 88 ms; TR = 9822 ms; no cardiac gating; total scan duration 296 s). Two DTI scans instead of one were acquired to increase the signal-to-noise ratio (SNR). The MTR was computed on the basis of a three-dimensional magnetization transfer scan comprising two volumes (transverse; 60 slices of 2.5 mm; 128×128 acquisition matrix; FOV 240 mm; flip angle 8 degrees; TE = 3.7 ms; TR = 37.5 ms; SENSE factor 2.5). For the second volume an additional off-resonance prepulse was applied (frequency offset 1100 Hz; 620 degrees; three-lobe sync-shaped; total scan duration 394 s).

Image processing

The two DTI scans were simultaneously realigned and corrected for possible gradient induced distortions (Andersson and Skare, 2002). A robust estimation of the diffusion tensors was obtained using M-estimators (Chang et al., 2005) to limit the influence of possible outliers. From the diffusion tensors the FA was computed (Basser and Pierpaoli, 1996). The FA represents the elongation of the diffusion profile and assumes values between 0 (isotropic diffusion) and 1 (pure one-dimensional diffusion) and is defined by:

$$FA = \sqrt{\frac{3}{2}\left(\frac{(\lambda_1 - \overline{\lambda})^2 + (\lambda_2 - \overline{\lambda})^2 + (\lambda_3 - \overline{\lambda})^2}{\lambda_1^2 + \lambda_2^2 + \lambda_3^2}\right)},$$

$$\overline{\lambda} = \frac{\lambda_1 + \lambda_2 + \lambda_3}{3}$$

where λ_1 represents the eigenvalue of the diffusion tensor's major eigenvector pointing in the direction parallel to the fiber bundle and λ_2 and λ_3 represent the eigenvalues of both minor eigenvectors pointing in the radial directions.

To compute the MTR, the second volume of the magnetization transfer scan was rigidly aligned with the first volume using the ANIMAL software package (Collins et al., 1995). Mutual information was used as a similarity metric. The MTR was computed on the image I_m with the magnetization prepulse and the image I_0 without magnetization prepulse using the equation: MTR = $(I_0-I_m)/I_0 \times 100\%$. The MTR is expressed as a percentage where 0% represents no signal reduction and 100% represents total signal reduction due to magnetization transfer.

For both the MTR (here the scan without the magnetization prepulse was used) and the T1-weighted scan the rigid transformations were determined that spatially aligned them with the diffusion unweighted (b = 0 s/mm^2) volume of the DTI scan using mutual information as similarity metric. For each subject a nonlinear transformation was computed using the ANIMAL software package that spatially aligns the subject's T1-weighted scan with a T1-weighted model brain (Collins et al., 1995; Hulshoff Pol et al., 2004). This nonlinear transformation was used at a later stage to warp the reconstructed tracts into model space.
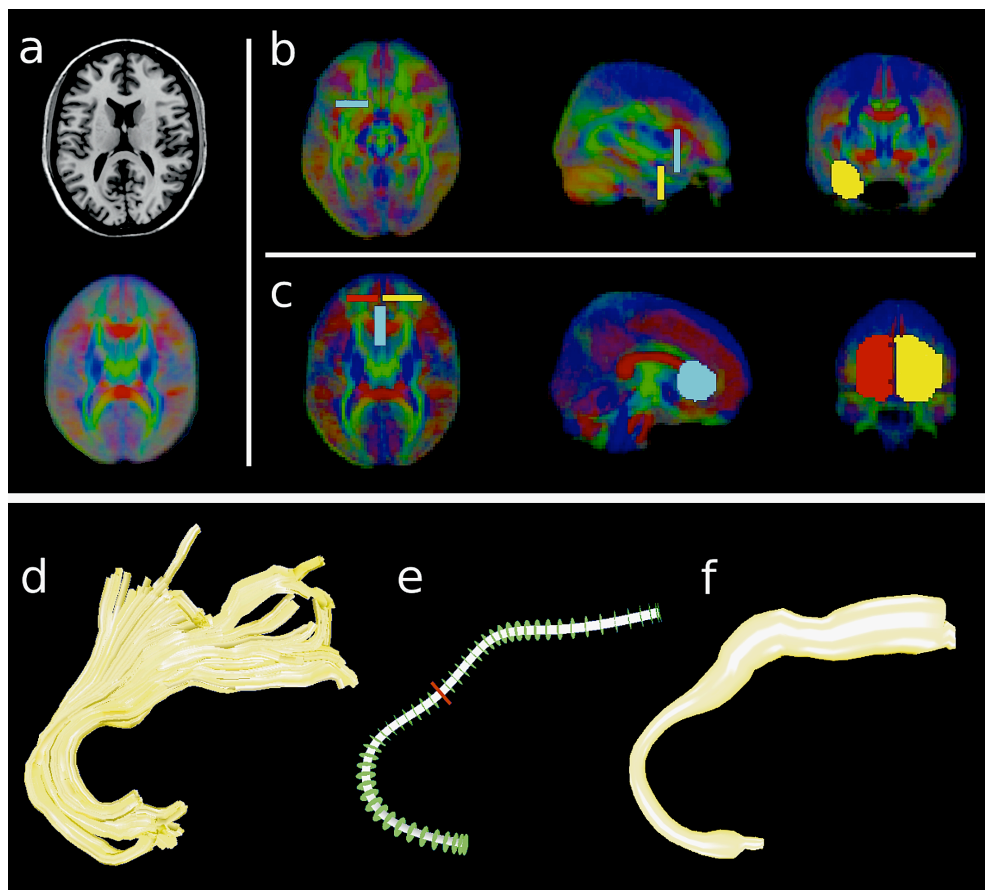
Figure 1. *(a) Transverse slice of the model brain (top) and the corresponding slice of the color-coded directional group map of the main direction of the tensors computed over all subjects (bottom). In this color-coded directional map, the left-right direction in model space is encoded with red, the anterior-posterior direction is encoded with green and blue encodes the inferior superior direction. (b) ROIs used for the selection of the tracts representing the left uncinate fasciculus. Note that the ROIs are overinclusive to ensure that they comprise the specific fiber bundles for all subjects. One ROI (light blue) was positioned in the prefrontal region and the other ROI (yellow) was positioned in the temporal region. The positioning of the ROIs for the right uncinate fasciculus was done in a similar fashion. (c) ROIs used for the selection of the genu of the corpus callosum. The first ROI (red) was placed in the left prefrontal region and the second ROI (yellow) was placed in the right prefrontal region. A third ROI (light blue) was added at the midline anterior to the ventricles to remove spurious tracts. Computation of the average fiber for the right uncinate fasciculus (d). The spline representation (e) of the fiber bundle was divided in 2 mm regular intervals starting from the centre of the spline (denoted by the red disk). (f) The radius of the average fiber denotes the variance of the cross-sectioned coordinates.*

Fiber tracking and fiber bundle selection

A multiple ROI fiber bundle selection approach (Wakana et al., 2004) was used to select the fiber tracts of interest where the reconstruction of the tracts was performed in native space and the selection and analysis of the tracts representing the genu and the left and right uncinate fasciculus was performed in model space.

In the first step, all possible tracts in brain were reconstructed individually in native space using the diffusion tensor images with an in-house implementation of the FACT algorithm (Mori et al., 1999) with the following parameter settings: 8 seed-points per voxel, minimum FA = 0.1, maximum angle = 45 degrees, maximum average angle with neighboring voxels = 45 degrees. Note that we used a relatively low FA threshold (0.1) to reduce the possibility that systematic group differences in the lower regime of FA values introduce a bias in the reconstruction of the tracts for the patients and controls. It was previously shown that a lowering of the FA threshold does not alter the findings of the tract-based analysis of FA values itself (Kanaan et al., 2006). Next, the points of the reconstructed tracts were labeled with the corresponding FA and MTR values after which the tracts were warped into the model space.

In the second step, the ROIs that were needed to select the tracts representing the genu and the left and right uncinate fasciculus were manually delineated on the model brain using an average map with color-coded directional information of the main direction of the tensors (**Figure 1a**). For the left and right uncinate fasciculus the ROIs were placed in the temporal and prefrontal regions (**Figure 1b**). For the genu two ROIs were placed, one in the left and one in the right prefrontal region (**Figure 1c**). To remove spurious tracts a third ROI was placed at the mid-line, anterior to the ventricles (the blue colored ROI in **Figure 1c**).

Instead of (nonlinear) transforming the ROIs defined in model space to each individual subject (native space) to select the genu and uncinate fasciuli tracts from the reconstructed tracts we transformed all reconstructed tracts from each subject into model space. The advantage is that tracts are geometric representations (polylines) that can be transformed without the need for interpolation. This is not the case when the ROIs are transformed from model to native space, as they are defined by voxels.

Computation of average fibers

We computed an average fiber (Gerig et al., 2004) in model space of the genu and left and right uncinate fasciculus of each individual subject. **Figure 1** shows an example of the computation of the average fiber for the right uncinate fasciculus. In short, first a spline representation of the shape of the original reconstructed fiber tracts (**Figure 1d**) was created. This spline was then divided in 2 mm regular intervals starting from the center of the spline. This center was defined by the geometric centre of the midpoint coordinates of all tracts of the fiber bundle perpendicularly projected onto the spline (the center is denoted by the red plane in **Figure 1e**). For each of these points we defined planes that are perpendicular to the spline. These planes (the position and direction of these planes are

denoted by the green disks in **Figure 1e**) were used to resample the original reconstructed fiber tracts (**Figure 1d**). Each plane was cross-sectioned with the original tracts of the fiber bundle. The cross-sectional coordinates were averaged to form the coordinate of the average fiber in this plane. For each separate plane the MTR and FA values of the cross-sectional coordinates of the original tracts were averaged to produce the average FA and MTR values for that plane. (Note that averaging was done over the reconstructed tracts in model space and did not incorporate resampling of the original voxel data.) The average cross-sectional coordinates of all the planes together with the corresponding average FA and MTR values then formed the average fiber. For each subject the final mean FA and mean MTR values were computed by averaging the FA and MTR values respectively of all points of an average fiber. These final mean FA and MTR values were computed for each subject and for each average fiber representation of the genu and the left and right uncinate fasciculus.

In addition we computed group average fibers over all individual average fibers for visualization purposes (**Figure 2**). These group average fibers allowed us to resample each individual average fiber to visualize the locality of possible group effects.

Statistical analysis

Mean MTR and mean FA measurements were analyzed using SPSS 15.0. Data were examined for outliers, extreme values and normality of distribution. No normality transformations were needed. Using general linear modeling, multiple univariate analyses of covariance were done with the mean MTR and mean FA of each separate average fiber as dependent variables, group (schizophrenia, healthy participants) entering as fixed factor, and age and gender as covariates. For dependent variables that differed significantly between groups Pearson product-moment correlations were computed for each group separately (or in patients only) between mean MTR and mean FA, between mean MTR/FA and level of education, and between mean MTR/FA and clinical variables. For the genu and the left and right uncinate fasciculus the correlations between age and mean FA, and age and mean MTR were computed separately for schizophrenia patients and healthy participants. A z-statistic was computed (after Fisher's Z-transform) to test if these correlations differ between groups.

Results

FA and MTR

A significant increase in mean MTR was found in the right uncinate fasciculus in patients with schizophrenia compared to healthy participants ($F(1,76) = 15.56$, $p = 0.0001$), which remained significant after Bonferroni correction for multiple comparisons (**Table 2**). No changes in mean FA were found in the right uncinate fasciculus in patients with schizophrenia compared to healthy participants ($F(1,76) = 0.76$, $p = 0.31$). No significant
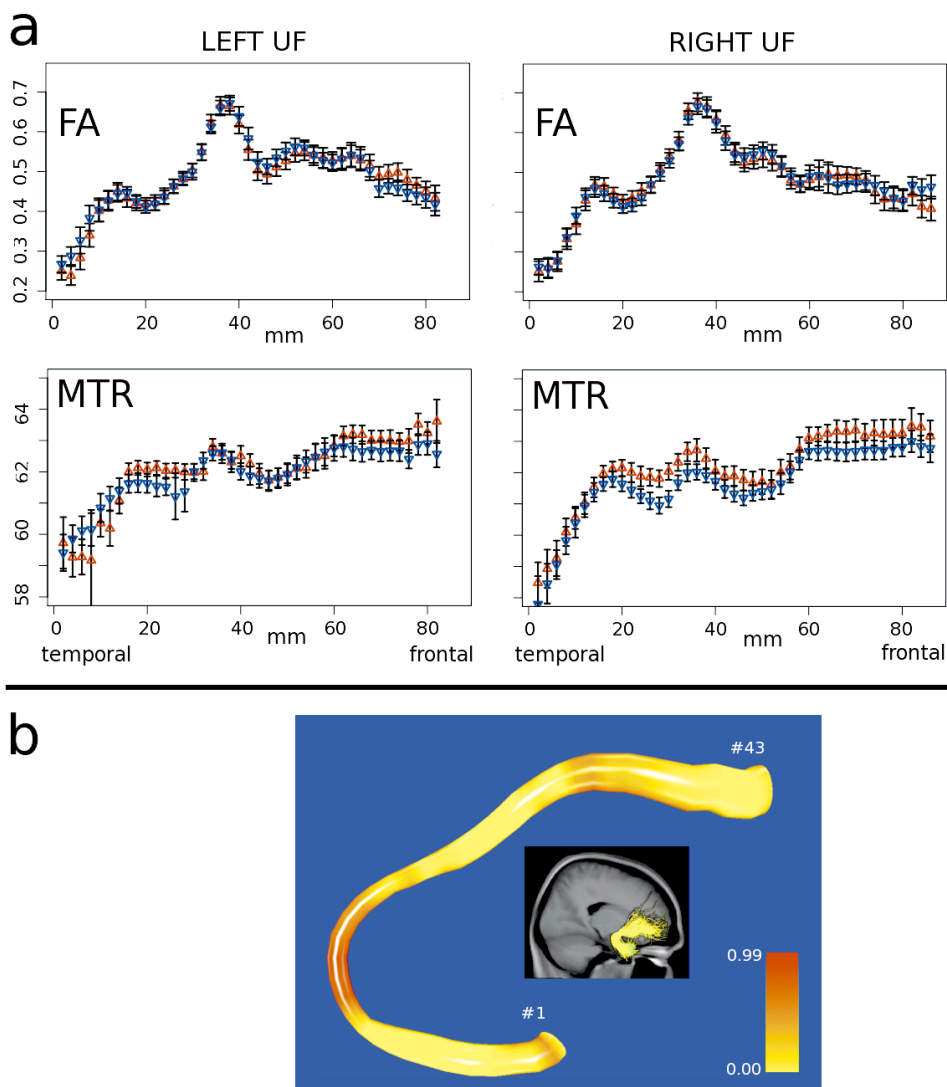
Figure 2. *(a) FA and MTR values in patients with schizophrenia (red triangle up) and healthy participants (blue triangle down) with a 2 mm interval along the left uncinate fasciculus (left) and right uncinate fasciculus (right). Note that the bars represent plus one and minus one standard error of the mean. For both uncinate fasciculi no differences in FA were found between patients and healthy participants. The MTR in the right uncinate fasciculus measured along the complete fiber was significantly higher in patients than in healthy participants. In contrast, comparison at a local level (i.e. per 2 mm interval) did not reveal significant differences in MTR or FA (after Bonferroni correction for multiple comparisons with the number of comparisons set to 43). (b) Local differences in MTR between patients and healthy participants along the average group fiber of the right uncinate fasciculus (more reddish color represents higher local MTR in patients).*

changes in mean FA or mean MTR in the left uncinate fasciculus or genu were found between groups. Excluding subjects with drug abuse or drug dependency from the sample did not alter the findings. To obtain additional information on whether the measured MTR group differences could be related to myelin concentrations, a post-hoc analysis was performed on the so-called transverse diffusivity. The transverse diffusivity is defined as the average of the two minor eigenvalues: $(\lambda_2 + \lambda_3)/2$, and shows a higher correlation with myelin concentrations than FA (Gulani et al., 2001). No significant group differences were found in transverse diffusivity for any of the fiber bundles.

A significant difference between correlations of mean FA with age ($z = -2.28$, $p = 0.02$) was found between schizophrenia patients and healthy participants in the left uncinate fasciculus (**Figure 3**). To determine whether possible medication effects could explain this finding an additional post-hoc analysis was performed where the cumulative medication was regressed out from the measured FA values in patients before computing the difference in correlations between age and FA between patients with schizophrenia and healthy comparison subjects. This resulted in a difference in correlations between age and FA in patients with schizophrenia compared to healthy participants for the left uncinate fasciculus that was significant at trend level ($z = -1.91$, $p = 0.056$). For the genu the difference ($z = -1.43$) found between schizophrenia patients and healthy participants did not reach significance.

Correlation analysis between mean MTR and mean FA in the genu, the left and right uncinate fasciculus in patients or in healthy participants did not reveal any significant correlations.

Table 2. FA and MTR values in individual tracts of patients with schizophrenia and healthy participants†

Tracts	Mean (sd) FA values			Mean (sd) MTR values		
	patients	healthy participants	F(1,76)	patients	healthy participants	F(1,76)
Genu of corpus callosum	0.58 (0.04)	0.57 (0.04)	1.45	61.96 (1.16)	61.95 (0.78)	0.00
Left uncinate fasciculus	0.46 (0.03)	0.47 (0.03)	0.83	61.43 (0.68)	61.29 (0.66)‡	0.06‡
Right uncinate fasciculus	0.47 (0.03)	0.46 (0.03)	0.76	61.77 (0.62)	61.17 (0.62)	15.56**

† Fiber-based comparisons between groups are corrected for age and gender. FA and MTR measurements are based on 39 patients and 40 control subjects for the right uncinate fasciculus because in one patient the right uncinate fasciculus could not be tracked
‡ after removal of one outlier from healthy participants (MTR values including outlier were 61.28 (0.90) for healthy participants and F(1,76) was 0.51)
** p<0.0001

Associations of the uncinate fasciculus with clinical symptoms, education, and antipsychotic medication

No significant correlations of mean FA and mean MTR in the right uncinate fasciculus were found with age at first symptoms, duration of illness, positive and negative and general symptoms of the PANSS, total CAN score, and antipsychotic medication intake at the time of the scan. There were no significant correlations (corrected for age, gender, and duration of illness) between cumulative antipsychotic medication use and mean MTR nor between cumulative antipsychotic medication use and mean FA, in the genu, the left or right uncinate fasciculus.

A significant correlation was found between mean MTR in the left uncinate fasciculus with extent of negative symptoms (r = -0.55, p < 0.0001), which remained significant after Bonferroni correction for multiple comparisons. There were no significant correlations of mean MTR and mean FA in the left uncinate fasciculus with any of the other clinical variables. No significant correlations were found between mean MTR in the genu and mean MTR in the right uncinate fasciculus with any of the clinical variables.

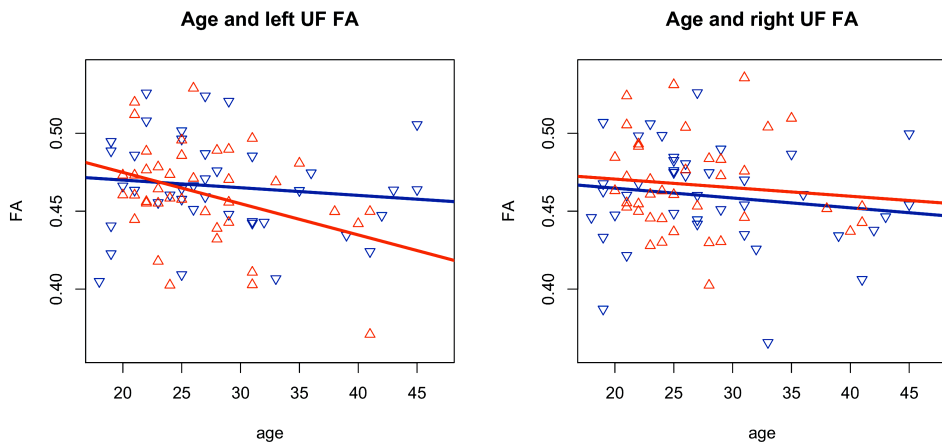**Figure 3.** *Correlation between age and FA for patients (-0.36, p = 0.02) (red triangle up) and healthy participants (-0.15, p = 0.36) (blue triangle down) in the left uncinate fasciculus (left figure) and right uncinate fasciculus (right figure).*

Discussion

In this study fractional anisotropy (FA) and the magnetization transfer ratio (MTR) were measured using DTI and MTR imaging along the uncinate fasciculi and the genu of the corpus callosum in the brains of 40 patients with schizophrenia and compared to those of 40 healthy participants. Our main finding is a significantly higher mean MTR of 1%, with no differences in mean FA, in the right uncinate fasciculus in the patients with schizophrenia compared to healthy participants. The MTR increases were found along large parts of the fiber (**Figure 2**), and were not limited to local changes of the tract which serves as an indication that these increases reflect schizophrenia-related changes that affect entire fiber tracts. In addition, a significant negative correlation between age and mean FA in the left uncinate fasciculus was found in schizophrenia patients but not in healthy participants.

The significant difference in correlations between age and FA in patients compared to healthy participants (**Figure 3**) suggests that in patients FA reductions become more apparent with age (mean age in patients was 26.8 years, range between 20-41 years). However, medication effects could be an important factor that should be taken into account when interpreting the results. The results of the additional post-hoc analysis where cumulative medication was taken into account indicate that, although medication effects may play a role, they cannot completely explain the measured differences in correlations between age and FA values. Our results support recent findings (Rosenberger et al., 2008) of a tract-based analysis that reported significant differences in correlations between age and FA in patients with schizophrenia compared to healthy participants for the left and right uncinate fasciculus combined. That fact that we found this correlation in the left and not the right uncinate fasciculus is in keeping with previous findings showing decreases in FA in the left but not in the right uncinate fasciculus of schizophrenia patients who were on average 43 years (Kubicki et al., 2002).

If the difference in correlation between age and FA predominantly relates to changes in myelination then one may expect to find similar differences in correlation between age and MTR because MTR appears to show a higher correlation with myelin levels than FA (Madler et al., 2008). We did not find a difference in correlations between age and MTR in patients compared to healthy participants. Therefore, our findings at least suggest that the differences in correlation between age and FA in the left uncinate fasciculus are not myelin-related.

Our finding of increased MTR in the right uncinate fasciculus suggests altered connectivity between the right frontal and temporal cortices in schizophrenia and may imply increased myelin concentrations in the largest fiber bundle connecting the medial frontal and temporal cortices. Since increased myelin concentrations along the fiber have been associated with more efficient axonal signal transport (Bozzali and Wrabetz, 2004), an increase in myelin in the uncinate fasciculus suggests an increased level of signal transfer between frontal and temporal cortices that could reflect a compensation mechanism for decreased interhemispheric connectivity in schizophrenia (Innocenti et al., 2003; Hulshoff Pol et al., 2004). The notion that increased MTR reflects increased myelination in the right hemisphere is in keeping with results of functional studies showing increased levels of

activation in the right frontal cortex in schizophrenia (Kircher et al., 2002; Sommer et al., 2003; Sommer et al., 2004; Weiss et al., 2006). In this context it should be noted that increased communication speed does not necessarily lead to increased communication efficiency (Laughlin and Sejnowski, 2003). The increased MTR could also result from compensation of aberrant brain functioning elsewhere in the brain, for instance in the left hemisphere (Mcguire et al., 1995). If, however, increases in myelin are responsible for the measured increase in MTR then one might also expect (to some extent) a reduction in transverse diffusivity, which is defined by the average of the minor eigenvalues of the diffusion tensor (Gulani et al., 2001). However, the post-hoc analysis of the transverse diffusivity in the right uncinate fasciculus did not reveal any group-related differences suggesting that our MTR findings may not (only) reflect increased myelination. An alternative explanation for the increased mean MTR in the right uncinate fasciculus in patients should therefore be considered, namely that it might reflect compromised connectivity not directly related to myelin.

MTR does not only depend on the macro-molecule concentration but also (amongst others) on T1-relaxation times of free water molecules (Henkelman et al., 2001). Prolonged T1-relaxation times in white matter do not reflect myelination, but a change in the free/bound water fraction. Interestingly, prolonged T1-relaxation times in the white matter of the right hemisphere have been reported for schizophrenia (Andreasen et al., 1991). Such an increase in T1 could effectively lead to an increase in MTR. Hence, an alternative explanation for the increased mean MTR in the right uncinate fasciculus in patients might involve changes in metabolites in white matter. Although we can only speculate, the increased mean MTR may be (indirectly) related to decreased glutamate and glutamine levels. In that case the increased mean MTR could be due to a prolonged T1 relaxation time reflecting an altered free/bound water fraction possibly related to changes in glial glutamate uptake (Coles, 2005; Kukley et al., 2007). MTR levels have been negatively correlated with glutamate and glutamine levels in white matter as measured with MR spectroscopy (Rovira et al., 2001; Wyckoff et al., 2003; Miese et al., 2006).

The average FA in the genu of the corpus callosum appeared lower in older patients as compared to older control participants, but this finding did not reach significance. In the genu of the corpus callosum a decrease in FA in patients compared to healthy participants was reported earlier (Kanaan et al., 2006; Price et al., 2007; Kubicki et al., 2008) although others did not find group differences in mean FA (Foong et al., 2000a; Jones et al., 2005). The absence of such a difference in FA in this study may be due to the relative low mean age (22.6 years) combined with an age-span of 18 - 45 years of our population as such FA reductions appear to become more pronounced with age (Friedman et al., 2008). Another possible explanation may be that the reported differences in FA are of more focal nature while tract-based analysis is most sensitive to changes to group differences that occur along large parts of the tracts. Both explanations may hold for the fact that in a previous study from our group (Hulshoff Pol et al., 2004) structural decreases in density were found using voxel-based morphometry in the genu for patients with schizophrenia (age span 16.3-67.9 years of age, mean age 36.6 years).

Although the measured difference in MTR in the right uncinate fasciculus was only in the order of one percent, we note that it is a robust and statistically highly significant finding as increased MTR values were consistently found in schizophrenia along large parts of the tract. Although small, these differences could, for instance, have large consequences for the synchronization of the signal because small alterations of signal transport along large parts of the fiber may cumulate into large alterations of various aspects of the signal transport (e.g. signaling speed, signal response function).

A limitation of this study is that the applied fiber-tracking algorithm requires sufficient directional information to successfully reconstruct the fibers. If, at a certain point, this information is not available (for instance due to crossings with other fibers) then the algorithm cannot reconstruct the complete fiber tract. Another limitation is that like DTI, MTR is an indirect measure of white matter microstructure. Since both FA and MTR are indirect measures and other factors than fiber orientation or macromolecule content may alter FA or MTR values as well, one should interpret group differences between FA or MTR values with caution (Laule et al., 2007).

In conclusion, a subtle but significant increase in mean MTR was found along large parts of the right uncinate fasciculus of schizophrenia patients. This increase appears to be specific for the right uncinate fasciculus and points towards increased connectivity between the medial frontal cortex and temporal pole provided that increases in myelin fully account for the increases found in mean MTR. Possibly, the right uncinate fasciculus may be part of a compensation mechanism for aberrant functioning of the left uncinate fasciculus, as suggested by the decreased FA in the older patients with schizophrenia. However, other mechanisms such as prolonged T1 relaxation times may also be implicated.

References

Andersson JL, Skare S (2002) A model-based method for retrospective correction of geometric distortions in diffusion-weighted EPI. Neuroimage 16:177-199.

Andreasen NC, Ehrhardt JC, Swayze VW, 2nd, Tyrrell G, Cohen G, Ku JS, Arndt S (1991) T1 and T2 relaxation times in schizophrenia as measured with magnetic resonance imaging. Schizophr Res 5:223-232.

Antosik-Biernacka A, Peuskens H, De Hert M, Peuskens J, Sunaert S, Van Hecke P, Goraj B (2006) Magnetization transfer imaging in chronic schizophrenia. Med Sci Monit 12:MT17-21.

Bagary MS, Symms MR, Barker GJ, Mutsatsa SH, Joyce EM, Ron MA (2003) Gray and white matter brain abnormalities in first-episode schizophrenia inferred from magnetization transfer imaging. Arch Gen Psychiatry 60:779-788.

Barkovich AJ (2000) Concepts of myelin and myelination in neuroradiology. AJNR Am J Neuroradiol 21:1099-1109.

Basser PJ, Pierpaoli C (1996) Microstructural and physiological features of tissues elucidated by quantitative-diffusion-tensor MRI. J Magn Reson B 111:209-219.

Beaulieu C (2002) The basis of anisotropic water diffusion in the nervous system - a technical review. NMR Biomed 15:435-455.

Bleuler E (1911) Dementia Praecox or the Group of Schizophrenias. NewYork: International Universities Press.

Bozzali M, Wrabetz L (2004) Axonal signals and oligodendrocyte differentiation. Neurochemical Research 29:979-988.

Chang LC, Jones DK, Pierpaoli C (2005) RESTORE: robust estimation of tensors by outlier rejection. Magn Reson Med 53:1088-1095.

Coles JA, Deitmer JW (2005) Extracellular potassium and pH: homeostasis and signaling. In: Neuroglia (Kettenmann H, Ransom BR, ed). Oxford: Oxford University Press.

Collins DL, Holmes CJ, Peters TM, Evans AC (1995) Automatic 3-D model-based neuroanatomical segmentation. Human Brain Mapping 3:190-208.

Davis KL, Stewart DG, Friedman JI, Buchsbaum M, Harvey PD, Hof PR, Buxbaum J, Haroutunian V (2003) White matter changes in schizophrenia - Evidence for myelin-related dysfunction. Archives of General Psychiatry 60:443-456.

Foong J, Maier M, Clark CA, Barker GJ, Miller DH, Ron MA (2000a) Neuropathological abnormalities of the corpus callosum in schizophrenia: a diffusion tensor imaging study. J Neurol Neurosurg Psychiatry 68:242-244.

Foong J, Maier M, Barker GJ, Brocklehurst S, Miller DH, Ron MA (2000b) In vivo investigation of white matter pathology in schizophrenia with magnetisation transfer imaging. J Neurol Neurosurg Psychiatry 68:70-74.

Friedman JI, Tang C, Carpenter D, Buchsbaum M, Schmeidler J, Flanagan L, Golembo S, Kanellopoulou I, Ng J, Hof PR, Harvey PD, Tsopelas ND, Stewart D, Davis KL (2008) Diffusion Tensor Imaging Findings in First-Episode and Chronic Schizophrenia Patients. Am J Psychiatry. 165:1024-1032.

Gerig G, Gouttard S, Corouge I (2004) Analysis of brain white matter via fiber tract modeling. Conf Proc IEEE Eng Med Biol Soc 6:4421-4424.

Gulani V, Webb AG, Duncan ID, Lauterbur PC (2001) Apparent diffusion tensor measurements in myelin-deficient rat spinal cords. Magn Reson Med 45:191-195.

Henkelman RM, Stanisz GJ, Graham SJ (2001) Magnetization transfer in MRI: a review. NMR Biomed 14:57-64.

Honea R, Crow TJ, Passingham D, Mackay CE (2005) Regional deficits in brain volume in schizophrenia: a meta-analysis of voxel-based morphometry studies. Am J Psychiatry 162:2233-2245.

Hulshoff Pol HE, Schnack HG, Mandl RC, Cahn W, Collins DL, Evans AC, Kahn RS (2004) Focal white matter density changes in schizophrenia: reduced inter-hemispheric connectivity. Neuroimage 21:27-35.

Hulshoff Pol HE, Schnack HG, Mandl RC, van Haren NE, Koning H, Collins DL, Evans AC, Kahn RS (2001) Focal gray matter density changes in schizophrenia. Arch Gen Psychiatry 58:1118-1125.

Innocenti GM, Ansermet F, Parnas J (2003) Schizophrenia, neurodevelopment and corpus callosum. Molecular Psychiatry 8:261-274.

Jones DK (2008) Studying connections in the living human brain with diffusion MRI. Cortex 44:936-952.

Jones DK, Catani M, Pierpaoli C, Reeves SJ, Shergill SS, O'Sullivan M, Maguire P, Horsfield MA, Simmons A, Williams SC, Howard RJ (2005) A diffusion tensor magnetic resonance imaging study of frontal cortex connections in very-late-onset schizophrenia-like psychosis. Am J Geriatr Psychiatry 13:1092-1099.

Jones DK, Catani M, Pierpaoli C, Reeves SJC, Shergill SS, O'Sullivan M, Golesworthy P, McGuire P, Horsfield MA, Simmons A, Williams SCR, Howard RJ (2006) Age effects on diffusion tensor magnetic resonance imaging tractography measures of frontal cortex connections in schizophrenia. Human Brain Mapping 27:230-238.

Kanaan RA, Kim JS, Kaufmann WE, Pearlson GD, Barker GJ, McGuire PK (2005) Diffusion tensor imaging in schizophrenia. Biol Psychiatry 58:921-929.

Kanaan RA, Shergill SS, Barker GJ, Catani M, Ng VW, Howard R, McGuire PK, Jones DK (2006) Tract-specific anisotropy measurements in diffusion tensor imaging. Psychiatry Res 146:73-82.

Kircher TT, Liddle PF, Brammer MJ, Williams SC, Murray RM, McGuire PK (2002) Reversed lateralization of temporal activation during speech production in thought disordered patients with schizophrenia. Psychol Med 32:439-449.

Konrad A, Winterer G (2008) Disturbed structural connectivity in schizophrenia - Primary factor in pathology or epiphenomenon? Schizophrenia Bulletin 34:72-92.

Kraepelin E (1919) Dementia Praecox and Paraphrenia., 8 Edition. Edinburgh, Livingstone.

Kubicki M, McCarley R, Westin CF, Park HJ, Maier S, Kikinis R, Jolesz FA, Shenton ME (2007) A review of diffusion tensor imaging studies in schizophrenia. J Psychiatr Res 41:15-30.

Kubicki M, Styner M, Bouix S, Gerig G, Markant D, Smith K, Kikinis R, McCarley RW, Shenton ME (2008) Reduced interhemispheric connectivity in schizophrenia-tractography based segmentation of the corpus callosum. Schizophr Res. 106:125-131.

Kubicki M, Westin CF, Maier SE, Frumin M, Nestor PG, Salisbury DF, Kikinis R, Jolesz FA, McCarley RW, Shenton ME (2002) Uncinate fasciculus findings in schizophrenia: a magnetic resonance diffusion tensor imaging study. Am J Psychiatry 159:813-820.

Kubicki M, Park H, Westin CF, Nestor PG, Mulkern RV, Maier SE, Niznikiewicz M, Connor EE, Levitt JJ, Frumin M, Kikinis R, Jolesz FA, McCarley RW, Shenton ME (2005) DTI and MTR abnormalities in schizophrenia: analysis of white matter integrity. Neuroimage 26:1109-1118.

Kukley M, Capetillo-Zarate E, Dietrich D (2007) Vesicular glutamate release from axons in white matter. Nature Neuroscience 10:311-320.

Laughlin SB, Sejnowski TJ (2003) Communication in neuronal networks. Science 301:1870-1874.

Laule C, Vavasour IM, Kolind SH, Li DKB, Traboulsee TL, Moore GRW, MacKay AL (2007) Magnetic resonance imaging of myelin. Neurotherapeutics 4:460-484.

Lin X, Tench CR, Morgan PS, Constantinescu CS. (2008): Use of combined conventional and quantitative MRI to quantify pathology related to cognitive impairment in multiple sclerosis. J Neurol Neurosurg Psychiatry 79(4):437-41.

Madler B, Drabycz SA, Kolind SH, Whittall KP, Mackay AL (2008) Is diffusion anisotropy an accurate monitor of myelination? Correlation of multicomponent T(2) relaxation and diffusion tensor anisotropy in human brain. Magn Reson Imaging 26:874-888.

Mcguire PK, Silbersweig DA, Wright I, Murray RM, David AS, Frackowiak RSJ, Frith CD (1995) Abnormal Monitoring of Inner Speech - a Physiological-Basis for Auditory Hallucinations. Lancet 346:596-600.

Miese F, Kircheis G, Wittsack HJ, Wenserski F, Hemker J, Modder U, Haussinger D, Cohnen M (2006) 1H-MR spectroscopy, magnetization transfer, and diffusion-weighted imaging in alcoholic and nonalcoholic patients with cirrhosis with hepatic encephalopathy. AJNR Am J Neuroradiol 27:1019-1026.

Mori S, van Zijl PC (2002) Fiber tracking: principles and strategies - a technical review. NMR Biomed 15:468-480.

Mori S, Crain BJ, Chacko VP, van Zijl PC (1999) Three-dimensional tracking of axonal projections in the brain by magnetic resonance imaging. Ann Neurol 45:265-269.

Mori T, Ohnishi T, Hashimoto R, Nemoto K, Moriguchi Y, Noguchi H, Nakabayashi T, Hori H, Harada S, Saitoh O, Matsuda H, Kunugi H (2007) Progressive changes of white matter integrity in schizophrenia revealed by diffusion tensor imaging. Psychiatry Res 154:133-145.

Price G, Cercignani M, Parker GJ, Altmann DR, Barnes TR, Barker GJ, Joyce EM, Ron MA (2007) Abnormal brain connectivity in first-episode psychosis: a diffusion MRI tractography study of the corpus callosum. Neuroimage 35:458-466.

Rosenberger G, Kubicki M, Nestor PG, Connor E, Bushell GB, Markant D, Niznikiewicz M, Westin CF, Kikinis R, A JS, McCarley RW, Shenton ME (2008) Age-related deficits in fronto-temporal connections in schizophrenia: A diffusion tensor imaging study. Schizophr Res. 102:181-188.

Rovira A, Grive E, Pedraza S, Rovira A, Alonso J (2001) Magnetization transfer ratio values and proton MR spectroscopy of normal-appearing cerebral white matter in patients with liver cirrhosis. AJNR Am J Neuroradiol 22:1137-1142.

Sommer IE, Ramsey NF, Mandl RC, Kahn RS (2003) Language lateralization in female patients with schizophrenia: an fMRI study. Schizophr Res 60:183-190.

Sommer IE, Ramsey NF, Mandl RC, van Oel CJ, Kahn RS (2004) Language activation in monozygotic twins discordant for schizophrenia. Br J Psychiatry 184:128-135.

van Buchem MA, McGowan JC, Grossman RI (1999) Magnetization transfer histogram methodology: its clinical and neuropsychological correlates. Neurology 53:S23-28.

van den Heuvel MP, Mandl RCW, Luigjes J, Hulshoff Pol HE (2008) Microstructural organization of the cingulum tract and the level of default mode functional connectivity. Journal of Neuroscience 28:10844-10851.

Wakana S, Jiang HY, Nagae-Poetscher LM, van Zijl PCM, Mori S (2004) Fiber tract-based atlas of human white matter anatomy. Radiology 230:77-87.

Weiss EM, Hofer A, Golaszewski S, Siedentopf C, Felber S, Fleischhacker WW (2006) Language lateralization in unmedicated patients during an acute episode of schizophrenia: a functional MRI study. Psychiatry Res 146:185-190.

Wolff SD, Balaban RS (1994) Magnetization transfer imaging: practical aspects and clinical applications. Radiology 192:593-599.

Wright IC, Rabe-Hesketh S, Woodruff PW, David AS, Murray RM, Bullmore ET (2000) Meta-analysis of regional brain volumes in schizophrenia. Am J Psychiatry 157:16-25.

Wright P, Nimgaonkar VL, Donaldson PT, Murray RM (2001) Schizophrenia and HLA: a review. Schizophr Res 47:1-12.

Wyckoff N, Kumar A, Gupta RC, Alger J, Hwang S, Thomas MA (2003) Magnetization transfer imaging and magnetic resonance spectroscopy of normal-appearing white matter in late-life major depression. Journal of Magnetic Resonance Imaging 18:537-543.

Chapter 3

Microstructural organization of the cingulum tract and the level of default mode functional connectivity

Martijn van den Heuvel, René Mandl, Judith Luigjes
and Hilleke Hulshoff Pol

Abstract

The default mode network is a functionally connected network of brain regions that show highly synchronized intrinsic neuronal activation during rest. However, less is known about the structural connections of this network, which could play an important role in the observed functional connectivity patterns. In this study, we examined the microstructural organization of the cingulum tract in relation to the level of resting-state default mode functional synchronization. Resting-state functional Magnetic Resonance Imaging and Diffusion Tensor Imaging data of 45 healthy subjects were acquired on a 3 Tesla scanner. Both structural and functional connectivity of the default mode network were examined. In all subjects, the cingulum tract was identified from the total collection of reconstructed tracts to interconnect the precuneus / posterior cingulate cortex and medial frontal cortex, key regions of the default mode network. A significant positive correlation was found between the average fractional anisotropy value of the cingulum tract and the level of functional connectivity between the precuneus / posterior cingulate cortex and medial frontal cortex. Our results suggest a direct relationship between the structural and functional connectivity measures of the default mode network and contribute to the understanding of default mode network connectivity.

Multiple cortical and sub-cortical regions show coherent time-series during rest and are suggested to form resting-state networks (Damoiseaux et al., 2006; Van den Heuvel et al., 2008). In particular, a set of regions called the default mode network (Raichle et al., 2001; Greicius et al., 2003) has been reported to show high levels of intrinsic neuronal activity during rest (Gusnard et al., 2001; Greicius et al., 2003; Raichle and Snyder, 2007). The most often reported and most influential regions of this network are the precuneus / posterior cingulate cortex (PCC), involved in responding to salient stimuli in the world around us (Gusnard et al., 2001; Corbetta et al., 2000) and medial frontal cortex (MFC), involved in emotional processing and the monitoring of one's mental state (Northoff and Bermpohl, 2004; Northoff et al., 2006; Schmitz and Johnson, 2007). Neuronal activation patterns of the PCC and MFC have been reported to be highly coherent during rest (Greicius et al., 2003; Fox and Raichle, 2007), indicating a high level of functional connectivity (Biswal et al., 1995) and ongoing communication between the PCC and MFC during rest. This supports the idea of the default mode network as a cohesive brain network that may be involved in important functions of human cognition (Gusnard et al., 2001; Greicius et al., 2003; Mason et al., 2007).

However, less is known about the structural connections of the default mode network. The cingulum bundle is a collection of white matter tracts that connect regions of the frontal lobe with the precuneus, posterior cingulate cortex, hippocampus and parahippocampus (Wakana et al., 2004; Schmahmann et al., 2007; Lawes et al., 2008). These termination regions show large overlap with key regions of the default mode network. Indeed, Greicius et al. recently reported that the PCC and MFC regions of the default mode network are connected by the cingulum tract (Greicius et al., 2009). These results suggest an anatomical basis of the default mode network and raise the question about a possible association between the structural and functional connectivity measures of the default mode network. We hypothesize that an association exists between the microstructural organization of the cingulum tract and the level of default mode functional connectivity. Examining this association could add to the understanding of default mode network connectivity. In this study, resting-state functional Magnetic Resonance Imaging (fMRI) recordings and Diffusion Tensor Imaging (DTI) scans were acquired on a 3 Tesla MR scanner in 45 subjects. The unique level of functional connectivity between the PCC and MFC regions of the default mode network was computed as the partial correlation between their resting-state time-series. Cingulum tracts interconnecting the PCC and MFC were reconstructed using the DTI scans and fractional anisotropy (FA) values of these tracts were calculated as an indication of white matter integrity (Kim et al., 2007). Over the group of subjects, the mean FA value of the cingulum tract was correlated with the level of functional connectivity between the PCC and MFC regions of the default mode network.

Materials and Methods

Subjects

45 healthy subjects (mean age: 24.8 years, SD: 4.8, 25 male, 20 female) participated in this study after giving written consent as approved by the medical ethics committee for research in humans (METC) of the University Medical Centre Utrecht, the Netherlands. All subjects underwent a 45 minute scanning session. During the resting-state recordings, subjects were instructed to relax, keep their eyes closed without falling asleep and to think of nothing in particular.

Image acquisition

Resting-state functional Magnetic Resonance Imaging (resting-state fMRI) and Diffusion Tensor Imaging (DTI) data were acquired on a 3 Tesla Philips Achieva Medical Scanner (Philips Medical Systems, Best, The Netherlands) at the University Medical Center Utrecht, The Netherlands. During the rest experiment, resting-state blood oxygenation level dependent (BOLD) signals were recorded during a period of 8 minutes using a fast fMRI sequence (3D PRESTOSENSE p/s-reduction 2/2 (Golay et al., 2000; Neggers et al., 2008); TR/TE 22 ms/32 ms using shifted echo, flip-angle 9 degrees; dynamic scan time 0.5 sec, 1000 timeframes; FOV 256×256 mm, 4 mm isotropic voxel size, 32 slice volume covering the whole brain). Directly after the fMRI time-series an additional functional scan was acquired with identical parameters, but with a high anatomical contrast due to an increased flip-angle of 25 degrees. This additional high contrast functional scan was acquired to improve the co-registration of the functional images with the anatomical image. In the same scanning session DTI scans were acquired (DTI-MR using parallel imaging SENSE p-reduction 3; high angular gradient set of 30 weighted directions (Jones, 2004; Jones et al., 1999), TR = 7035 ms, TE = 68 ms, EPI factor 35; FOV 240×240 mm, 2 mm isotropic voxel size, 75 slices covering the whole brain). In total, 2 DTI sets of 30 weighted diffusion scans with different weighting directions (b = 1000 s/mm^2) and 2 unweighted B0 scans (b = 0 s/mm^2) were acquired. The second DTI set was acquired with a reversed k-space read-out direction (anterior direction) in comparison to the first set (posterior direction) (Andersson et al., 2003). In addition, a T1-weighted image (3D FFE using parallel imaging; TR/TE 10 ms/4.6 ms; FOV 240×240 mm, 200 slices, 0.75 mm isotropic voxel size) was acquired for anatomical reference of the functional time-series and structural DTI scans.

Image preprocessing

fMRI preprocessing was performed with the SPM2 software package (http://www.fil.ion.ucl.ac.uk). The functional scans were corrected for small head movements by realigning all scans to the last functional scan. Both the T1-weighted image and the functional scans were co-registered with the high contrast functional scan, to enable spatial

overlap between the functional time-series and the T1-weighted image. Cortical voxels were selected based on a cortical segmentation of the T1-weighted image. Cortical segmentation was performed with the widely used and freely available Freesurfer software package (http://surfer.nmr.mgh.harvard.edu/). The T1-weighted image was normalized to match the MNI 305 T1 template brain (Collins et al., 1994). Next, the fMRI time-series and cortical segmentation map were normalized to standard space by using the normalization parameters of the T1-weighted image. The normalized cortical segmentation map was resliced to the spatial resolution of the fMRI images.

DTI preprocessing was performed with the diffusion toolbox of Andersson et al. (Andersson and Skare, 2002) and in-house developed software. First, susceptibility distortions, often reported in single-shot EPI images, were corrected by combining the 2 sets of DTI images. A field distortion map was computed based on the two unweighted B0 images and applied to the weighted images (Andersson et al., 2003), resulting in a single set of corrected scans, which were realigned with the corrected B0 image (Andersson and Skare, 2002). For each voxel, the main diffusion direction was calculated by fitting a tensor to the diffusion scans using a robust tensor fit method based on an M-estimator (Chang et al., 2005). The Fiber Assignment by Continuous Tracking (FACT) algorithm (Mori et al., 1999; Mori and van Zijl, 2002) was used to reconstruct the white matter tracts of the brain. In each voxel, 27 fiber seeds were started. Fiber tracking was stopped when the fiber touched a voxel with a FA value lower than 0.1 or when it had an average angle change between the neighboring eigenvectors of more than 45 degrees or when the trajectory of the traced fiber exceeded the brain. Only fibers with a minimum length of 50 mm were considered. Next, the B0 image was registered (linear) to the anatomical image and normalized using the normalization parameters of the T1-weighted image, to overlap with the normalized resting-state fMRI time-series.

Selection of default mode network

Resting-state networks (RSNs) across the group of subjects were selected with the voxel-based Normalized Cut Group Clustering approach, described in detail elsewhere (Van den Heuvel et al., 2008). This method involves the clustering of voxels that show a high level of functional connectivity consistently over a group of subjects. In brief, for each individual dataset, the resting-state fMRI dataset was represented as a network that was constructed out of all cortical voxels with weighted connections between all voxel pairs. Cortical voxels were identified from the individual cortical segmentation map. The weights of the connections between the voxels in the network were computed as the zero-lag temporal correlation between the filtered resting-state time-series. The resulting connectivity graph was then clustered, resulting in the grouping of voxels that showed a high level of functional connectivity. Next, the overlap of the individual voxel-wise clustering results defined a group graph, with weighted connections between the cortical voxels reflecting the level of consistency of the clustering results over the group of subjects. The voxels in the group graph were selected from the group cortical segmentation map, which resulted from overlapping the individual cortical segmentation maps. The group graph was clustered,

clustering voxels into resting-state networks that showed a high level of functional connectivity consistently over the group of subjects. Using the Normalized Cut Group Clustering approach, the number of RSN clusters are defined as an optimal clustering fit of the group graph, which is defined as a clustering fit that minimizes the total cost of partitioning the graph into separate networks (Van den Heuvel et al., 2008). This optimization procedure resulted in an optimal clustering fit of the data in 7 RSNs (**Figure 1**). Group clustering revealed the extensively described default mode network (Raichle et al., 2001; Greicius et al., 2003), overlapping the PCC (Brodmann Area (BA) 23/31), bilateral middle/superior temporal gyrus (BA 21/39) and inferior/superior parietal cortex (SPC) (BA 39/40), and frontal cortices, including both superior frontal cortex (BA 8/9) and MFC (BA 10/11). The other clustered RSNs included two lateralized frontal-parietal networks, a motor/sensory/auditory network, a network consisting of insula and anterior cingulate cortex and two singular networks that overlapped the medial frontal gyrus and a posterior part of BA 7 (**Figure 1**). The clustered RSNs showed resemblance with the resting-state networks found by previous studies reporting on the group-wise selection of resting-state networks (Beckmann et al., 2005; Damoiseaux et al., 2006; De Luca et al., 2006; Van den Heuvel et al., 2008).

Functional connectivity

The PCC and MFC were selected from the default mode network clustermap (**Figure 1a**). For each of the individual datasets, the functional connectivity between the PCC and MFC was calculated as follows. The fMRI time-series of all voxels were filtered using a bandpass filter, extracting the low resting-state frequencies of interest (0.01 - 0.08 Hz) (Achard et al., 2006; Biswal et al., 1995; Biswal et al., 1997; Cordes et al., 2001). The representative time-series of the PCC and MFC were obtained by averaging the time-series of the voxels within these regions. Next, the level of functional connectivity between the PCC and MFC regions was computed as a partial correlation between their filtered time-series, controlling for third-party influences of other RSN regions (Stam, 2004; Sun et al., 2004; Salvador et al. 2005; Achard et al., 2006; Liu et al., 2008). Besides the default mode network, the group clustering revealed 6 other resting-state networks, which in total consisted of 13 anatomically separate regions. For each of these 13 other RSN regions and the two bilateral SPC regions of the default mode network, representative time-series were computed by averaging the time-series of all voxels within this particular RSN region (Liu et al., 2008). The partial correlation between the time-series of the PCC and MFC was computed by correlating the resting-state time-series of the PCC and MFC, factoring out the contributions of the time-series of the other 13 RSN regions and the two bilateral superior parietal cortex (SPC) regions of the default mode network (**Figure 1a**). This procedure was similar to the methodology used in previous studies examining functional connectivity between brain regions (Achard et al., 2006; Liu et al., 2008; Salvador et al.,
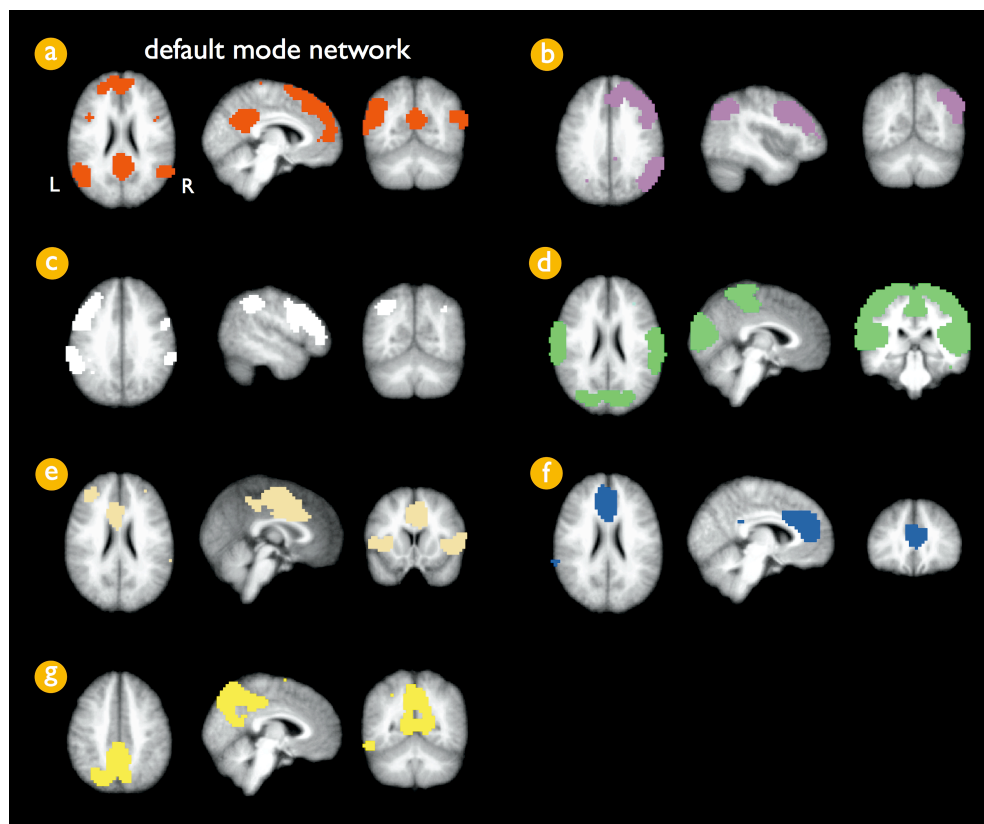
Figure 1. Group clustered resting-state networks. Normalized cut group clustering of the resting-state time series of the group of 45 subjects revealed seven resting-state networks. Cluster a (a) shows the default mode network, consisting of frontal regions, including superior frontal gyrus (BA 8/9) and medial frontal gyrus (BA 10/11) and precuneus/posterior cingulate cortex (BA 23/31) and bilateral regions overlapping middle/superior temporal tyrus (BA 21/39) and inferior/superior parietal cortex (BA 39/40). Clusters b and c (b, c) show lateralized frontoparietal networks in the right and left hemisphere, overlapping regions in the superior parietal lobule, inferior parietal lobule, supramarginal gyrus (BA 40), and medial and superior frontal gyrus (BA 8/9). Cluster d (d) shows a combined network of both visual and motor regions, consisting of medial, lateral, and superior occipital gyrus and peristriate regions (BA 17/18/19), precentral (BA 4), and postcentral gyrus (BA 3/1/2). Cluster e (e) shows a network of cingulate gyrus (BA 24) and bilateral insular and superior temporal gyrus (BA 13/22), a network that is also commonly found in resting-state studies. Cluster f (f) involves a singular region consisting of a medial part of the medial frontal gyrus (BA 9) and cingulate gyrus (BA 32). Cluster g (g) involves a singular region consisting of a posterior part of BA 7. L, Left; R, right.

 2005). In these studies the brain was partitioned into a fixed number of regions based on a predefined anatomical template, normally around 90 regions and partial correlations between the time-series of each pair of regions was computed by factoring out the contributions of the time-series of the other 88 regions. In our study, the third-party regions were defined as the brain regions of the other RSNs (**Figure 1**) that resulted from the group clustering. The use of a partial correlation ensured the examination of the specific level of functional connectivity between the PCC and MFC (Achard et al., 2006; Liu et al., 2008; Salvador et al., 2005). To verify this specificity, the straight correlation coefficient (i.e. non-partialized correlation) between the filtered time-series of the PCC and MFC was computed, correlating the fMRI time-series of the PCC and MFC, without factoring out the contributions of the other RSN regions. In addition, to examine the level of overall default mode functional connectivity, the time-series of the PCC and MFC regions were correlated, factoring out the third-party effects of the other RSN regions (**Figure 1**, network b-g), but not the effects of the two SPC regions of the default mode network (**Figure 1**). Finally, a Fisher's r-to-z transformation was used to improve the normality of the partial correlation coefficients (Fox and Raichle, 2007; Salvador et al., 2005). The partial correlation Fisher's z coefficient reflected the unique level of functional connectivity between the PCC and MFC of the default mode network (Achard et al., 2006; Salvador et al., 2005).
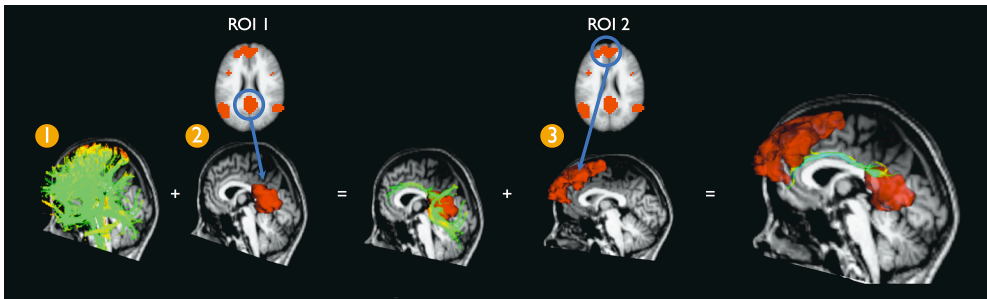

Figure 2. *Selection of tracts that interconnect the regions of the default mode network. In each individual dataset, interconnecting tracts between the PCC and MFC of the default mode network were selected as follows. First, the FACT algorithm was used to trace the total collection of tracts in the human brain. 27 fiber seeds were started in all voxels of the brain, reconstructing the total collection of fibers (step 1). Second, the PCC was selected from the default mode network clustermap (Figure 1a). Fibers that touched the PCC region were selected (step 2). Third, the MFC was selected from the default mode network clustermap and from the resulting fibers of step 2 the fibers that touched the MFC regions were selected (step 3). This procedure resulted in the fibers that touched both regions of interest, selecting the fibers that interconnect the PCC and MFC of the default mode network.*

Selection of interconnecting tracts

It was verified for each individual dataset whether or not the two PCC and MFC regions of interest were interconnected with white matter tracts. First, to overlap the regions of interest with the individual structural DTI data, the default mode network clustermap was registered to the individual unweighted B0 image (using the reversed normalization and registration parameters generated in the matching of B0 and T1-weighted images). Next, from the total collection of reconstructed tracts, the tracts that touched both the PCC and the MFC were selected, using a three step procedure (**Figure 2**). From the total collection of reconstructed tracts (**Figure 2**, step 1), the tracts that touched the PCC were selected (**Figure 2**, step 2). Next, from the resulting tracts, the tracts that touched the MFC were selected (**Figure 2**, step 3). To enable group comparison, the resulting tracts were normalized using the registration and normalization parameters of the B0 image. The mean FA value of the resulting tracts, an estimate of the microstructural organization within these white matter tracts (Beaulieu, 2002), was calculated by averaging the FA values of the points along the selected left and right hemispheric tracts. This procedure was repeated for each individual dataset, obtaining a mean FA value for the connecting tracts in each subject. In addition, for each individual DTI dataset the mean FA value of the total collection of fibers in the brain was computed.

Association between structural and functional connectivity

The association between the level of structural connectivity and the level of functional connectivity of the default mode network was computed by correlating the mean FA value of the connecting tracts with the unique level of functional connectivity (Fisher's z score) between the PCC and MFC over the group of subjects, correcting for age. Possible age effects were regressed out of the FA and functional connectivity measures separately, as recent studies have demonstrated that normal aging is associated with both decreased microstructural organization (i.e. lower FA values) of the cingulum tract (Andrews-Hanna et al., 2007) and decreased levels of default mode functional connectivity (Andrews-Hanna et al., 2007; Damoiseaux et al., 2007). In addition, an alternative approach to correct for aging effects was examined by taking age as a covariate in assessing the correlation between default mode functional connectivity and mean cingulum FA values. Furthermore, to examine whether the association between mean FA and default mode functional connectivity was specific to the interconnecting cingulum tracts or instead was related to a more global effect, two additional analyses were performed. One, the level of functional connectivity between the PCC and MFC regions was correlated with the mean FA value of the total collection of reconstructed fibers in the brain. Two, the functional connectivity levels of the other clustered RSNs were correlated with the mean FA value of the cingulum tract. Group clustering revealed 6 additional RSNs, with 4 RSNs consisting of two or more anatomically separate cortical regions (**Figure 1**). In total, these 4 RSNs consisted of 11 regions. Functional connectivity measures of these RSNs were computed in a similar manner as the computation of the level of functional connectivity of the default mode

network. The level of functional connectivity was defined as the partial correlation between the filtered resting-state time-series of the regions of the selected RSN, correcting for third-party effects of the time-series of the regions of the other clustered RSNs. The resulting partial correlation coefficient was correlated with the mean FA value of the cingulum, after controlling for age on both measures.

Results

Normalized Cut Group Clustering of the resting-state fMRI data revealed 7 resting-state networks, including the often reported default mode network (**Figure 1**, cluster a). The level of overall default mode connectivity (i.e. the correlation between the PCC and MFC, factoring out the effects of the other RSNs, but not the two SPC regions) was significantly nonzero over the group of subjects (mean: 0.51, SD: 0.23, $p < 0.001$). The level of unique default mode functional connectivity between the PCC and MFC was found to be significant non-zero over the group of subjects (mean: 0.19, SD: 0.24, $p < 0.001$). All 45 subjects showed interconnecting tracts between the PCC and MFC of the default mode network. The normalized connecting tracts of all 45 subjects are shown in **Figure 3**, together with the PCC and MFC regions of interest from the default mode network clustermap. The selected connecting tracts reflected the left and right cingulum fiber bundle (Lawes et al., 2008; Wakana et al., 2004). The average FA value of the cingulum tracts over the group of subjects was 0.52 (SD: 0.05). Correlating the straight correlation coefficient (i.e. non-partialized) between the PCC and MFC time-series with the mean FA value of the cingulum tracts revealed a positive, but non-significant association ($r = 0.18$, $p = 0.17$, mean: 0.18, SD: 0.33, corrected for age). Correlating the level of overall default mode functional connectivity with the FA value of the cingulum tract revealed a positive trend ($r = 0.23$, $p = 0.07$, corrected for age). Correlating the partial correlation coefficient as a measure of the unique level of default mode PCC - MFC functional connectivity with the mean FA value of the cingulum tracts revealed a significant positive association ($r = 0.29$, $p < 0.05$, **Figure 4**), after controlling for age on each measure. The association between default mode functional connectivity and mean cingulum FA values was also examined by taking age as a covariate when assessing the correlation of mean cingulum FA and resting-state functional connectivity measures. This alternative approach also revealed a significant association between default mode functional connectivity and mean cingulum FA ($r = 0.34$, $p < 0.05$). Furthermore, the association between the level of default mode functional connectivity and FA measures was found to be specific to the cingulum since no significant association was found between the level of default mode functional connectivity and the mean FA value of the total collection of reconstructed tracts in the brain (i.e. all other white matter tracts in the brain) ($r = 0.12$, $p = 0.37$). In addition, no significant correlation was found between the mean FA value of the cingulum tract and the level of functional connectivity between the regions of the other RSNs (RSN b, **Figure 1b**, $r = -0.16$, $p = 0.29$; RSN c, **Figure 1c**, $r = -0.11$, $p = 0.43$; RSN d, **Figure 1d**, left - right primary motor/sensory cortex, $r = 0.05$, $p=0.74$; RSN d, **Figure 1d**, left - right primary visual cortex, $r = 0.16$,

p = 0.33, RSN e, **Figure 1e**, left - right inferior/superior temporal cortex r = 0.08, p = 0.61; RSN e, **Figure 1e**, left inferior/superior temporal cortex - anterior cingulate gyrus, r = 0.03, p = 0.85; RSN e, **Figure 1e**, right inferior/superior temporal cortex - anterior cingulate gyrus, r = 0.17, p = 0.26). No significant association was found between mean cingulum FA values and age (r = -0.05, p = 0.73) or the level of default mode functional connectivity and age (r = 0.06, p = 0.68), which is likely to result from the relative young age of the subjects that were included in this study (mean age: 24.8 years, SD: 4.8).
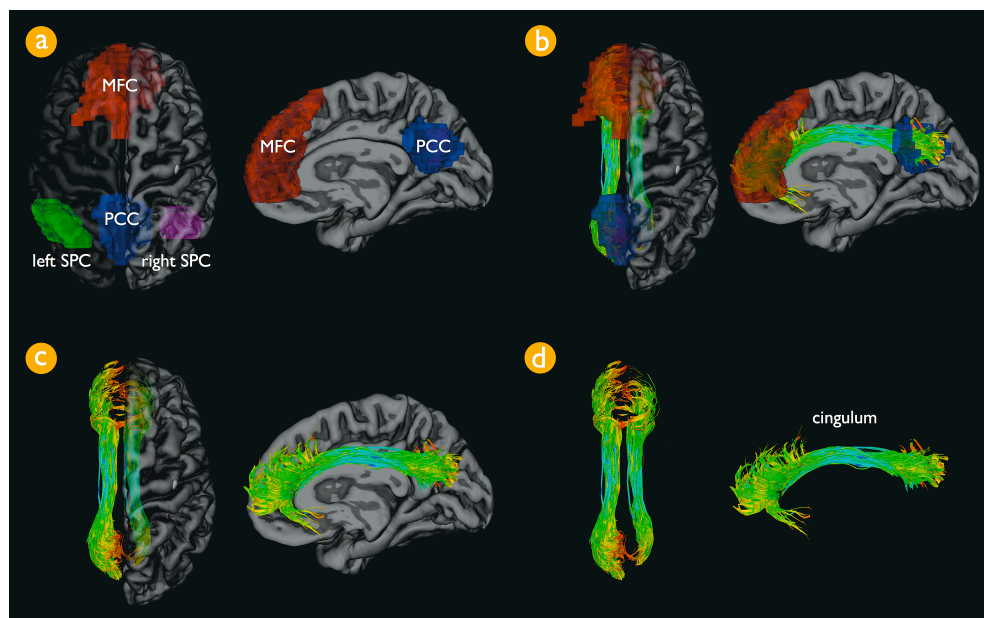

Figure 3. The cingulum tract connects precuneus and posterior cingulate cortex and medial frontal cortex of the default mode network. Figure 3a shows the regions of interest of the default mode network on a 3D rendering of the averaged normalized T1-weighted scan. The default mode network was selected by using a Normalized Cut Group Clustering approach of the resting-state data. Clustering revealed the default mode network, including the precuneus / posterior cingulate cortex (PCC, blue region of interest), medial frontal cortex (MFC, red region of interest) and bilateral superior parietal cortex (SPC, green and magenta regions). Figure 3b, c and d show the interconnecting tracts between the PCC and MFC regions over all subjects combined. Figure 3b shows both the tracts together with the PCC (blue) and MFC (red) regions of the default mode network projected on the averaged normalized anatomical brain of the group of subjects.

Discussion

The main finding of this study is that the microstructural organization (fractional anisotropy) of the interconnecting cingulum tract was found to be directly associated with

the level of functional connectivity of the default mode network. We combined resting-state functional MRI and structural DTI in a group of 45 subjects on a 3 Tesla MR scanner. The cingulum tract was confirmed to interconnect the precuneus / posterior cingulate cortex (PCC) and medial frontal cortex (MFC) of the default mode network in all subjects (**Figure 3**). Furthermore, the mean FA value of the cingulum tract was positively correlated with the level of unique coherency between the resting-state fMRI time-series of the PCC and MFC of the default mode network (**Figure 4**). These results suggest a specific association between the microstructural organization of the cingulum tract and the level of default mode functional connectivity. Our findings suggest an important role of the cingulum tract in the default mode network.
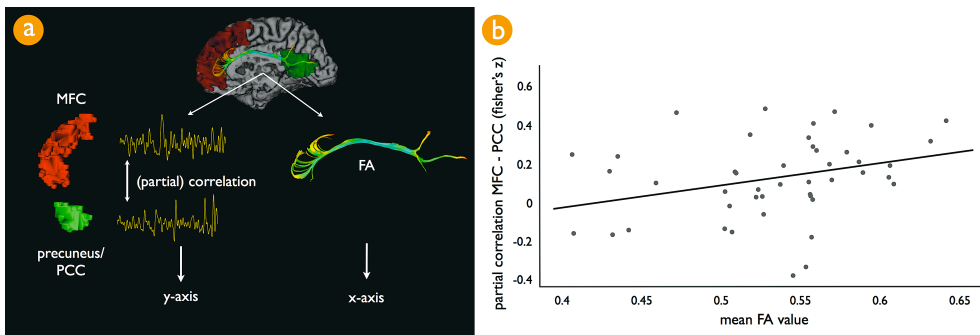

Figure 4. Association between the level of default mode functional connectivity and the microstructural organization of the cingulum tract. Figure 4a illustrates the analysis that was used to compute the level of functional and structural connectivity between the regions of interest from the default mode network. In each individual dataset, the spatially averaged filtered rest-recorded time-series (0.01 - 0.08 Hz) of the PCC and MFC of the default mode network clustermap were correlated, correcting for third-party effects. This resulted in a partial correlation between the PCC and MFC regions, which reflected the unique level of functional connectivity between these two key regions of the default mode network. The normality of the partial correlation coefficient was improved by using a Fisher's r-to-z transformation. For each individual dataset, the mean FA value of the found interconnecting cingulum tract was calculated, by averaging the FA values along all points of the found interconnecting tracts. Correlating the level of default mode functional connectivity and mean cingulum FA revealed a significant positive correlation, correcting for age (r = 0.29, p < 0.05) (Figure 4b). This suggests a direct positive association between the microstructural organization of the cingulum tract and the level of functional connectivity of the default mode network during rest. Note that the partial correlation between the PCC and MFC regions represented the partial correlation between these regions, factoring out the pair-wise correlations between the time-series of the other resting-state network regions, including the two lateralized superior parietal regions of the default mode network. This relationship was found to be specific for the cingulum tract, as no significant association was found between the partial correlation between the PCC and MFC and the mean FA value of the total collection of reconstructed tracts in the brain. Furthermore, functional connectivity measures between the regions of the other clustered resting-state networks (Figure 1, network b - g) did not show a significant association with the mean FA value of the cingulum tract.

The observed interconnecting role of the cingulum tract in the default mode network is consistent with studies demonstrating that the cingulum tract forms a direct neuroanatomical link between the precuneus and medial frontal cortex (Wakana et al., 2004; Schmahmann et al., 2007; Lawes et al., 2008). Our results are coherent with the recent study of Greicius et al. reporting on an important role of the cingulum tract in interconnecting PCC and MFC of the default mode network (Greicius et al., 2009). This direct anatomical connection reflects a vast number of axonal connections between the PCC and MFC, responsible for the facilitation of neuronal communication between these regions. This communication is likely to be ongoing during rest as suggested by the high level of neuronal activity (Gusnard et al., 2001; Raichle et al., 2001; Damoiseaux et al., 2007; Raichle and Snyder, 2007) and the observed high level of resting-state synchronization between the PCC and MFC (Greicius et al., 2003; Damoiseaux et al., 2007). Furthermore, our results show that the temporal coherency between the activation patterns of the PCC and MFC regions is specifically related to the microstructural organization (i.e. FA value) of the cingulum. It is believed that the major contribution to the directional dependent diffusion signal is due to axonal membranes hindering the diffusion process of water molecules (Beaulieu, 2002) and increased FA values may be associated with a more dense packing of axonal fibers. In this context, it is reasonable to speculate about a positive relationship between the microstructural organization of white matter tracts, reflected by the FA value, and the level of default mode neuronal communication. A possible interpretation of our results could be that a higher level of microstructural organization of the cingulum tract is associated with increased communication between PCC and MFC of the default mode network during rest.

Supporting evidence for our findings comes from studies reporting on decreased default mode functional connectivity in combination with studies reporting on degenerative brain abnormalities in the cingulum bundle. Alzheimer patients show a decreased level of functional connectivity within the default mode network (Greicius et al., 2004; Rombouts et al., 2005) as well as reduced FA values in the cingulum tract (Xie et al., 2005; Zhang et al., 2007). In addition, normal aging has been associated with decreased resting-state activation within the default mode network (Andrews-Hanna et al., 2007; Damoiseaux et al., 2007) and with lower FA values of the cingulum (Schneiderman et al., 2007; Yoon et al., 2008; Makris et al., 2007). Furthermore, decreased default mode functional connectivity (Friston, 1999; Liang et al., 2006; Micheloyannis et al., 2006; Salvador et al., 2007; Williamson, 2007; Liu et al., 2008; Bluhm et al., 2007) and reduced microstructural organization of the cingulum tract (Sun et al., 2003; Nestor et al., 2007) have been suggested to play an important role in schizophrenia.

The results of this study can be interpreted as supporting evidence for a general association between structural and functional connectivity in the human brain (Koch et al. 2002; Toosy et al., 2004; Greicius et al., 2009). A number of recent studies have suggested a direct link between white matter organization and fMRI BOLD activation patterns. FA values of splenial fibers have been associated with BOLD activation in the primary visual regions (Toosy et al., 2004) and inter-hemispheric synchronization in the developing brain

(Fornari et al., 2007). Furthermore, complete section of the corpus callosum has been reported to result in loss of interhemispheric resting-state functional connectivity (Johnston et al., 2008).

What does it mean when subjects show a higher level of resting-state default mode neuronal activation and synchronization? The results of our study cannot be used to draw conclusions about the functional relevance of the default mode network. However, other studies have suggested that increased recruitment of the default mode network is related to the tendency of a person's mind to wander (Mason et al., 2007) and it may be linked to the integration of cognitive and emotional processing (Greicius et al., 2003) and relating oneself to the outside world (Gusnard et al., 2001). These processes are likely to be ongoing during rest and to involve the integration of multiple cognitive functions. Structural pathways interconnecting the regions of default mode network may facilitate this kind of functional integration. It is of interest to further examine the found structural-functional relationship and its effect on cognitive and emotional processes that are related to default mode activation (Andrews-Hanna et al., 2007).

The level of overall default mode functional connectivity was significantly nonzero over the group of 45 subjects (Salvador et al., 2005; Greicius et al., 2003; Beckmann et al., 2005; De Luca et al., 2006; Damoiseaux et al., 2007; Van den Heuvel et al., 2008). Interestingly, the unique level of default mode functional connectivity between the PCC and MFC (i.e. controlling for the third-party influences of the two superior parietal cortex (SPC) regions) was found to be negative in 10 of the 45 subjects, with 2 subjects showing a partial correlation lower than -0.2 (**Figure 4**). Negative levels of default mode connectivity have been related to advanced aging (Andrews-Hanna et al., 2007). However, such an effect could not be concluded from our results. The 10 subjects who showed a negative level of connectivity were not significantly older than the 35 subjects who showed a positive level of default mode connectivity. This is likely to result from the relatively young age of the included group of subjects (mean age 24.8 years). Most other resting-state studies have reported only positive levels of default mode connectivity in young adults (Greicius et al., 2003). However, these studies have mainly focused on the level of overall default mode connectivity, defined as a straight correlation between the resting-state time-series of the PCC and MFC. In this study, we focused on the level of unique default mode connectivity between the PCC and MFC (by factoring out the contribution of the two SPC regions), as these are the two regions of the default mode network that are specifically connected by the cingulum. Indeed, supporting the results of previous resting-state studies, the level of overall default mode connectivity was found to be positive in all 45 subjects (mean: 0.51). Future studies are needed to examine the meaning of these specific negative synchronization patterns and how they relate to cognitive processes that involve default mode network activity. In this study, negative synchronization patterns between the PCC and MFC were interpreted as lower levels of default mode functional connectivity.

Some limitations of this study have to be taken into account when interpreting its results. The PCC and MFC regions are the most often reported regions of the default mode network. Therefore, the focus of this study was on the tracts that interconnected these two regions of the default mode network. As mentioned, bilateral parietal and temporal cortices

have also been found to participate in the default mode network (Raichle et al., 2001; Greicius et al., 2003; Fox et al., 2005; Damoiseaux et al., 2006) (**Figure 3**). However, tracts connecting these regions are likely to cross other white matter pathways, making the reconstruction of these tracts more difficult. Future studies are aimed to examine these tracts using other methods of representing the diffusion signal in combination with other tractography algorithms. Furthermore, the level of functional connectivity is expressed as a (partial) correlation between the rest-recorded BOLD time-series, believed to result from synchronization of neuronal activation (Biswal et al., 1997; Cordes et al., 2001; Greicius et al., 2003; Salvador et al., 2005; Buckner and Vincent, 2007). However, it has been suggested that physiological temporal patterns, including respiratory and cardiac oscillations could confound the BOLD signal (Wise et al., 2004), making the resting-state correlations less specific. We used a high temporal fMRI acquisition sequence to minimize these effects (Cordes et al., 2001).

In this study, we found a significant role for the cingulum tract in the default mode network in interconnecting the precuneus / posterior cingulate cortex and medial frontal cortex, key regions of the default mode network. Higher fractional anisotropy values of the cingulum were found to be associated with increased default mode functional connectivity, suggesting a direct association between the microstructural organization of the cingulum tract and the level of neuronal synchronization between key regions of the default mode network. Our results suggest an important role for the cingulum tract in default mode functional connectivity.

References

Achard S, Salvador R, Whitcher B, Suckling J, Bullmore E (2006) A resilient, low-frequency, small-world human brain functional network with highly connected association cortical hubs. J Neurosci 26:63-72.

Andersson JL, Skare S (2002) A model-based method for retrospective correction of geometric distortions in diffusion-weighted EPI. Neuroimage 16:177-199.

Andersson JL, Skare S, Ashburner J (2003) How to correct susceptibility distortions in spin-echo echo-planar images: application to diffusion tensor imaging. Neuroimage 20:870-888.

Andrews-Hanna JR, Snyder AZ, Vincent JL, Lustig C, Head D, Raichle ME, Buckner RL (2007) Disruption of large-scale brain systems in advanced aging. Neuron 56:924-935.

Beaulieu C (2002) The basis of anisotropic water diffusion in the nervous system - a technical review. NMR Biomed 15:435-455.

Beckmann CF, DeLuca M, Devlin JT, Smith SM (2005) Investigations into resting-state connectivity using independent component analysis. Philos Trans R Soc Lond B Biol Sci 360:1001-1013.

Biswal B, Yetkin FZ, Haughton VM, Hyde JS (1995) Functional connectivity in the motor cortex of resting human brain using echo-planar MRI. Magn Reson Med 34:537-541.

Biswal BB, Van Kylen J, Hyde JS (1997) Simultaneous assessment of flow and BOLD signals in resting-state functional connectivity maps. NMR Biomed 10:165-170.

Bluhm RL, Miller J, Lanius RA, Osuch EA, Boksman K, Neufeld R, Theberge J, Schaefer B, Williamson P (2007) Spontaneous Low-Frequency Fluctuations in the BOLD Signal in Schizophrenic Patients: Anomalies in the Default Network. Schizophr Bull 33:1004-1012.

Buckner RL, Vincent JL (2007) Unrest at rest: Default activity and spontaneous network correlations. Neuroimage 37:1091-1096.

Chang LC, Jones DK, Pierpaoli C (2005) RESTORE: robust estimation of tensors by outlier rejection. Magn Reson Med 53:1088-1095.

Collins DL, Neelin P, Peters TM, Evans AC (1994) Automatic 3D intersubject registration of MR volumetric data in standardized Talairach space. J Comput Assist Tomogr 18:192-205.

Corbetta M, Kincade JM, Ollinger JM, McAvoy MP, Shulman GL (2000) Voluntary orienting is dissociated from target detection in human posterior parietal cortex. Nat Neurosci 3:292-297.

Cordes D, Haughton VM, Arfanakis K, Carew JD, Turski PA, Moritz CH, Quigley MA, Meyerand ME (2001) Frequencies contributing to functional connectivity in the cerebral cortex in "resting-state" data. AJNR Am J Neuroradiol 22:1326-1333.

Damoiseaux JS, Rombouts SA, Barkhof F, Scheltens P, Stam CJ, Smith SM, Beckmann CF (2006) Consistent resting-state networks across healthy subjects. Proc Natl Acad Sci U S A 103:13848-13853.

Damoiseaux JS, Beckmann CF, Arigita EJ, Barkhof F, Scheltens P, Stam CJ, Smith SM, Rombouts SA (2007) Reduced resting-state brain activity in the "default network" in normal aging. Cereb Cortex. 18:1856-1864.

De Luca M, Beckmann CF, De Stefano N, Matthews PM, Smith SM (2006) fMRI resting state networks define distinct modes of long-distance interactions in the human brain. Neuroimage 29:1359-1367.

Fornari E, Knyazeva MG, Meuli R, Maeder P (2007) Myelination shapes functional activity in the developing brain. Neuroimage 38:511-518.

Fox MD, Raichle ME (2007) Spontaneous fluctuations in brain activity observed with functional magnetic resonance imaging. Nat Rev Neurosci 8:700-711.

Fox MD, Snyder AZ, Vincent JL, Corbetta M, Van Essen DC, Raichle ME (2005) The human brain is intrinsically organized into dynamic, anticorrelated functional networks. Proc Natl Acad Sci U S A 102:9673-9678.

Friston KJ (1999) Schizophrenia and the disconnection hypothesis. Acta Psychiatr Scand Suppl 395:68-79.

Golay X, Pruessmann KP, Weiger M, Crelier GR, Folkers PJ, Kollias SS, Boesiger P (2000) PRESTO-SENSE: an ultrafast whole-brain fMRI technique. Magn Reson Med 43:779-786.

Greicius MD, Krasnow B, Reiss AL, Menon V (2003) Functional connectivity in the resting brain: a network analysis of the default mode hypothesis. Proc Natl Acad Sci U S A 100:253-258.

Greicius MD, Srivastava G, Reiss AL, Menon V (2004) Default-mode network activity distinguishes Alzheimer's disease from healthy aging: evidence from functional MRI. Proc Natl Acad Sci U S A 101:4637-4642.

Greicius MD, Supekar K, Menon V, Dougherty RF (2009) Resting-State Functional Connectivity Reflects Structural Connectivity in the Default Mode Network. Cereb Cortex.19:72-78.

Gusnard DA, Raichle ME, Raichle ME (2001) Searching for a baseline: functional imaging and the resting human brain. Nat Rev Neurosci 2:685-694.

Johnston JM, Vaishnavi SN, Smyth MD, Zhang D, He BJ, Zempel JM, Shimony JS, Snyder AZ, Raichle ME (2008) Loss of resting interhemispheric functional connectivity after complete section of the corpus callosum. J Neurosci 28:6453-6458.

Jones DK (2004) The effect of gradient sampling schemes on measures derived from diffusion tensor MRI: a Monte Carlo study. Magn Reson Med 51:807-815.

Jones DK, Horsfield MA, Simmons A (1999) Optimal strategies for measuring diffusion in anisotropic systems by magnetic resonance imaging. Magn Reson Med 42:515-525.

Kim JH, Loy DN, Liang HF, Trinkaus K, Schmidt RE, Song SK (2007) Noninvasive diffusion tensor imaging of evolving white matter pathology in a mouse model of acute spinal cord injury. Magn Reson Med 58:253-260.

Koch MA, Norris DG, Hund-Georgiadis M (2002) An investigation of functional and anatomical connectivity using magnetic resonance imaging. Neuroimage 16:241-250.Lawes IN, Barrick TR, Murugam V, Spierings N, Evans DR, Song M, Clark CA (2008) Atlas-based segmentation of white matter tracts of the human brain using diffusion tensor tractography and comparison with classical dissection. Neuroimage 39:62-79.

Liang M, Zhou Y, Jiang T, Liu Z, Tian L, Liu H, Hao Y (2006) Widespread functional disconnectivity in schizophrenia with resting-state functional magnetic resonance imaging. Neuroreport 17:209-213.

Liu Y, Liang M, Zhou Y, He Y, Hao Y, Song M, Yu C, Liu H, Liu Z, Jiang T (2008) Disrupted small-world networks in schizophrenia. Brain 131:945.

Makris N, Papadimitriou GM, van der Kouwe A, Kennedy DN, Hodge SM, Dale AM, Benner T, Wald LL, Wu O, Tuch DS, Caviness VS, Moore TL, Killiany RJ, Moss MB, Rosene DL (2007) Frontal connections and cognitive changes in normal aging rhesus monkeys: a DTI study. Neurobiol Aging 28:1556-1567.

Mason MF, Norton MI, Van Horn JD, Wegner DM, Grafton ST, Macrae CN (2007) Wandering minds: the default network and stimulus-independent thought. Science 315:393-395.

Micheloyannis S, Pachou E, Stam CJ, Breakspear M, Bitsios P, Vourkas M, Erimaki S, Zervakis M (2006) Small-world networks and disturbed functional connectivity in schizophrenia. Schizophr Res 87:60-66.

Mori S, van Zijl PC (2002) Fiber tracking: principles and strategies - a technical review. NMR Biomed 15:468-480.

Mori S, Crain BJ, Chacko VP, van Zijl PC (1999) Three-dimensional tracking of axonal projections in the brain by magnetic resonance imaging. Ann Neurol 45:265-269.

Neggers SF, Hermans EJ, Ramsey NF (2008) Enhanced sensitivity with fast three-dimensional blood-oxygen-level-dependent functional MRI: comparison of SENSE-PRESTO and 2D-EPI at 3 T. NMR Biomed 21:663-676.

Nestor PG, Kubicki M, Spencer KM, Niznikiewicz M, McCarley RW, Shenton ME (2007) Attentional networks and cingulum bundle in chronic schizophrenia. Schizophr Res 90:308-315.

Northoff G, Bermpohl F (2004) Cortical midline structures and the self. Trends Cogn Sci 8:102-107.

Northoff G, Heinzel A, de Greck M, Bermpohl F, Dobrowolny H, Panksepp J (2006) Self-referential processing in our brain--a meta-analysis of imaging studies on the self. Neuroimage 31:440-457.

Raichle ME, Snyder AZ (2007) A default mode of brain function: A brief history of an evolving idea. Neuroimage 37:1083-1090.

Raichle ME, MacLeod AM, Snyder AZ, Powers WJ, Gusnard DA, Shulman GL (2001) A default mode of brain function. Proc Natl Acad Sci U S A 98:676-682.

Rombouts SA, Barkhof F, Goekoop R, Stam CJ, Scheltens P (2005) Altered resting state networks in mild cognitive impairment and mild Alzheimer's disease: an fMRI study. Hum Brain Mapp 26:231-239.

Salvador R, Suckling J, Coleman MR, Pickard JD, Menon D, Bullmore E (2005) Neurophysiological architecture of functional magnetic resonance images of human brain. Cereb Cortex 15:1332-1342.

Salvador R, Martinez A, Pomarol-Clotet E, Sarro S, Suckling J, Bullmore E (2007) Frequency based mutual information measures between clusters of brain regions in functional magnetic resonance imaging. Neuroimage 35:83-88.

Schmahmann JD, Pandya DN, Wang R, Dai G, D'Arceuil HE, de Crespigny AJ, Wedeen VJ (2007) Association fibre pathways of the brain: parallel observations from diffusion spectrum imaging and autoradiography. Brain 130:630-653.

Schmitz TW, Johnson SC (2007) Relevance to self: A brief review and framework of neural systems underlying appraisal. Neurosci Biobehav Rev 31:585-596.

Schneiderman JS, Buchsbaum MS, Haznedar MM, Hazlett EA, Brickman AM, Shihabuddin L, Brand JG, Torosjan Y, Newmark RE, Tang C, Aronowitz J, Paul-Odouard R, Byne W, Hof PR (2007) Diffusion tensor anisotropy in adolescents and adults. Neuropsychobiology 55:96-111.

Stam CJ (2004) Functional connectivity patterns of human magnetoencephalographic recordings: a 'small-world' network? Neurosci Lett 355:25-28.

Sun FT, Miller LM, D'Esposito M (2004) Measuring interregional functional connectivity using coherence and partial coherence analyses of fMRI data. Neuroimage 21:647-658.

Sun Z, Wang F, Cui L, Breeze J, Du X, Wang X, Cong Z, Zhang H, Li B, Hong N, Zhang D (2003) Abnormal anterior cingulum in patients with schizophrenia: a diffusion tensor imaging study. Neuroreport 14:1833-1836.

Toosy AT, Ciccarelli O, Parker GJ, Wheeler-Kingshott CA, Miller DH, Thompson AJ (2004) Characterizing function-structure relationships in the human visual system with functional MRI and diffusion tensor imaging. Neuroimage 21:1452-1463.

Van den Heuvel MP, Mandl RC, Hulshoff Pol HE (2008) Normalized group clustering of resting-state fMRI data. PLoS ONE 3:e2001

Wakana S, Jiang H, Nagae-Poetscher LM, van Zijl PC, Mori S (2004) Fiber tract-based atlas of human white matter anatomy. Radiology 230:77-87.

Williamson P (2007) Are Anticorrelated Networks in the Brain Relevant to Schizophrenia? Schizophr Bull 33:994-1003.

Wise RG, Ide K, Poulin MJ, Tracey I (2004) Resting fluctuations in arterial carbon dioxide induce significant low frequency variations in BOLD signal. Neuroimage 21:1652-1664.

Xie S, Xiao JX, Wang YH, Wu HK, Gong GL, Jiang XX (2005) Evaluation of bilateral cingulum with tractography in patients with Alzheimer's disease. Neuroreport 16:1275-1278.

Yoon B, Shim YS, Lee KS, Shon YM, Yang DW (2008) Region-specific changes of cerebral white matter during normal aging: A diffusion-tensor analysis. Arch Gerontol Geriatr. 47:129-138.

Zhang Y, Schuff N, Jahng GH, Bayne W, Mori S, Schad L, Mueller S, Du AT, Kramer JH, Yaffe K, Chui H, Jagust WJ, Miller BL, Weiner MW (2007) Diffusion tensor imaging of cingulum fibers in mild cognitive impairment and Alzheimer disease. Neurology 68:13-19.

Chapter 4

Functional diffusion tensor imaging: measuring task-related fractional anisotropy changes in the human brain along white matter tracts

René C. W. Mandl, Hugo G. Schnack, Marcel P. Zwiers, Arjen van der Schaaf, René S. Kahn and Hilleke E. Hulshoff Pol

Abstract

Functional neural networks in the human brain can be studied from correlations between activated gray matter regions measured with fMRI. However, while providing important information on gray matter activation, no information is gathered on the co-activity along white matter tracts in neural networks. We report on a functional diffusion tensor imaging (fDTI) method that measures task-related changes in fractional anisotropy (FA) along white matter tracts. We hypothesize that these fractional anisotropy changes relate to morphological changes of glial cells induced by axonal activity although the exact physiological underpinnings of the measured FA changes remain to be elucidated. As expected, these changes are very small as compared to the physiological noise and a reliable detection of the signal change would require a large number of measurements. However, a substantial increase in signal-to-noise ratio was achieved by pooling the signal over the complete fiber tract. Adopting tract-based statistics enabled us to measure the signal within a practically feasible time period. Activation in the sensory thalamocortical tract and optic radiation in eight healthy human subjects was found during tactile and visual stimulation, respectively. The results of our experiments indicate that these FA changes may serve as a functional contrast mechanism for white matter. This noninvasive fDTI method may provide a new approach to study functional neural networks in the human brain.

Neurobehavioral functions depend on a dynamic flow of information between various gray matter brain regions which are interconnected via white matter pathways (Catani and Ffytche, 2005; Mesulam, 2005). Activation of the human brain's gray matter regions have been extensively studied with neuroimaging techniques such as functional magnetic resonance imaging (fMRI), positron emission tomography (PET), single photon emission computed tomography (SPECT), electro-encephalography (EEG) and magneto-encephalography (MEG). However, these techniques do not provide information on the white matter pathways and their corresponding activity. Imaging techniques such as DTI (Le Bihan et al., 1986; Basser et al., 1994) in combination with fiber tractography (Conturo et al., 1999; Jones et al., 1999; Mori and van Zijl, 2002) allow us to non-invasively study the anatomy of these pathways - but not their activity. In this paper we present a functional diffusion tensor imaging (fDTI) method that is able to detect task-related changes in FA that may represent the activity of white matter tracts. Directly testing the white matter tracts for activation would provide us with a unique opportunity to study the connections of neural networks that become active during various cognitive functions. In addition, it may allow the study of dysfunctional neural networks in patients with neurological and psychiatric diseases, such as schizophrenia in which structural and functional brain abnormalities have been found (Wright et al., 2000; Hulshoff Pol et al., 2004; Sommer et al., 2004).

In DTI the diffusion profile of water molecules is measured. In white matter fibers, which are formed by large numbers of heavily myelinated axons running in parallel, the diffusion is more hindered in the radial directions (i.e. perpendicular to the fibers' principal direction) than in the direction parallel to the fibers. As a result, the diffusion profile in white matter is elongated (cigar shaped), pointing in the direction of the fibers. In DTI the diffusion profile is represented by a positive definite tensor of which the major eigenvector with eigenvalue λ_1 represents the direction parallel to the fibers and both minor eigenvectors with eigenvalues λ_2 and λ_3 represent the radial directions.

The fractional anisotropy (Basser and Pierpaoli, 1996) (FA) defined by:

$$FA = \sqrt{\frac{3}{2}\left(\frac{(\lambda_1 - \bar{\lambda})^2 + (\lambda_2 - \bar{\lambda})^2 + (\lambda_3 - \bar{\lambda})^2}{\lambda_1^2 + \lambda_2^2 + \lambda_3^2}\right)},$$

$$\bar{\lambda} = \frac{\lambda_1 + \lambda_2 + \lambda_3}{3}$$

is a relative measure that describes the variance between the levels of diffusion measured in the different directions. It is therefore not sensitive to fluctuations in the diffusion unweighted ($b = 0$ s/mm^2) image, which serves as normalization factor in the eigenvalue computation. This in contrast to other measures such as radial diffusivity defined by (λ_2 + λ_3) / 2, parallel diffusivity defined by λ_1, or mean diffusivity defined by (λ_1+ λ_2 + λ_3) / 3,

which are sensitive to intensity fluctuations in the diffusion unweighted image, for instance due to task-related onset changes in T2* (the basis of the fMRI BOLD contrast). The FA is therefore well-suited to study activity-related changes in white matter as it is insensitive to possible task-related T2* changes in neighboring gray matter.

fDTI is based on the assumption that changes in FA are a sign of local fiber activity. We hypothesize that morphological changes of glial cells (in particular oligodendrocytes) lead to shape changes of the extra-cellular space (ECS) (Ransom et al., 1985; Sykova, 2004; Beshay et al., 2005) and, in turn, lead to a measurable increase in FA. Indeed, changes in the diffusion profile due to changes in the ECS in white matter have been shown *in vitro* using diffusion weighted imaging in the rat optic nerve (Anderson et al., 1996). An earlier study (Prichard et al., 1995) reported that electrical stimulation induced significant changes in the diffusion properties of brain tissue in rats. Using intrinsic optical signal (IOS) measurements (MacVicar et al., 2002) slowly varying activity-related signal changes were measured in the rat optical nerve and were attributed to glial cell swelling. However, a study using the real-time tetramethylammonium (TMA$^+$) iontophoretic method in combination with IOS measurements (Sykova et al., 2003) showed that the concentration of TMA$^+$ in the extra-cellular space (ECS) did not change although similar changes in the IOS signal were measured. Therefore the authors concluded that it was unlikely that glial cell swelling was the primary mechanism for these IOS changes and they suggested that a more plausible explanation may be found in morphological changes of glial cells. A recent study (Stroman et al., 2008) showed that increased levels of potassium lead to changes in both IOS values and MRI proton density measurements for gray and subcortical white matter in rats, suggesting that activity-related changes in the ECS of gray matter as well as white matter can be measured using MRI. The authors therefore conclude that cell swelling arising from neuronal depolarization is detectable with fMRI-like acquisitions.

Regarding the measurement of activation in gray matter there is an ongoing discussion whether diffusion weighted MRI provides a more direct way to measure activation than functional MRI methods that are based on vascular responses such as BOLD contrasted fMRI. Le Bihan and colleagues (Le Bihan et al., 2006) hypothesized that for functional imaging of gray matter diffusion-sensitized images can be used to measure neuronal activity related cell swelling. This would provide a more direct way to measure neuronal activation than standard BOLD contrasted fMRI does. The results of their experiments not only suggested that the measured diffusion-sensitized MRI signal changes could be linked to activity-related cell swelling but also that the delay between stimulus onset and measured signal change was notably smaller for the diffusion-sensitized MRI signal than the delay between the stimulus onset and the BOLD fMRI signal. However, another study (Miller et al., 2007), which compared signal changes induced by neuronal activation and signal changes due to hypercapnia, was not able to replicate this difference in delays. Moreover, the results of that study suggested that even with strong diffusion weighting vascular effects could not be ruled out as a possible source for the measured task-related MRI signal change.

Regarding the measurement of activity in white matter, several different physiological processes - other than morphological changes of glial cells - that are part of (or accompany) fiber activity could, in theory, alter the diffusion profile and therefore the measured FA value as well. For instance, the changes in FA value may also have been altered by local changes in capillary blood flow (Le Bihan et al., 1986), in capillary blood volume (Lu et al., 2003) or by activity-related anisotropic magnetic susceptibility variations (Richard P. Kennan, 1995). These other possible explanations for the observed task-related changes in FA should be considered and will be addressed in the discussion section.

Normal activity-induced changes in the diffusion profile of white matter are expected to be very small as compared to the physiological noise (Gulani et al., 1999) and a reliable detection of the signal change would require a large number of measurements. But if it is assumed that activity-related FA-signal changes extends the whole tract, then a substantial increase in signal-to-noise ratio can be achieved by pooling the signal over the entire tract. It is the adoption of a tract-based statistics -rather than a voxel-based statistics- that enables us to measure the signal within a practically feasible time period. The principle of the fDTI method is outlined in **Figure 1**.

To assess the validity of the fDTI method, eight healthy right-handed subjects participated in both tactile and visual fDTI experiments. Afterwards, three other subjects participated in a second, time course experiment. The second experiment provided more specific information on when the maximum of the measured signal change is found for the different types of stimuli. Throughout the rest of this paper we will refer to the first experiment as the fDTI experiment and to the second experiment as the time course experiment. These experiments were approved by the medical ethical committee for human subjects of the University Medical Center Utrecht, The Netherlands, and all subjects provided written informed consent prior to participation.

Materials and Methods

fDTI experiment

In the tactile experiment the subjects were instructed to keep their eyes closed for the duration of the whole experiment. During the active condition, the palm and fingers of the subject's right hand were brushed in a random fashion by an investigator. In the visual experiment the subjects were instructed to look at a red fixation cross that was projected on the center of a screen visible from inside the scanner at all times. During the active condition a black and white checkerboard was shown that alternated at a frequency of 8 Hertz. During the rest condition only the red fixation cross was visible. In both fDTI experiments the same active versus rest paradigm was used and the scan parameter settings were identical. These two fDTI experiments were selected for their expected lack of overlap in activated tracts, which allowed us to study both the method's specificity and sensitivity. Moreover, a subject's response was not required in either of the tasks reducing the chance of task-related motion artifacts.
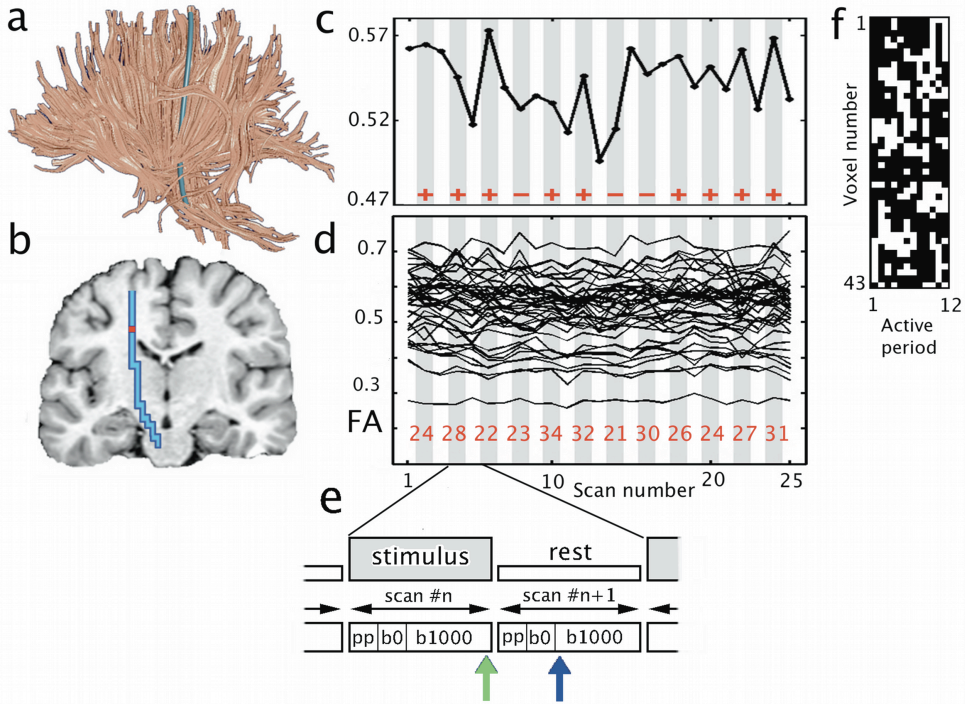
Figure 1. *Overview of the fDTI analysis. (a) The fDTI method starts with the reconstruction of anatomical tracts in the brain without any region specific selection criteria using conventional fiber tracking. All the tracts (here the total count for the whole white matter was 20,193 tracts) are then tested individually for activation. (b) The blue colored tract is an example tract used to explain the test for activation. (c) In the fDTI method the FA values during rest are compared to the FA values during the task. These changes in FA value are encoded per voxel using a series of '+'s and '-'s. If the FA value of an active period (gray column) was higher than the average FA value of its temporal neighbors (both resting periods, shown in a white column) then a '+' was assigned, and otherwise a '-', here shown for the individual red voxel. Note that the test for activation is done over the complete tract, and not at the level of individual voxels, as we assumed that during a task the whole tract is active. In this way the statistical power is increased allowing subtle FA-changes to be detected. (d) The FA values measured for all 43 voxels that are part of the tract that is tested. The numbers shown for each active period at the lower part of the graph (in red) depict the number of '+'s encoded over all 43 voxels of the tested tract. The total number of '+'s found was 322 from a total of 516 (12×43) signs. The sign-test yielded p = 0.000000001 for the tested tract and remained significant at the 0.05 level even after Bonferroni-correction for the total number of tracts tested (Bonferroni corrected threshold is 0.05 / 20193 = 0.000002). (e) In this timing plot of a stimulus and resting epoch pp stands for preparation phase (12 s), b0 denotes the time period in which the b = 0 s/mm^2 volume is acquired (12 s), and b1000 denotes the time period in which the six b = 1000 s/mm^2 volumes are acquired (36 s). The green and blue arrows denote where (according to the results of the time course experiment) the maximum signal change is expected for the tactile and visual stimulus, respectively. (f) shows the matrix with all the signs of the active tract. The '+'s are represented by black and white denotes the '-'s. This sign matrix shows that the positive correlation of the tract with the task is likely to represent signal changes over large parts of the tract over a considerable time period.*

For each fDTI experiment a separate anatomy scan, a conventional high-resolution DTI scan and an fDTI scan were acquired (see MRI scan acquisition). The subjects left the scanner room to rest between the two experiments for at least 15 minutes. For one subject the results of the visual task were excluded because of visibility problems of the checkerboard reported afterwards. The conventional DTI-scan was used for reconstruction of the tracts (**Figure 1a**) using the FACT-algorithm (Mori et al., 1999). The anatomy scan was used for inter-subject registration and visualization of the results. We did not use cardiac gating as it would lengthen the acquisition time considerably. Identical timing parameters for the visual task and the tactile task were used to make direct comparison possible between the results of the tactile and visual task.

MRI scan acquisition

For the fDTI experiment the following scans were acquired on a Philips Achieva 1.5 Tesla whole-body MR scanner (Intera Achieva, Philips, Best, The Netherlands). First, a T1-weighted whole brain scan was acquired for anatomical reference. Next, a conventional transverse single shot spin-echo, echo planar imaging (SS-EPI) DTI scan was acquired for reconstruction of the white matter tracts in the whole brain (acquisition matrix = 128×96; FOV = 240 mm; 60 slices; slice-thickness = 2.5 mm; no gap; TE = 86 ms; TR = 10000 ms; parallel imaging SENSE factor = 2; 32 different diffusion gradient directions with b-factor = 1000 s/mm^2; scan duration = 354 s). The functional time series of DTI scans (the fDTI set) were acquired during the execution of an alternating sequence of a neurobehavioral task and a resting condition. A total of 29 transverse SS-EPI DTI scans (acquisition matrix = 64×64; FOV = 256 mm; 40 slices; slice-thickness = 4 mm; no gap; TE = 74 ms; TR = 6000 ms; parallel imaging SENSE factor = 2.5; 1 scan without diffusion gradients and 6 non-collinear diffusion gradient directions with b-factor = 1000 s/mm^2; scan duration per DTI scan = 60 s) were collected (15 during the resting condition and 14 during the active condition; beginning and ending with a resting condition).

These DTI scans started with a calibration period of 12 seconds. For a stimulus period the stimulus started at the beginning of the calibration to eliminate possible onset effects of a BOLD related signal during the acquisition of the data (BOLD signal has a time-to-peak that is typically below 10 seconds). Next, two diffusion unweighted volumes (which are averaged) with a total duration of 12 seconds were acquired, followed by 6 diffusion-weighted volumes (36 seconds) using the following diffusion gradient scheme: (Gx, Gy, Gz) = (1, 0, 0), (0, 1, 0), (0, 0, 1), (-½√2, 0, -½√2), (½√2, ½√2, 0), (0, ½√2, ½√2), where the x-, y-, and z-axis correspond to the patient's right-left, anterior-posterior, and feet-head direction, respectively. The first 4 DTI scans were disregarded to eliminate possible onset effects (for example, due to heating of the scanner gradients) leaving 13 rest scans and 12 active scans.

Post processing

The diffusion unweighted scan of the first fDTI image was used to compute the rigid body transformation that aligns the first fDTI image with the conventional DTI image. Because the application of parallel imaging substantially reduces susceptibility artifacts (e.g. nonlinear spatial deformations) we assumed that rigid body transformations could be used in this registration step. All other images in the fDTI set were then registered (using cross correlation) towards the first fDTI image. In this step each diffusion weighted scan in the other series was registered to its corresponding diffusion weighted scan of the first fDTI image. Subsequently the FA was computed for each separate voxel of each image in the fDTI set. The conventional DTI image was used to reconstruct the tracts for the whole brain with an in house implementation of the FACT algorithm (Mori et al., 1999). Parameter settings: minimum FA > 0.2, maximum angle between current major eigenvector and previous major eigenvector < 26 degrees, average maximum angle between current major eigenvector and major eigenvectors of neighboring voxels (R-value) < 37 degrees, minimum tract length 50 mm, number of tract starting points per voxel = 8.

Statistical analysis

Considering that the FA-signal change extends over the whole tract we postulated that a switch to statistical testing at the level of complete tracts instead of single voxels, yields the necessary increase in statistical power (see the legend of **Figure 1** for a detailed explanation). However, white matter voxels that are part of an active tract may all have different baseline FA values and their (non Gaussian) distributions are likely to differ as well. Because of these differences in baseline FA values the comparison between active and rest FA values should be done per voxel to keep the within variation as low as possible. Also, because of the expected different distributions, the conservative nonparametric sign-test (Armitage et al., 2002) was used as a test-statistic because this test does not require normally distributed data. For each separate voxel that was part of the tested tract, the FA values measured during the active conditions were compared to rest FA values and were encoded by a series of '+' and '-' signs as follows. An active condition was assigned a '+' if its FA value was higher than the average of the FA values of its two temporal neighbors (the rest conditions just before and just after the active condition), otherwise a '-' was assigned. To test if a complete tract was active, the sign-test was applied to the set of '+' and '-' signs combined for all voxels that were part of the tract. Thus, if the number of voxels which are part of the tract that is tested for activation is n and the number of signs per voxel is m, then the sign-test is applied to a set of $n \times m$ signs. If, by using the sign-test with a significance threshold of $p < 0.05$, the number of '+'s found differed significantly from what was expected according to the binomial distribution with equal probabilities for '+' and '-', the tract was considered active. When all tracts were tested for activity in this manner, the significance level of 0.05 should be properly adjusted to correct for multiple testing. In this study the Bonferroni correction was used.

Multi-subject averaging

To compare the results of the tactile and the visual fDTI experiment at a group level the individual results were placed in a common space as follows. For each subject a binary map of the complete set of voxels that coincides with the active tracts found was placed in one common space using the affine transformation that registers the subject's anatomy scan with the Montreal Neurological Institute MNI-305 template. The affine transformation was computed using the ANIMAL algorithm (Collins et al., 1995) and the resampling of the binary maps was performed using linear interpolation. Each of the transformed maps was then blurred with a 3-dimensional Gaussian kernel with a full width at half maximum of 7 mm (to partially overcome spatial inter-subject variability) followed by a threshold at a value of 0.1 yielding a second binary map. The result of this procedure is that the binary voxel representation of an active tract in the second binary map is a dilated version of the binary voxel representation of an active tract in the first binary map. Finally these binary maps of the subjects were accumulated and overlaid on the subjects' average anatomy. Thus the value of a (colored) voxel represents the number of subjects for which an active tract can be associated with that voxel.

Average percent FA-signal change

For each subject the per voxel average percent FA-signal change (($FA_{task} - FA_{rest}$) / FA_{rest}) $\times$ 100% was computed for the FA time series of the voxels that are part of active tracts. The per voxel average percent FA-signal change values were computed and were averaged over all active voxels of all subjects yielding an overall average percent FA-signal change. Likewise, the per voxel average percent signal change for the same set of active voxels was computed for the parallel diffusivity, the radial diffusivity and the mean diffusivity.

Estimation of the contribution of blood volume changes

To obtain a coarse estimate of the maximum contribution of possible task-related blood volume changes to the measured signal we used a two-compartment model (Harshbarger and Song, 2006) consisting of an intra- and extravascular component. The signal S_r during rest condition was modeled by:

$$S_r = S_0[f_r e^{-bD} + (1 - f_r)e^{-bD_{brain}}]$$

and the signal S_a during active condition was modeled by:

$$S_a = S_0[\delta_i f_a e^{-bD} + \delta_e(1 - f_a)e^{-bD_{brain}}]$$

where S_0 is the baseline signal without diffusion weighting, f_r and f_a are the volume fractions of the intravascular component during rest and activation, D is the apparent diffusion coefficient (ADC) of the vessel, D_{brain} is the ADC of brain tissue, and δ_i is a composite coefficient for intravascular and δ_e for extravascular contributions to the signal changes (reflecting T2 and potentially apparent T1 activation-related changes). The following parameter settings were used: $f_r = 0.01$ (for white matter, the fraction of the microvascular tissue is in the order of 1% (Norris, 2001; Nonaka et al., 2003)); $f_a = 0.015$ (i.e. 50% change in volume fraction with activation, based on (Donahue et al., 2006)); b-factor = 1000 s/mm^2; $D = 1 \times 10^{-3}$ mm^2/s (capillaries). Assuming that the extravascular component contains white matter two different ADC values ranges for brain tissue were used $D_{brain} = [2.46 \times 10^{-4}$ mm^2/s, 5.23×10^{-4} mm^2/s] (radial) and $[1.51 \times 10^{-3}$ mm^2/s, 1.83×10^{-3} mm^2/s] (parallel) (Bammer et al., 2000). The composite coefficients were set to $\delta_i = 1.2$ (here the estimate for gray is matter used) and $\delta_e = 1$ (no extravascular contribution). The range of the relative signal change $(S_a - S_r) / S_r$ in the radial direction is $[-1.2 \times 10^{-3}, -3.50 \times 10^{-5}]$ and the parallel direction range is $[8.27 \times 10^{-3}, 1.32 \times 10^{-2}]$ which correspond to changes in ADC in the range $[1.24 \times 10^{-6}$ mm^2/s, 3.50×10^{-8} mm^2/s] (radial diffusion) and $[-8.23 \times 10^{-6}$ mm^2/s, -1.31×10^{-5} mm^2/s] (parallel diffusion), respectively. Thus the maximum signal changes induced by blood volume are therefore estimated for radial diffusivity between 0.50% and 0.01% and for parallel diffusivity between -0.54% and -0.72%.

Time course experiment

Considering the results of the fDTI experiment the signal contrast between stimulus and rest conditions was expected to be maximal when the diffusion gradient direction is perpendicular to the tract. Because the "tracts of interest" were known beforehand (i.e. the sensory thalamocortical tract and the optic radiation), for the time course experiment, a single diffusion gradient direction was selected that is perpendicular to the tract of interest. By selecting only one diffusion gradient direction instead of six (necessary to compute the FA) the temporal resolution was increased to 2.6 seconds.

MRI scan acquisition

The scans for the time course experiment were acquired on a Philips Achieva 3 Tesla whole-body MR scanner (Intera Achieva, Philips, Best, The Netherlands). For the time course experiment with the tactile stimulus, a transverse SS-EPI diffusion weighted scan with 80 diffusion weighted volumes was acquired with the same diffusion gradient applied in the subject's left-right direction for each of these diffusion weighted volumes (acquisition matrix = 80×80; FOV = 200×200 mm; 28 slices; slice thickness 7.5 mm; no gap; TR = 2852 ms; TE = 68 ms; diffusion gradient b-factor = 1000 s/mm^2; parallel imaging SENSE factor = 3; total scan duration 239 s). Note that for this experiment no diffusion unweighted volumes were acquired because this would decrease the temporal

resolution. The scan was repeated 5 times and anisotropic voxels aligned with the tracts of interest were used to reduce partial voluming to increase the signal-to-noise ratio. The same tactile stimulus was used as in the tactile fDTI experiment. The stimulus started at the 4th scan and ended after the 26th scan (stimulus duration 60 s). The scan parameters for the time course experiment with the visual stimulus were identical to the scan parameters for the time course experiment with the tactile stimulus except that the slice direction was set to coronal and that the diffusion gradient was applied in the subject's upper-left bottom-right direction (the usage of a combined diffusion gradient in the visual task was necessary to keep the TE of the visual task identical to the TE of the tactile task). The stimulus used was the same stimulus as used in the visual fDTI experiment and the stimulus started at the 4th scan and ended after the 26th scan. The conventional DTI scan used in the time course experiment was identical to the one described in the fDTI experiment.

Post processing

For the analysis of the scans of the time course experiment with tactile stimulation all voxels that were part of the tracts connected to the left sensory thalamocortical tract were selected. From these voxels, 25 voxels with the highest MRI signal (averaged over all scans) were selected being the "voxels of interest" for these voxels a task-related signal change was expected. These voxels were selected in this way because a high MRI signal is expected in white matter when the direction of the diffusion gradient is perpendicular to the tract's main direction. The MRI signals of these voxels of interest were normalized by dividing their values by the (per voxel) medians. In contrast to the fDTI experiment, only diffusion weighted (b = 1000 s/mm^2) data were acquired for the time course experiment, and thus no normalization with respect to the diffusion unweighted signal (b = 0 s/mm^2) was possible, making these data susceptible to global signal variation. To correct for the influence of global signal variation, the MRI signal values of the voxels of interest were covariated with the MRI signal values of voxels that had similar signal intensity characteristics but were not expected to show a task-related signal change: the "background voxels". These background voxels were the 25 voxels with the highest average MRI signal value selected from tracts that were not part of the sensory thalamocortical tract. The 15 measurements (3 subjects; 5 measurements per subject) were averaged and temporally smoothed using a Gaussian kernel with sigma = 14 s. In a similar fashion the analysis of the scans for the time course experiment with the visual stimulus was carried out. The only difference was that the 25 voxels of interest were selected from the optic radiation and that the background voxels were selected from tracts other than the optic radiation.

Results

Positively correlated active tracts (that is, active tracts that show a significant positive correlation with the task) found for a single subject during the tactile task and the visual
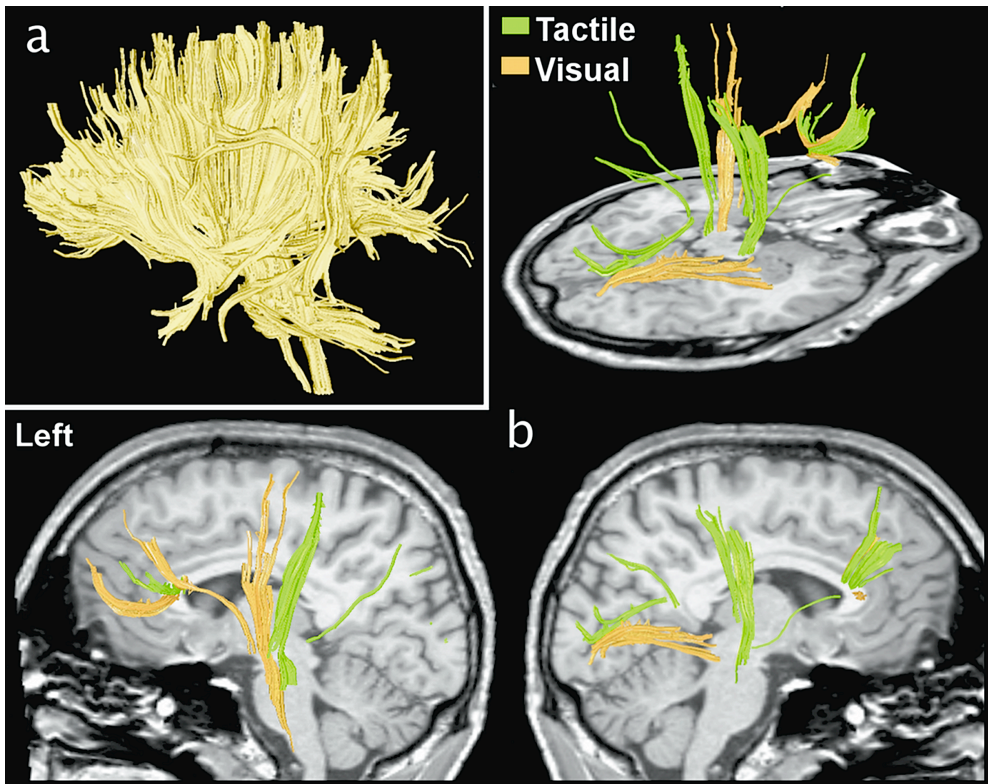
Figure 2. *Individual fDTI results for subject 5. (a) The reconstructed tracts that were tested for activity using the fDTI method. (b) Tracts that were found positively active during the visual task (orange) and the tactile task (green). The lower images show the tracts found for the left and the right hemisphere. During the tactile task, positively correlated activation was found predominantly contra-laterally for thalamocortical tracts running to the primary sensory cortical area. Positively correlated activation during the visual task was found amongst others for tracts that are part of the optic radiation.*

task in the fDTI experiment are shown in **Figure 2**. (See Movie S1 and Movie S2 for these fDTI results in combination with conventional fMRI results.) The results of all individuals for the fDTI experiment were placed in a common space to study the accumulated activation patterns for each task separately (**Figure 3**). For the tactile task, positively correlated activation was most consistently found for the afferent tracts of the left sensory thalamocortical tract and the splenium of the corpus callosum (**Figure 3a**). Negatively correlated activation was most consistently found for the afferent tracts of the right sensory thalamocortical tract (**Figure 3b**). For the visual task, positively correlated activation was most consistently found for the genu and splenium of the corpus callosum and to a lesser extent for the tracts of the right sensory thalamocortical tract (**Figure 3c**). For the visual task, negatively correlated activation was most consistently found for both left and right
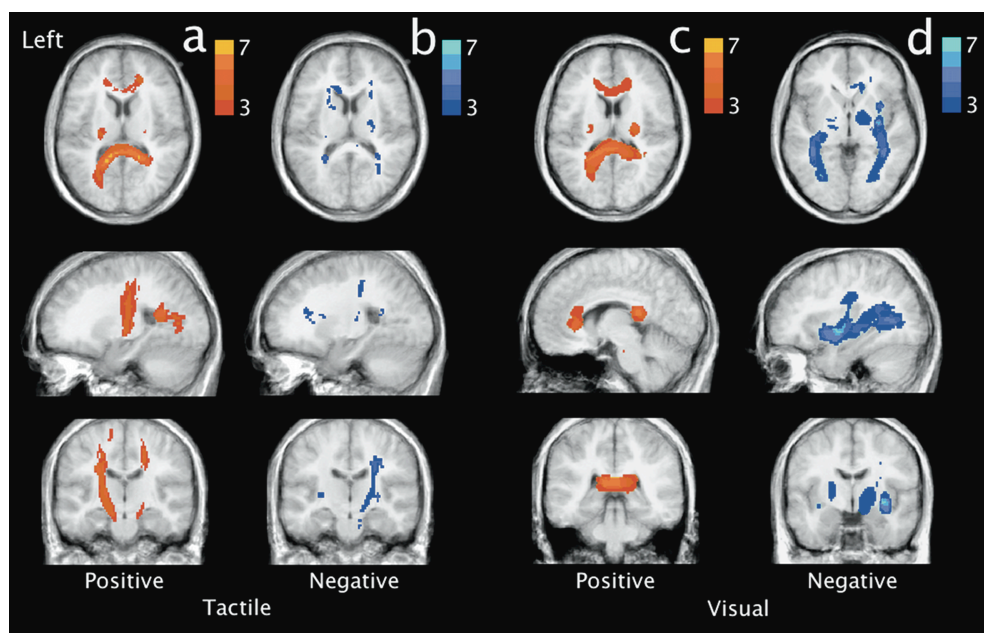
Figure 3. *Accumulated group fDTI results for the tactile and visual task. For both tasks the accumulated group fDTI results were computed and overlaid on the subjects' average anatomy. The color of the voxel represents the number of subjects for which active tracts are found at that position. Red voxels denote positively correlated activation (a,c) while blue voxels denote negatively correlated activation (b, d). Note that for the visual task the slices for the positively correlated activation (c) and negatively correlated activation (d) were taken at different positions. The results for the positively correlated activation showed that the majority of the positively correlated activation (c) was found for tracts that were part of the splenium. Negatively correlated activation (d) was found at the position that corresponded with the optic radiation.*

optic radiations. The average percent FA-signal change, averaged over all active tracts of all subjects were 0.98% and -1.40%, for the tactile positive and negative correlating tracts, and 1.06%, and -1.45%, for the visual positive and negative correlating tracts, respectively. The results for the average percent signal change for the same set of active tracts computed for the radial diffusivity was: -1.49%, 1.91%, -1.38%, 1.34%. For the parallel diffusivity the average percent signal change was: 0.39%, -0.44%, 0.27%, -0.47% and for the mean diffusivity: -0.03%, 0.08%, -0.21%, 0.04%. Note that the average percent signal changes for radial diffusivity and parallel diffusivity have opposite signs leading to reduced signal changes in mean diffusivity as the radial diffusivity and parallel diffusivity changes partially cancel each other out.

The results of the time course experiment showed that with the same stimulus length for the tactile task and the visual task the signal maximum was reached at 78 seconds and 98 seconds, respectively (**Figure 4**).
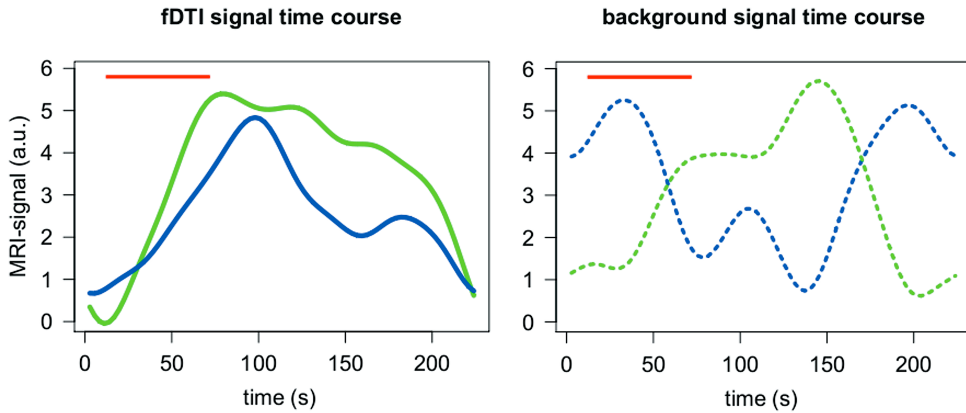
fDTI signal time course

background signal time course

Figure 4. *Time course experiment. The time courses of the diffusion weighted MRI signal for the visual and the tactile task measured perpendicular to the tract's main direction using a single stimulus. An increase in glial cell volume is expected to lead to an increase of the measured signal. The tactile and the visual stimulus period (red horizontal line) started at t = 12 s and ended at t = 72 s. a) The results represent the averages of 15 measurements (3 subjects; 5 measurements per subject) smoothed using a Gaussian kernel with sigma=14 s. For the tactile stimulus (green) the maximum signal was found at t = 78 s. For the visual stimulus (blue) the maximum signal was found at t = 98 s. b) The averages of the signals of the background voxels that were used to correct for global signal variations (dashed blue line for the visual task and green dashed line for the tactile task). Note that these signals were independently scaled for visualization.*

Discussion

In this study we present a method to measure task-related FA changes hypothesized to reflect white matter activity in the human brain. We found expected activation patterns of white matter tracts for both the tactile and the visual task albeit that for the visual task the correlation between signal change and task appears to be reversed. During the tactile task the sensory thalamocortical tract was active while the optic radiation was active during the visual task. These white matter tracts were expected to become active based on their anatomical connections with the sensory and occipital cortices, which are gray matter areas known to be involved in tactile and visual tasks.

In the tactile task the majority of the subjects showed the expected tactile task-specific white matter activation patterns. Positively correlated activation was found for the left sensory thalamocortical tract. The negatively correlated activation that was found in the ipsilateral sensory thalamocortical tract may reflect a suppression of inputs from the opposite hand as reported earlier during fMRI experiments (Blankenburg et al., 2003; Iguchi et al., 2005).

In the visual task, the majority of subjects showed positively correlated active callosal tracts connecting homotopic visual regions (Brandt et al., 2000) crossing the splenium as well as positively activated tracts in the frontal region. However, because

similar activation patterns were found for the results of the tactile experiment we must consider the possibility that these activation patterns are not directly linked to the visual stimulus. Activation of the optic nerve was less likely to be detected because of known large susceptibility artifacts at the base of the brain. The most prominent activation, as expected, was along the optic radiation (Kandel, 2000).

The majority of subjects showed negatively correlated activation in the optic radiation but deactivation of the optic radiation (**Figure 3d**) is less likely during a visual task. If, however, the underlying contrast mechanism does have a slow varying response function, as is suggested by the time course experiment, a more plausible explanation would be that this reversal of the sign of the activation actually reflects a difference in time course of the measured signal for the tactile and visual task. This could possibly be due to the checkerboard stimulus being perceived as a more intense stimulus than the tactile stimulus. Such an intensity difference could lead to differences in the time needed for the measured signal to reach its maximum or to return to baseline. Indeed the results of the time course experiment (**Figure 4**) suggest a difference in when the signal maximum is reached. For the tactile task the maximum signal is reached at 78 seconds, almost directly after the end of the stimulation period. The maximum signal for the visual task however is reached at 98 seconds. Thus for checkerboard stimulation experiments using stimulation and resting periods of 60 seconds, the signal maximum of a stimulation period is not reached within the stimulation period itself but well within the subsequent resting period. The substantial lag between the end of the checkerboard stimulus and the signal maximum could therefore result in an anti-correlation between the task and the measured fDTI signal resulting in negative activation. This because, for visual stimuli, the period of acquisition of the diffusion weighted volumes (b1000) (see **Figure 1e**) of the resting period is now positioned more closely in time to the (delayed) signal maximum (**Figure 1e** blue arrow) than the b1000 of the stimulus period itself.

Our fDTI method is based on the assumption that changes in FA are a sign of local fiber activity. At this point the biophysical underpinning of the measured fDTI signal is not known. Several different physiological processes that are part of (or accompany) fiber activity could, in theory, alter the diffusion profile and therefore the measured FA value. For instance, a possible mechanism that could change the shape of the ECS and therefore the measured FA value is activity-related swelling of glial cells (Anderson et al., 1996). As a result of neural fiber activity, the level of potassium (K+) in the ECS increases (for sensory stimulation up to 0.4 mM and for visual stimulation up to 1 mM (Sykova and Chvatal, 2000; Coles, 2005)) and leads to cell swelling of its surrounding glial cells (particularly oligodendrocytes and fibrous astrocytes). This glial cell swelling would then lead to anisotropic changes of the ECS in white matter (Ransom et al., 1985; Sykova, 2004). Such an anisotropic change of the ECS could result in a measurable increase in FA because DTI with a diffusion weighting and echo time as used in this study (b-factor = 1000 s/mm^2, TE = 74 ms) is believed to be primarily sensitive to the diffusion of water in the ECS (Clark and Le Bihan, 2000). Indeed, changes in the diffusion profile due to changes of the ECS in white matter have been shown *in vitro* using diffusion weighted imaging in the rat optic nerve (Anderson et al., 1996). In that study a larger relative decrease in diffusivity was

found in the radial direction than in the parallel direction as is reflected by an increased FA value. Also it was shown that the time required for full glial cell swelling may involve tens of seconds or longer, depending on the strength of the stimulus (Ransom et al., 2000; Sykova, 2004). Intrinsic optical signal (IOS) measurements during electrical stimulation of the rat optic nerve (MacVicar et al., 2002) showed a response function that was in the order of tens of seconds and was interpreted as a decrease of ECS volume due to glial cell swelling. Interestingly, the measured IOS signal continuously increased during the stimulation period and reached its maximum well after the end of the stimulus period similar to the results of our time course experiment. This similarity in time course suggests that glial cell swelling could indeed be one of the underlying physiological mechanisms that is responsible for the measured FA-signal change. Considering their results a coarse estimate can be made indicating that an increase of the concentration of K+ in the ECS with 1 mM would lead to a decrease of the ECS in the order of 1%. But how this 1% decrease relates to changes in the measured FA value is very difficult to determine because the relation between the measured diffusivity and ECS volume is not well understood (Sykova, 2004; Chvatal et al., 2007).

Recent findings indicate that elevated levels of K+ in the ECS not only result in volumetric changes but also result in complex morphological changes of astrocytes (Sykova et al., 2003; Pangrsic et al., 2006; Chvatal et al., 2007; Neprasova et al., 2007; Stroman et al., 2008). If glial cell swelling is the underlying mechanism of the signal changes measured in this study then an overall decrease of the measured diffusion profile (the mean diffusivity) would be expected. However, if morphological changes of glial cells underlie the measured signal changes then changes in the shape of the diffusion profile (reflected by the FA) would be more probable than changes in mean diffusivity. The results of the average percent FA-signal change and the average percent signal change in mean diffusivity do suggest that morphological glial cell changes are more likely to be responsible for the measured signal changes measured in this study than glial cell swelling because the changes in FA were larger than the changes in mean diffusivity.

In gray matter an activity-related increase in blood flow in the capillaries can be detected with intravoxel incoherent motion (Le Bihan et al., 1986). Although intravoxel incoherent motion typically uses moderate diffusion weighting (up to b = 700 s/mm^2) it was suggested (Harshbarger and Song, 2006) that even with stronger diffusion gradients as used in this study (b = 1000 s/mm^2) changes in blood flow in the smallest capillaries could still contribute to the measured MRI signal. If the capillaries in white matter have a preferential direction then the changes in blood flow within a voxel may be anisotropic and alter the shape of the diffusion profile, which would be reflected by a change in FA.

Another possible mechanism, closely linked to changes in blood flow, that could lead to changes in FA would be an activity-related increase in microvascular blood volume (Lu et al., 2003). An increase in blood volume within a voxel would result in a decrease of the volume of the white matter's parenchyma in that voxel (Lu et al., 2003) hence reducing the fraction of tissue that is responsible for the measured anisotropy with DTI. In addition, the dilatation of the blood vessels may result in an anisotropic shape change of the extra-cellular space (ECS).

Changes in the level of blood oxygenation resulting in changes in local susceptibility (which is the contrast mechanism of BOLD-fMRI) could also alter the FA value. If the microvascular system in white matter has a preferential direction within a voxel then anisotropic task-related changes in susceptibility could potentially contribute to the measured FA-signal change, as was shown in a computer simulation (Richard P. Kennan, 1995). However, the effect of possible task-related anisotropic susceptibility changes on the FA measurements is probably limited. If the capillary bed in white matter has a preferential direction, then task-related changes in susceptibility will be very small in all tracts for which the preferential direction of the capillary bed runs parallel to the main magnetic field. This because a change in the level of blood oxygenation in capillaries running parallel to the main magnetic field does not lead to changes in susceptibility (Norris, 2001). But the results of the fDTI experiments showed active tracts in all major directions. If task-related anisotropic susceptibility changes do substantially contribute to the measured FA-signal changes then one would expect that no active tracts were found in at least one of the major directions.

The last three possible mechanisms are all based on microvascular changes. Using a two-compartment model (Harshbarger and Song, 2006) we estimated that in the fDTI experiment the maximum activity-related signal changes by blood volume changes is 0.5% for radial diffusivity and for parallel diffusivity -0.72%. These results show that for parallel diffusivity the task-related signal changes could, in theory, be explained by activity-related blood volume changes. However, for radial diffusivity the maximum possible task-related signal change induced by the changes in blood volume are about three times smaller than the measured average percent FA-signal change. This suggests that the measured signal changes cannot be explained by microvascular changes alone and that other contrast mechanisms are responsible for the major part of the measured signal change.

The order of the acquisition of the different diffusion weighted volumes of a single DTI scan may affect the measurements due to the slow varying time course of the measured signal. Although the ordering itself could not be responsible for the measured FA-signal change (as the ordering of the different diffusion directions is identical for the DTI scans collected during rest as for the DTI scans collected during stimulation) it may introduce different sensitivities in different directions. In future experiments the influence of such possible order-specific effects could be reduced by using a round robin scheme for the diffusion gradients of consecutive DTI scans.

The sheer presence of a person at the entrance of the MRI bore (e.g. to apply the tactile stimulus) can lead to changes in the experienced main magnetic field strength within the scanner's field of view. However, it is not likely that these changes influence the measurements because the FA is a relative measure and these changes do not occur within a single fDTI acquisition.

Although the results of the time course experiment suggest the need for different timing parameters for different types of single stimulus intervals, it does not provide information on possible saturation effects in the case when repetitive stimulation periods are used. For glial cell swelling for example, saturation effects may be due to a resting period that is too short to allow the glial cells to shrink to their normal size. Additional

experiments are needed to study the fDTI signal during repetitive stimulation to optimize the experimental design.

The results of the fDTI method are to a large extent determined by the quality of the conventional DTI scan and the applied fiber tracking algorithm. For instance, it is known that sensory information enters the thalamus via the ventral spinothalamic fasciculus and is then projected via the thalamus onto the sensory cortex via the sensory thalamocortical tract. However, results for the tactile task show some active tracts that appear to start in the thalamus and run into the sensory cortex as expected, while other tracts appear to originate in the pons, passing the thalamus and run directly towards the sensory cortex. The latter tracts could be the result of the fiber tracking algorithm erroneously combining separate fibers (in this case tracts from the spinothalamic fasciculus and sensory thalamocortical tract) into one single tract. Besides erroneously combining separate tracts, the erroneously splitting of one tract into parts also occurs. For instance, fiber tracking algorithms utilizing the single tensor model cannot adequately reconstruct crossing fibers (Mori and van Zijl, 2002). Even if all constituent (separate) parts of a set of crossing active fibers were successfully reconstructed, these parts may be too short and therefore insufficiently profit from the increased sensitivity of the tract-based statistics approach to be marked as active. The number of false negatives of the fDTI method is therefore directly related to the quality of the fiber tracking algorithm used.

One of the limitations of this study is the relatively large voxel size used (64 mm^3 in the fDTI experiment) which leads to considerable partial voluming. This limits the detection of tract activation to the major tracts such as the optic radiation and the sensory thalamocortical tract. The latter, for instance, has a diameter of several millimeters (Hardy et al., 1980; Zarei et al., 2007).

The sign-test, the statistical test used in this study to test for tract activation, is a non-parametric statistical test that ignores the size of the measured differences between active and rest conditions and only takes the signs of these differences into account. This is an important feature of the sign-test as the FA value along a fiber tract will vary considerably and the sizes of the task-related FA signal changes at different levels of FA values are incomparable. An important aspect of tract-based analysis is that all direct comparisons of FA signals (when the FA-signal changes are encoded into a series of '+'s and '-'s) are done within a voxel where the FA signals for task and rest conditions will be of similar magnitude. As the sign-test limits the effect of possible outliers it is very robust in the sense that tracts will not be considered active based on the FA signal behavior of a few voxels alone (See **Figure 5**). This reduces the chance of finding spurious active tracts, which is important because the aim of this study was to show that the fDTI method can successfully be applied to detect activation of white matter tracts. Moreover, we applied the conservative Bonferroni correction for multiple testing thereby assuming that each test for fiber activation is an independent test. However, this is not the case as fibers may (partly) overlap and as a consequence the Bonferroni correction is too conservative. On the other hand the degrees of freedom for the sign-test are based on the assumption that the signals of neighboring voxels are independent and a violation of this assumption may lead to an

overestimation of fiber activation. Further research is needed to obtain a better estimate of the required correction factor for multiple testing.
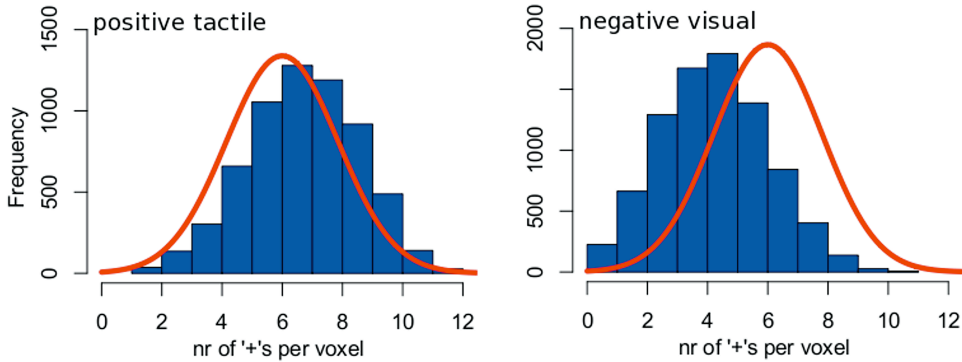

Figure 5. *Histogram distributions of voxels that are part of active fibers. Here two histograms are shown of the number of '+'s per voxel, for all voxels along active fiber tracts, separately for positive correlation and negative correlation, combined for all subjects. In the case that there would not be an activity-related signal change, the distribution of +'s in these voxels would follow a normal distribution (solid red line). If only a small group of voxels (the active voxels) is responsible for a tract to be considered active then these voxels must show a high correlation (i.e. a high number of +'s) with the task while the distribution of +'s of the other (non-active) voxels that are part of the active tract would remain unchanged. This would result in a histogram built up from a large and a small normal distribution. The large group of non-active voxels would produce the original (large) normal distribution (solid red line) while the small group of active voxels would produce a second smaller distribution left (negative correlation) or right (positive correlation) from the original distribution. However, if not a small group but the majority of the voxels along the active fibers belong to the set of active voxels, one would expect a single normal distribution which is shifted to left (negative correlation) or to the right (positive correlation). Left, the histogram for the (positive) active voxels for the tactile task is shown while on the right side the histogram for the (negative) active voxels of the visual task is shown. Both histograms appear to follow a single normal distribution but are shifted to the right (positive correlation with tactile task) or to the left (negative correlation with visual task). This suggests that the task-related signal changes found with fDTI indeed occur along large parts of the fibers and are not confined to small parts of the fibers.*

To make sure that these findings do not depend on the choice of a particular statistical analysis method used the data was also analyzed using parametric statistics. In this analysis conventional t-statistics as in ROI/VOI based fMRI (here a VOI was defined by the voxels that were part of the tract that was tested for activation) were used. First, t-tests are used to test differences in mean FA value between active and rest conditions per voxel. Second, a t-test is used to test whether the average t-value of all voxels in the VOI (i.e. the tract to be tested for activation) is significantly greater than - or smaller than zero. In that case the tract is considered to show a positive correlation or negative correlation, respectively. Note, that in this particular case we conduct a t-statistic over t-values and not a t-statistic over b-values because at this stage we only want to establish tract activation. The results of this

analysis did not change our findings. In **Figure 6** the results of the analyses based on the sign test as well as on parametric statistics are shown for a single subject.

It was shown that the FA measure is robust against noise induced bias for higher values (FA > 0.4) but it is not rotationally invariant when 6 different diffusion gradients are used (here used in fDTI data acquisition) (Skare et al., 2000). Possible effects of this rotational dependency on the fDTI results are expected to be very limited because deviations due to this dependency form a constant factor within a voxel over the subsequent rest and task conditions (assuming no gross subject motion).

In conclusion, we propose a noninvasive method to identify white matter tract activation *in vivo*. Active tracts were identified using a tract-based statistical analysis. The results of the experiments indicate that the task-related FA signal changes can be detected but have a low temporal resolution (tens of seconds), which is in line with previously reported results of glial cell swelling in white matter. Furthermore the results suggest that there may be a relation between the time the signal reaches its maximum and the intensity of the presented stimuli. The low temporal resolution as well as the possible dependency on stimulus intensity should be to taken into account in the design of future experiments. We believe that the fDTI method may become a valuable tool to study the brain's active connections that could help us to get a better understanding of the functional architecture of the neural networks in the human brain.
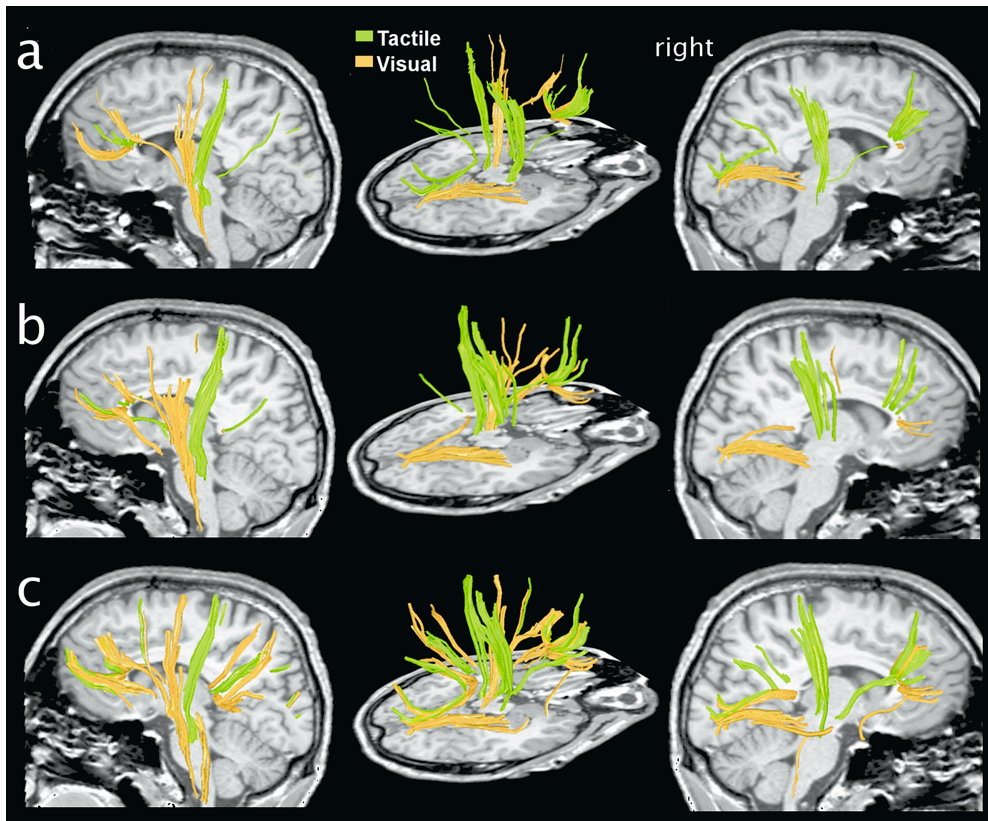
Figure 6*. Positively correlated fDTI results for subject #5 computed in three different ways. (a) The original active tracts found based on changes in FA using the sign-test (See Figure 1). (b) Analysis of the same data set using conventional t-statistics as in ROI/VOI based fMRI. For each voxel in the fDTI scan a multiple regression was carried out. Two regressors were used, one encoding for the stimulus (0/1) and the other representing possible linear scanner drift. Each tract that was tested for activation was considered active if the mean of the stimulus regressor values of the voxels in the tract was found significantly higher than zero using a one-sided Student's t-test (p < 0.05; Bonferroni corrected for the number of tested tracts). (c) Active tracts based on changes in the radial diffusion component using the sign-test. The three different methods yielded very similar activation patterns. The similar results for (a) and (b) indicate that the results do not depend on the chosen statistical method. The similar results for (a) and (c) indicate that the measured signal change stems predominantly from a change in diffusion in the radial direction.*

References

Anderson AW, Zhong J, Petroff OA, Szafer A, Ransom BR, Prichard JW, Gore JC (1996) Effects of osmotically driven cell volume changes on diffusion-weighted imaging of the rat optic nerve. Magn Reson Med 35:162-167.

Armitage P, Berry G, Matthews JNS (2002) Statistical Methods in Medical Research, fourth Edition. Malden: Blackwell Science.

Bammer R, Augustin M, Strasser-Fuchs S, Seifert T, Kapeller P, Stollberger R, Ebner F, Hartung HP, Fazekas F (2000) Magnetic resonance diffusion tensor imaging for characterizing diffuse and focal white matter abnormalities in multiple sclerosis. Magn Reson Med 44:583-591.

Basser PJ, Pierpaoli C (1996) Microstructural and physiological features of tissues elucidated by quantitative-diffusion-tensor MRI. J Magn Reson B 111:209-219.

Basser PJ, Mattiello J, LeBihan D (1994) Estimation of the effective self-diffusion tensor from the NMR spin echo. J Magn Reson B 103:247-254.

Beshay JE, Hahn P, Beshay VE, Hargittai PT, Lieberman EM (2005) Activity-dependent change in morphology of the glial tubular lattice of the crayfish medial giant nerve fiber. Glia 51:121-131.

Blankenburg F, Taskin B, Ruben J, Moosmann M, Ritter P, Curio G, Villringer A (2003) Imperceptible stimuli and sensory processing impediment. Science 299:1864.

Brandt T, Stephan T, Bense S, Yousry TA, Dieterich M (2000) Hemifield visual motion stimulation: an example of interhemispheric crosstalk. Neuroreport 11:2803-2809.

Catani M, Ffytche DH (2005) The rises and falls of disconnection syndromes. Brain. 128:2224-2239.

Chvatal A, Anderova M, Hock M, Prajerova I, Neprasova H, Chvatal V, Kirchhoff F, Sykova E (2007) Three-dimensional confocal morphometry reveals structural changes in astrocyte morphology in situ. J Neurosci Res 85:260-271.

Clark CA, Le Bihan D (2000) Water diffusion compartmentation and anisotropy at high b values in the human brain. Magn Reson Med 44:852-859.

Coles JA, Deitmer JW (2005) Extracellular potassium and pH: homeostasis and signaling. In: Neuroglia (Kettenmann H, Ransom BR, ed). Oxford: Oxford University Press.

Collins DL, Holmes CJ, Peters TM, Evans AC (1995) Automatic 3-D model-based neuroanatomical segmentation. Human Brain Mapping 3:190-208.

Conturo TE, Lori NF, Cull TS, Akbudak E, Snyder AZ, Shimony JS, McKinstry RC, Burton H, Raichle ME (1999) Tracking neuronal fiber pathways in the living human brain. Proc Natl Acad Sci U S A 96:10422-10427.

Donahue MJ, Lu H, Jones CK, Edden RA, Pekar JJ, van Zijl PC (2006) Theoretical and experimental investigation of the VASO contrast mechanism. Magn Reson Med 56:1261-1273.

Gulani V, Iwamoto GA, Lauterbur PC (1999) Apparent water diffusion measurements in electrically stimulated neural tissue. Magn Reson Med 41:241-246.

Hardy TL, Bertrand G, Thompson CJ (1980) Organization and topography of sensory responses in the internal capsule and nucleus ventralis caudalis found during stereotactic surgery. Appl Neurophysiol 42:335-351.

Harshbarger TB, Song AW (2006) Endogenous functional CBV contrast revealed by diffusion weighting. NMR Biomed 19:1020-1027.

Hulshoff Pol HE, Schnack HG, Mandl RC, Cahn W, Collins DL, Evans AC, Kahn RS (2004) Focal white matter density changes in schizophrenia: reduced inter-hemispheric connectivity. Neuroimage 21:27-35.

Iguchi Y, Hoshi Y, Tanosaki M, Taira M, Hashimoto I (2005) Attention induces reciprocal activity in the human somatosensory cortex enhancing relevant- and suppressing irrelevant inputs from fingers. Clin Neurophysiol 116:1077-1087.

Jones DK, Simmons A, Williams SC, Horsfield MA (1999) Non-invasive assessment of axonal fiber connectivity in the human brain via diffusion tensor MRI. Magn Reson Med 42:37-41.

Kandel ER, Schwartz, J.H., and Jessell, T.M. (2000) Principles of Neural Science, 4th Edition: McGraw-Hill Inc.

Le Bihan D, Urayama SI, Aso T, Hanakawa T, Fukuyama H (2006) Direct and fast detection of neuronal activation in the human brain with diffusion MRI. Proc Natl Acad Sci U S A. 103:8263-8268.

Le Bihan D, Breton E, Lallemand D, Grenier P, Cabanis E, Laval-Jeantet M (1986) MR imaging of intravoxel incoherent motions: application to diffusion and perfusion in neurologic disorders. Radiology 161:401-407.

Lu H, Golay X, Pekar JJ, Van Zijl PC (2003) Functional magnetic resonance imaging based on changes in vascular space occupancy. Magn Reson Med 50:263-274.

MacVicar BA, Feighan D, Brown A, Ransom B (2002) Intrinsic optical signals in the rat optic nerve: Role for K+ uptake via NKCC1 and swelling of astrocytes. Glia 37:114-123.

Mesulam M (2005) Imaging connectivity in the human cerebral cortex: the next frontier? Ann Neurol 57:5-7.

Miller KL, Bulte DP, Devlin H, Robson MD, Wise RG, Woolrich MW, Jezzard P, Behrens TE (2007) Evidence for a vascular contribution to diffusion FMRI at high b value. Proc Natl Acad Sci U S A 104:20967-20972.

Mori S, van Zijl PC (2002) Fiber tracking: principles and strategies - a technical review. NMR Biomed 15:468-480.

Mori S, Crain BJ, Chacko VP, van Zijl PC (1999) Three-dimensional tracking of axonal projections in the brain by magnetic resonance imaging. Ann Neurol 45:265-269.

Neprasova H, Anderova M, Petrik D, Vargova L, Kubinova S, Chvatal A, Sykova E (2007) High extracellular K(+) evokes changes in voltage-dependent K(+) and Na (+) currents and volume regulation in astrocytes. Pflugers Arch 453:839-849.

Nonaka H, Akima M, Hatori T, Nagayama T, Zhang Z, Ihara F (2003) Microvasculature of the human cerebral white matter: arteries of the deep white matter. Neuropathology 23:111-118.

Norris DG (2001) The effects of microscopic tissue parameters on the diffusion weighted magnetic resonance imaging experiment. NMR Biomed 14:77-93.

Pangrsic T, Potokar M, Haydon PG, Zorec R, Kreft M (2006) Astrocyte swelling leads to membrane unfolding, not membrane insertion. J Neurochem 99:514-523.

Prichard JW, Zhong J, Petroff OA, Gore JC (1995) Diffusion-weighted NMR imaging changes caused by electrical activation of the brain. NMR Biomed 8:359-364.

Ransom BR, Yamate CL, Connors BW (1985) Activity-dependent shrinkage of extracellular space in rat optic nerve: a developmental study. J Neurosci 5:532-535.

Ransom CB, Ransom BR, Sontheimer H (2000) Activity-dependent extracellular K+ accumulation in rat optic nerve: the role of glial and axonal Na+ pumps. J Physiol 522 Pt 3:427-442.

Richard P. Kennan JZaJCG (1995) Effects of Magnetic Susceptibility Variations on the Apparent Diffusion Measured by NMR. In: Diffusion and perfusion magnetic resonance imaging: applications to functional MRI (Bihan DL, ed), pp 110-121. New York: Raven Press Ltd.

Skare S, Li T, Nordell B, Ingvar M (2000) Noise considerations in the determination of diffusion tensor anisotropy. Magn Reson Imaging 18:659-669.

Sommer IEC, Ramsey NF, Mandl RCW, Van Oel CJ, Kahn RS (2004) Language activation in monozygotic twins discordant for schizophrenia. British Journal of Psychiatry 184:128-135.

Stroman PW, Lee AS, Pitchers KK, Andrew RD (2008) Magnetic Resonance Imaging of Neuronal and Glial Swelling as an Indicatior of Function in Cerebral Tissue Slices. Magnetic Resonance in Medicine 59:700-706.

Sykova E (2004) Extrasynaptic volume transmission and diffusion parameters of the extracellular space. Neuroscience 129:861-876.

Sykova E, Chvatal A (2000) Glial cells and volume transmission in the CNS. Neurochem Int 36:397-409.

Sykova E, Vargova L, Kubinova S, Jendelova P, Chvatal A (2003) The relationship between changes in intrinsic optical signals and cell swelling in rat spinal cord slices. Neuroimage 18:214-230.

Wright IC, Rabe-Hesketh S, Woodruff PWR, David AS, Murray RM, Bullmore ET (2000) Meta-analysis of regional brain volumes in schizophrenia. American Journal of Psychiatry 157:16-25.

Zarei M, Johansen-Berg H, Jenkinson M, Ciccarelli O, Thompson AJ, Matthews PM (2007) Two-dimensional population map of cortical connections in the human internal capsule. J Magn Reson Imaging 25:48-54.

Chapter 4

Chapter 5

Functional diffusion tensor imaging at 3 Tesla

René C. W. Mandl, Hugo G. Schnack, Marcel P. Zwiers, René S. Kahn and Hilleke E. Hulshoff Pol

Abstract

In a previous study we reported on a noninvasive functional diffusion tensor imaging (fDTI) method to measure neuronal signals directly from subtle changes in fractional anisotropy along white matter tracts. We hypothesized that these fractional anisotropy changes relate to morphological changes of glial cells induced by axonal activity. In the present study we set out to replicate the results of the first fDTI study using an improved fDTI scan acquisition scheme at a higher MRI field strength. A group of twelve healthy participants were scanned on a 3 Tesla MRI scanner revealing activation in the contralateral thalamo-cortical tract and optic radiations during tactile and visual stimulation, respectively. These activation patterns were very similar to the activation patterns found in the first fDTI experiment at 1.5 Tesla using the same types of stimuli. Moreover, these results support the notion of different response functions for tactile and visual stimuli. The results suggest that the non-invasive fDTI method is robust enough to study the functional neural networks in the human brain within a clinically feasible time period.

Neurobehavioral functions depend on a dynamic flow of information between different gray matter brain regions that are interconnected via white matter pathways (Catani and Ffytche, 2005; Mesulam, 2005). Activation in gray matter regions of the human brain have been extensively studied with neuroimaging techniques such as functional magnetic resonance imaging (fMRI), positron emission tomography (PET), single photon emission computed tomography (SPECT), electro-encephalography (EEG) and magneto-encephalography (MEG). However, these techniques do not provide any information on the white matter pathways and their corresponding activity. Imaging techniques such as diffusion tensor imaging (DTI) (Le Bihan et al., 1986; Basser et al., 1994) in combination with fiber tracking (Conturo et al., 1999; Jones et al., 1999; Mori and van Zijl, 2002) allow us to non-invasively study the anatomy of these pathways. However, these techniques do not provide information on the pathways' activity. In a recent study (Mandl et al., 2008) we proposed a non-invasive functional diffusion tensor imaging (fDTI) method that has the potential to detect white matter tracts that are active during neurobehavioral functioning. In that first fDTI study, eight healthy participants were scanned on a 1.5 Tesla scanner during a tactile experiment and a visual experiment to assess the validity of the fDTI method. The results of these experiments revealed activation in the contralateral thalamo-cortical tract and optic radiations during tactile and visual stimulation, respectively. Furthermore, the results not only suggested a slow varying response function for both the tactile and visual stimuli but also that these response functions are different for the different types of stimuli. fDTI is based on the assumption that changes in fractional anisotropy (Basser and Pierpaoli, 1996) (FA) are a sign of local fiber activity. We hypothesized that morphological changes of glial cells (e.g. oligodendrocytes) lead to shape changes of the extra-cellular space (ECS) (Ransom et al., 1985; Sykova, 2004; Beshay et al., 2005) and, in turn, lead to a measurable increase in FA. Indeed, changes in the diffusion profile due to changes in the ECS in white matter have been shown *in vitro* using diffusion weighted imaging in the rat optic nerve (Anderson et al., 1996). An earlier study (Prichard et al., 1995) reported that electrical stimulation induced significant changes in the diffusion properties of brain tissue in rats. Using intrinsic optical imaging (MacVicar et al., 2002) slowly varying activity-related signal changes were measured in the rat optical nerve, which were attributed to glial cell swelling. However, a study using the real-time tetramethylammonium (TMA+) iontophoretic method in combination with intrinsic optical imaging (Sykova et al., 2003) showed that the concentration of TMA+ in the extra-cellular space (ECS) did not change although similar changes in the intrinsic optical imaging signal were measured. Therefore the authors concluded that it was unlikely that glial cell swelling was the primary mechanism for these intrinsic optical signal changes and they suggested that a more plausible explanation may be found in morphological changes of glial cells. The first fDTI results (Mandl et al., 2008) support this conclusion as the FA-signal changes in the active tracts measured in that study were due to opposite changes in parallel and transverse diffusion coefficients which (for a large part) cancel each other out leading to only small changes in mean diffusivity. If cell swelling was the underlying mechanism for the measured FA-signal changes then an overall reduction in mean diffusivity (MD) is expected because cell swelling would result in a decrease in both transverse and parallel diffusivity

in the active conditions. A recent study (Stroman et al., 2008) showed that increased levels of potassium lead to changes in both intrinsic optical signal values and MRI proton density measurements for gray and subcortical white matter in rats, suggesting that activity-related changes in the ECS of gray matter as well as white matter can be measured using MRI. Normal activity-induced ECS changes, however, are expected to be very small as compared to the physiological noise (Gulani et al., 1999) and a reliable detection of the signal change would require a large number of measurements. In the fDTI method we assume that these activity-related glial shape changes extend over the entire active fiber so that a substantial increase in signal-to-noise ratio can be achieved by pooling the signal changes over the complete tract. It is the adoption of a tract-based statistics - rather than a voxel-based statistics - that enables us to measure the signal within a practically feasible time period.

In the present study we used visual and tactile stimuli on a 3 Tesla MRI scanner. For white matter voxels that are part of an active tract, we expected that the FA was higher during the active condition than during the rest condition, thus showing a positive correlation with the task. For the tactile task, activation was expected for the afferent fibers of the thalamo-cortical tracts that connect the thalamus and the contralateral primary sensory area (Kandel, 2000). For the visual task, activation was expected mainly for fibers that are bilaterally part of the optic radiation (Kandel, 2000).

Materials and methods

The principle of the fDTI method as applied in this study is outlined in **Figure 1**. Twelve healthy subjects participated in this study. All experiments presented in this study were approved by the medical ethical committee for human subjects of the University Medical Center Utrecht, the Netherlands, and all subjects signed written informed consent prior to participation. For the tactile stimulus experiment the participants were instructed to keep their eyes closed for the duration of the whole experiment. During the active condition, the palm and fingers of the subject's right hand were brushed in a random fashion by an investigator. For the visual stimulus experiment the subjects were instructed to look at a red fixation cross that was projected on the center of a screen visible from inside the scanner at all times. During the active condition a red and green checkerboard was shown that alternated at a frequency of 8 Hertz.

fDTI acquisition refinements

In the present study we utilized an fDTI acquisition scheme that was improved in several ways to increase specificity by further excluding possible confounding factors (the time settings of this acquisition scheme are detailed in **Figure 2**). (1) We optimized the time settings separately for the tactile stimulus and the visual stimulus because the results of the previous study suggested a considerable time lag in the order of tens of seconds for the visual stimulus, which was not found for the tactile stimulus (**Figure 2a**). (2) For each type of stimulus, scan slice directions were chosen perpendicular to the expected active tracts in
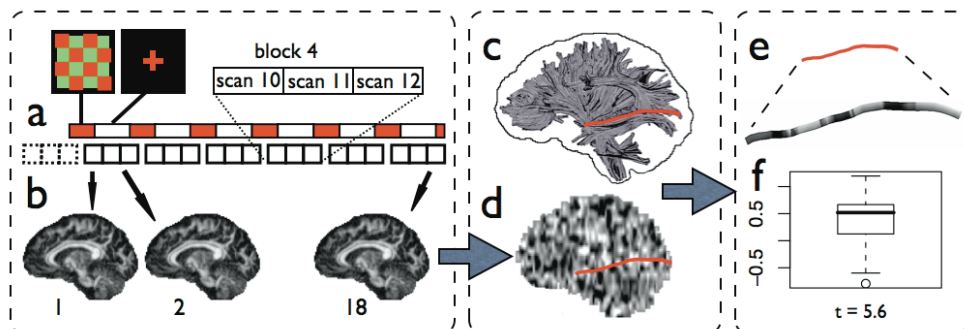
Figure 1. *The fDTI method (visual experiment) a) In the fDTI experiment 1+6 blocks of 3 DTI scans are acquired. The first block (dashed lines) is a dummy block added to correct for possible scanner onset effects and is disregarded in the further analysis. The necessity for the lag between task and scans is explained in Figure 2. For each of the 18 DTI scans an FA map is computed (b). A statistical parameter map (SPM) is computed (d) on the FA maps using a general linear model. Fiber tracts are reconstructed for the complete brain (c) and, for each tract, the t-values found in the SPM along that tract were grouped into a single set of t-values (e). For each tract a statistical test (student's t-test) is done (f) on the set of t-values to test if the average t-value found along the tract is significantly (t > 5) greater than zero.*

order to minimize the effects of possible motion artifacts that may introduce false positives. If a slice is corrupted because of motion artifacts then for a tract that runs completely through that slice, all points are affected. In contrast, for a tract that runs in the direction perpendicular to that slice only one point is affected. Therefore, the scan slice direction was set in the transverse direction for the tactile stimulus, which is perpendicular to the thalamo-cortical tracts and for the visual stimulus the scan slice direction was set in the coronal direction, which is perpendicular to the optic radiations. (3) The voxel size was set to be anisotropic pointing into the direction of the tracts that are expected to become active in order to reduce partial voluming. (4) In the fDTI experiment 6 blocks of 3 DTI scans were acquired (**Figure 1a**) where stimulus periods (60 s) alternated with resting periods (120 s). Thus, instead of a simple on/off task-design each stimulus period was now followed by two resting periods. In this way possible effects of any periodic signal changes that are not related to the task such as cerebrospinal fluid pulsations (Kao et al., 2008) were minimized. (5) For both tactile and visual fDTI experiments the stimulus period was shifted with respect to the corresponding acquisition. Now a stimulus period starts at the middle of the last scan of a block and stops at the middle of the first scan of the consecutive block. This shift between the start of the stimulus period and the start of the DTI scan(s) associated with activation was added for two reasons. First, because of the slowly varying response function the expected signal maximum now falls in the first DTI scan period for tactile stimulus and in the middle of the first and second DTI scans for the visual stimulus. Second, effects of possible fast varying signal changes (such as signal changes due to task-

related head motion or blood oxygen-level dependent (BOLD) signal) now affect activation and rest DTI scans equally, thereby canceling each other out. Because both activation and rest DTI scans were acquired partially during an activation period (**Figure 1a**). (6) In the first fDTI study the conservative non-parametric sign-test formed the statistical basis to test for tract activation. In the present study we used the more familiar parametric t-test because the findings from the first fDTI study (Mandl et al., 2008) suggested that the usage of the t-test instead of the sign-test produces very similar results. (7) We applied a round robin scheme for the applied diffusion gradients to minimize possible systematic interaction effects between diffusion gradient directions and fiber directions that could be misinterpreted as activation.
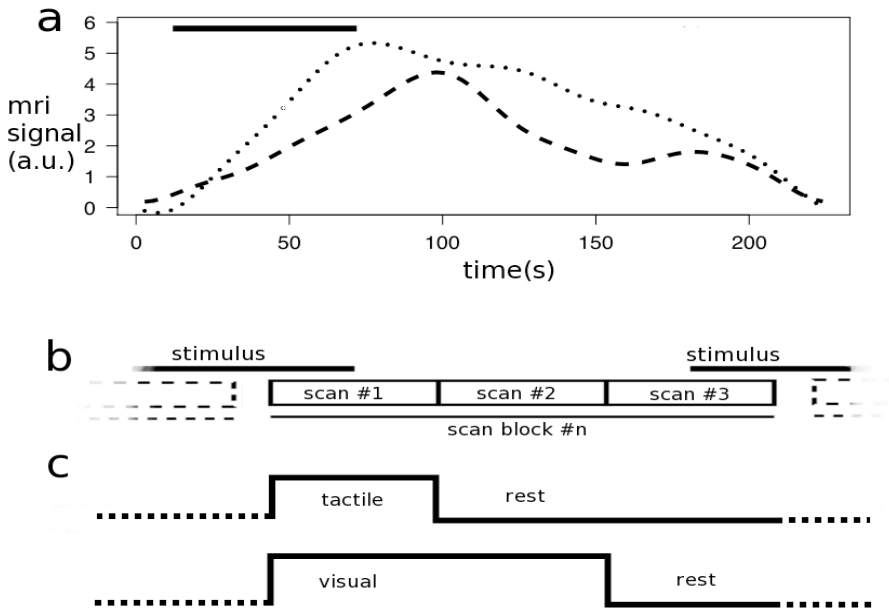

Figure 2. Response functions and task encoding. The graphs represent the time course of the measured diffusion weighted MRI signal for a single tactile stimulus (dots) and a visual stimulus (dashes) (adapted from (Mandl, et al. 2008)) and the scan in combination with a scan block as used in the fDTI experiment. (a) Both the tactile stimulus and visual stimulus (bar) started after 12 s with a duration of 60 s. The signal during the stimulus is constantly increasing (reflecting a reduction in diffusivity in the transverse direction of the tract). (b) The results of the response function experiment show that the maximum of the response function (dotted line) for the tactile stimulus (bar) falls within the first scan of a scan block while the maximum of the response function (dashed line) of the visual stimulus is found between the first and second scan. (c) Therefore in the tactile fDTI experiment the first scan is contrasted against the second and third scan, while for the visual fDTI experiment the first and second scan are contrasted against the third scan.

Scan acquisition parameters

For each experiment a separate T1-weighted scan, two conventional high-resolution DTI scans, and an fDTI scan were acquired. All scans were acquired on a Philips Achieva 3 Tesla whole-body MR scanner (Intera Achieva, Philips, Best, The Netherlands) using an eight-channel head coil. A sagittal 3D T1-weighted whole brain scan was acquired for anatomical reference, inter-subject registration, creation of a white matter mask and visualization of the results (acquisition matrix = 304×299×200; FOV = 240×240×160 mm; TR = 10 ms; TE = 4.6 ms; flip angle = 8 degrees; SENSE parallel imaging factor in both phase encoding directions = 1.5; total scan duration = 602 s). Next, two conventional transverse Stejskal-Tanner diffusion weighted single shot spin-echo, echo planar imaging (SS-EPI) DTI scans were acquired (FOV = 240×240 mm; 128×128 acquisition matrix; 128×128 reconstruction matrix; 2 mm slice thickness; 75 consecutive slices; flip angle = 90 degrees; TE = 68 ms; TR = 7047 ms; SENSE parallel imaging factor = 3; total scan duration = 268 s, no cardiac gating) (Mandl et al., 2008; van den Heuvel et al., 2008). The second conventional DTI scan differs from the first one in that the k-space readout direction (anterior-posterior) is reversed. These conventional DTI-scans were used for reconstruction of the tracts (**Figure 1c**). The functional time series of DTI scans (the fDTI set) were acquired during the execution of an alternating sequence of a neurobehavioral task and a resting condition. For the tactile experiment a total of seven sets of three transverse SS-EPI DTI scans (acquisition matrix = 96×96; FOV = 240 mm; 30 slices; slice-thickness = 7 mm; no gap; TE = 78 ms; TR = 6000 ms; SENSE parallel imaging factor = 3; 90 degrees flip angle; 6 non-collinear diffusion gradient directions with b-factor = 1000 s/mm^2 and 2 scans without diffusion gradients (b-factor = 0 s/mm^2); scan duration per DTI scan = 60 s) were collected. No cardiac gating was used as it would lengthen the experiments. For the visual experiment the fDTI scans were acquired in coronal direction with otherwise identical parameter settings. The first scan block is a dummy block that was added to eliminate possible scanner onset effects (e.g. gradient heating).

Table 1

	scan block 1	scan block 2	scan block 3	scan block 4	scan block 5	scan block 6
gradient 1	G(1, 0, 0)	G(0, ½√2, ½√2)	G(½√2,0, ½√2)	G(½√2, ½√2, 0)	G(0, 0, 1)	G(0, 1, 0)
gradient 2	G(0, 1, 0)	G(1, 0, 0)	G(0, ½√2, ½√2)	G(½√2, 0, ½√2)	G(½√2, ½√2, 0)	G(0, 0, 1)
gradient 3	G(0, 0, 1)	G(0, 1, 0)	G(1, 0, 0)	G(0, ½√2, ½√2)	G(½√2, 0, ½√2)	G(½√2, ½√2, 0)
gradient 4	G(½√2, ½√2, 0)	G(0, 0, 1)	G(0, 1, 0)	G(1, 0, 0)	G(0, ½√2, ½√2)	G(½√2, 0, ½√2)
gradient 5	G(½√2, 0, ½√2)	G(½√2, ½√2, 0)	G(0, 0, 1)	G(0, 1, 0)	G(1, 0, 0)	G(0, ½√2, ½√2)
gradient 6	G(0, ½√2, ½√2)	G(½√2, 0, ½√2)	G(½√2, ½√2, 0)	G(0, 0, 1)	G(0, 1, 0)	G(1, 0, 0)

G(x, y, z) is the gradient direction vector where x points in the subjects right-left direction, y points in anterior-posterior direction and z points in the inferior-superior direction. The set of six gradients is rotationally shifted by one for each subsequent scan block (i.e. a round-robin scheme).

Per scan block the order of the diffusion gradient directions was shifted in a round robin scheme (**Table 1**). For the dummy block the same ordering of the diffusion gradients was used as for the first real scan block. For each scan block one stimulus period was presented. A stimulus period started at the middle of the acquisition period of the last DTI scan of the previous scan block and stopped at the middle of the acquisition period of the first scan of the current scan block (**Figure 1a**). The subjects left the scanner room for at least 15 minutes to rest between the two experiments. The order of the fDTI experiments (first tactile then visual or vice versa) was balanced and randomized.

Fiber tracking

The two conventional DTI scans were combined to remove susceptibility-induced distortions (Andersson, et al. 2003). After correction (Andersson and Skare 2002) of the gradient-induced distortions and subject motion the diffusion tensors were computed using robust tensor estimation (Chang, et al. 2005) based on M-estimators yielding a single DTI volume. The DTI volume was used to reconstruct the fiber tracts for the whole brain with the FACT algorithm (Mori, et al. 1999). Parameter settings: minimum FA > 0.15, maximum angle between current major eigenvector and previous major eigenvector < 37 degrees, average maximum angle between current major eigenvector and major eigenvectors of neighboring voxels (R-value) < 37 degrees, minimum tract length 50 mm, number of tract starting points per voxel = 8. The fiber tracking was constrained within the white matter by using a white matter mask that was created on the T1-weighted scan using SPM2 (Wellcome Department of Cognitive Neurology, London, UK) and overlaid on the conventional DTI set. The rigid transformation needed to align the T1-weighted scan with the conventional DTI volume was computed between the T1-weighted image and the diffusion unweighted scan from the (susceptibility corrected) conventional DTI image with the ANIMAL software package (Collins, et al. 1995) using mutual information as a similarity metric.

Statistical analysis

Because the measured FA values and noise characteristics may vary considerably at different positions along a tract, the effect size of a task-related signal change is not constant for all voxels that are part of the same fiber tract. Therefore statistical tests that assume equal effect sizes for all parts of the tract are not suited to test for fiber activation. In the fDTI method the comparison between active and rest FA values is performed per voxel using a general linear model. The resulting t-value then represents the difference between activation and rest independent of the effect size. The results for all voxels together form a statistical parameter map (SPM) that is used to test for task-related fiber activation (**Figure 1d**). The computation of the SPM is described below. For each of the reconstructed fibers (**Figure 1c**) the set of t-values in the SPM that coincides with the tract is selected (**Figure 1e**) and tested whether its mean t-value is significantly greater than zero

(here we used a fixed threshold of t > 5, uncorrected) (**Figure 1g**). Because of the differences in response functions for tactile and visual stimuli, different task encoding regressors for the reconstruction of the SPM were used in the tactile and visual experiment (**Figure 2**). The first DTI scan of the scan block (activation) was compared with the second and third DTI scan (rest) for the tactile stimulus, while for the visual stimulus the first and second DTI scan of the scan block (activation) were compared to the third DTI scan (rest).

Statistical Parameter Map creation

To correct for inter-scan subject motion all different diffusion weighted and unweighted volumes were rigidly aligned (using cross-correlation as similarity metric) with their counterparts from the first DTI scan. Next, the FA maps were computed for each of the 18 registered DTI scans. For each FA time series (i.e. the FA value of a single voxel followed over time) a t-statistic was computed using a general linear model (GLM) with two regressors. The first regressor encoded for activation (activation = 1, rest = 0). The second regressor (with linear increasing values between 0 and 1) was added to correct for effects of possible scanner drift although such effects are unlikely as the FA is a relative measure. The results of the first regressor form the statistical parameter map (SPM) that is used to test for activation of the entire fiber tracts (**Figure 1d**). Realignment of the SPM with the reconstructed tracts was done using a linear transformation that was computed between the average diffusion unweighted scan of the conventional DTI scan and the average diffusion unweighted scan of fDTI set using cross-correlation as a similarity metric.

Group results

The accumulated results here were created analogue to the accumulated results presented in (Mandl, et al. 2008). In short, for each subject a binary map of the complete set of voxels that coincides with the active tracts found is placed in one common space using the linear transformation that registers the subject's anatomy scan with the Montreal Neurological Institute MNI-305 template. Each of the transformed sets is then blurred with a 3-dimensional Gaussian kernel with a full width at half maximum of 7 mm followed by a threshold at a value of 0.1 yielding a second binary map. Finally these binary maps of the subjects are accumulated and overlaid on the subjects' average anatomy. Thus the value of a (colored) voxel represents the number of subjects for which an active tract can be associated with that voxel.

Results

Figure 3 shows the active tracts found for a single subject in the tactile fDTI experiment and the visual fDTI experiment. For each task, the results of all individuals were placed in a common space to study the cumulative activation patterns (**Figure 4**). For the tactile experiment contralateral activation of the sensory thalamo-cortical tract was found. Bilateral activation was found predominantly in the optic radiations for the visual experiment as well as in the splenium of the corpus callosum. The latter contains fibers that connect homotopic visual regions. Interestingly, activation was found in the right parietal lobe (**Figure 3** and **Figure 4**). These active tracts could represent parts of the dorsal pathway (which is involved in motion detection) because of the apparent motion component of the checkerboard stimulus (Larsen, et al. 2005).

Discussion

The white matter activation patterns found in this 3 Tesla fDTI study are very similar to the activation patterns found in our first fDTI study acquired at 1.5 Tesla. For the tactile stimulus, task-related changes in FA values were found in the contralateral sensory thalamo-cortical tract while for the visual stimulus task-related changes in FA values were predominantly found in the optic radiations. This replication of our previous fDTI results on a different group of healthy participants using a different MRI scanner operating at 3 Tesla can be seen as a further indication that the fDTI method can successfully be applied to measure white matter activation.
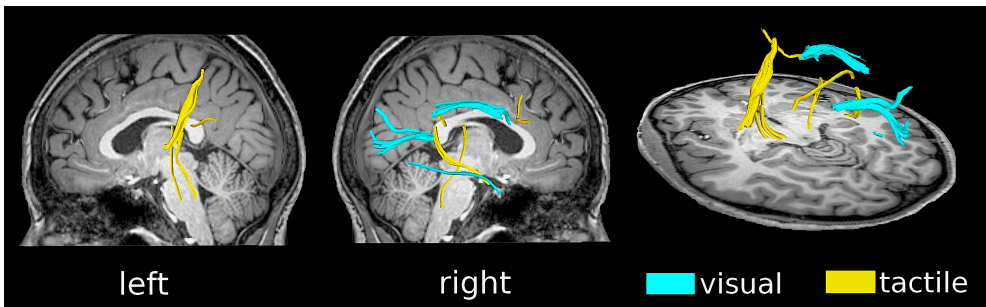
Figure 3. *fDTI results for a single subject. Tracts that were found active during the visual task (blue) and the tactile task (yellow) using the fDTI method. During the tactile task, activation was found predominantly contra-laterally for the thalamo-cortical tracts running from the thalamus to the primary sensory cortical area. Activation during the visual task was found, amongst others, for tracts that are part of the optic radiation.*
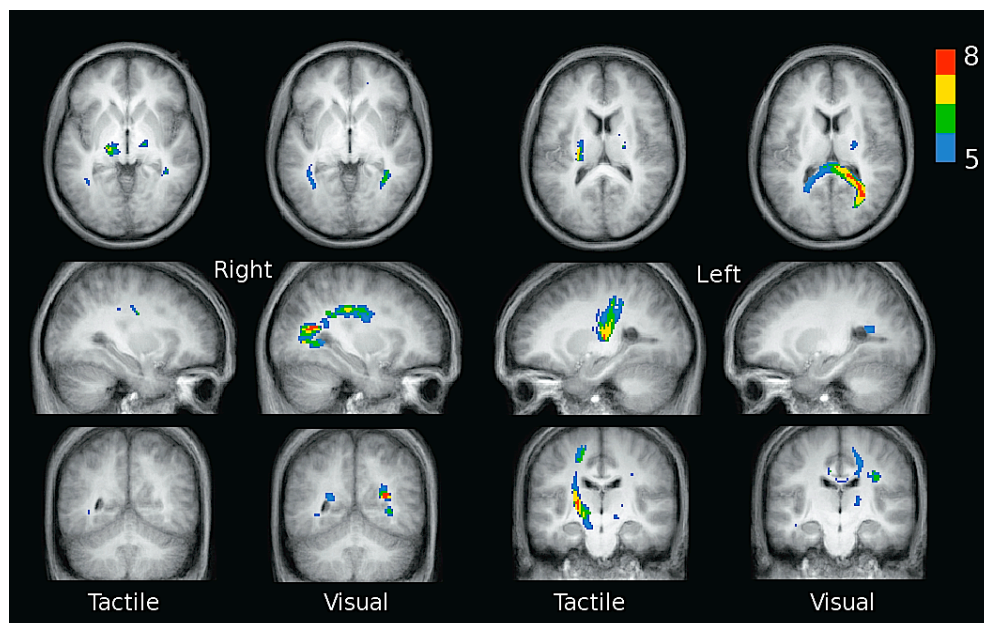
Figure 4. *Accumulated fDTI results of all 12 individuals for the tactile and visual task. For both tasks the cumulative fDTI results were computed and overlaid on the subjects' average anatomy. The value of a (colored) voxel represents the number of subjects for which active tracts are found at that position. The results show that the majority of the tactile activation is found in the contralateral tracts connecting the thalamus and sensory cortex. Visual activation is found for tracts that are part of the splenium and at positions that correspond with the optic radiations.*

One of the conclusions in the first fDTI study was that the measured FA-signal changes were more likely to be due to morphological changes of glial cells than due to glial cell swelling because the measured FA-signal changes were not accompanied by an overall decrease of the measured diffusion profile (reflected by a decrease in mean diffusivity). To determine if this finding could also be replicated we computed the overall average t-values of the task-related changes in FA and mean diffusivity (MD) for all voxels part of all the active tracts found in the tactile and the visual fDTI experiment. The higher t-values of the task-related changes found in FA (tactile experiment: average t-value (s.d.) = 0.41 (0.06), visual experiment: average t-value = 0.50 (0.03)) in the active tracts compared to the t-values for the task-related changes in MD (tactile experiment: -0.25 (0.15), visual experiment: -0.17 (0.13)) also suggest that morphological glial cell changes are responsible for the signal changes measured in this study instead of glial cell swelling (Sykova et al., 2003).

It is important to know which part of the measured FA-signal changes can actually be attributed to activity-related morphological changes of glial cells and which part may be induced by confounding factors. fMRI studies showed that a number of confounding factors can manifest themselves as false activation patterns. Indeed, when cell swelling was

used as a contrast mechanism to detect activity in gray matter of the human brain, focal changes in magnetic susceptibility could not be ruled out as a source of the signal changes found (Darquie et al., 2001). Moreover, in fMRI, changes in respiration patterns may introduce magnetic susceptibility changes leading to artificial activation patterns found in white matter (Windischberger et al., 2002). In our approach the role of these magnetic susceptibility changes are probably quite limited. Such magnetic susceptibility changes would have a larger effect on the size of the diffusion profile (reflected by the MD) than on the shape of the diffusion profile (reflected by the FA). This is not the case as the overall average t-values of the task-related changes in FA for all voxels part of all the active tracts found in the tactile and the visual fDTI experiment are in fact larger than the overall average t-values of the task-related changes in MD. Also, a possible contribution of fastly varying signal changes (e.g. BOLD contrast) to the measured FA-signal changes was largely canceled out by the introduction of the temporal shift for the stimulus onset (**Figure 1a**). Furthermore, the stimulus design used in this study (1 stimulus period followed by 2 rest periods) reduces the possibility that any type of periodic signal changes could interfere with task-related signal changes and therefore contribute to the measured changes in FA-signal.

Despite the application of the temporal lag to maximize the measured signal change and the increased signal-to-noise-ratio (SNR) due to the increased main magnetic field strength the bilateral activation predominantly found for the visual experiment in the optic radiations appears to be less pronounced at 3 Tesla than the activation found for the visual experiment in the optic radiations at 1.5 Tesla (Mandl et al., 2008). This difference in sensitivity may be explained by the lower number of stimulus periods (6) in the 3 Tesla experiment as compared to the number of stimulus periods (12) in the 1.5 Tesla experiment. Moreover, due to the smaller voxel size at 3 Tesla (43.75 mm^3) compared to the voxel size at 1.5 Tesla (64 mm^3) the SNR between a single fDTI scan 1.5 Tesla is comparable to a single fDTI scan at 3 Tesla because the expected increase in SNR with a factor of $\sqrt{2}$ due to a doubling of the main magnetic field strength (3 Tesla vs 1.5 Tesla) cancels out. Also, because of the thick slices used in the 3 Tesla experiments (7 mm) internal dephasing may contribute to a reduction of the SNR.

Both the 1.5 Tesla and 3 Tesla experiments were designed to maximize the specificity of the fDTI method to minimize the chance of spurious fiber activation because the main purpose of these experiments was to assess the feasibility of the fDTI method. Further experiments are needed to determine the optimal stimulus and MRI parameter settings to optimize the sensitivity of the fDTI method.

In conclusion, we replicated the results of our previous fDTI study using the same types of stimuli but with an improved MRI acquisition scheme on a different group of healthy participants using a 3 Tesla MRI scanner. This replication of our previous fDTI results suggests that the fDTI method can be applied within feasible time period and is robust enough to become a valuable tool that can help us to get a better understanding of the dynamics of functional neural networks in the human brain.

References

Anderson AW, Zhong J, Petroff OA, Szafer A, Ransom BR, Prichard JW, Gore JC (1996) Effects of osmotically driven cell volume changes on diffusion-weighted imaging of the rat optic nerve. Magn Reson Med 35:162-167.

Andersson JL, Skare S (2002) A model-based method for retrospective correction of geometric distortions in diffusion-weighted EPI. Neuroimage 16:177-199.

Andersson JL, Skare S, Ashburner J (2003) How to correct susceptibility distortions in spin-echo echo-planar images: application to diffusion tensor imaging. Neuroimage 20:870-888.

Basser PJ, Pierpaoli C (1996) Microstructural and physiological features of tissues elucidated by quantitative-diffusion-tensor MRI. J Magn Reson B 111:209-219.

Basser PJ, Mattiello J, LeBihan D (1994) Estimation of the effective self-diffusion tensor from the NMR spin echo. J Magn Reson B 103:247-254.

Beshay JE, Hahn P, Beshay VE, Hargittai PT, Lieberman EM (2005) Activity-dependent change in morphology of the glial tubular lattice of the crayfish medial giant nerve fiber. Glia 51:121-131.

Catani M, Ffytche DH (2005) The rises and falls of disconnection syndromes. Brain. 128:2224-2239.

Chang LC, Jones DK, Pierpaoli C (2005) RESTORE: robust estimation of tensors by outlier rejection. Magn Reson Med 53:1088-1095.

Collins DL, Holmes CJ, Peters TM, Evans AC (1995) Automatic 3-D model-based neuroanatomical segmentation. Human Brain Mapping 3:190-208.

Conturo TE, Lori NF, Cull TS, Akbudak E, Snyder AZ, Shimony JS, McKinstry RC, Burton H, Raichle ME (1999) Tracking neuronal fiber pathways in the living human brain. Proc Natl Acad Sci U S A 96:10422-10427.

Darquie A, Poline JB, Poupon C, Saint-Jalmes H, Le Bihan D (2001) Transient decrease in water diffusion observed in human occipital cortex during visual stimulation. Proc Natl Acad Sci U S A 98:9391-9395.

Gulani V, Iwamoto GA, Lauterbur PC (1999) Apparent water diffusion measurements in electrically stimulated neural tissue. Magn Reson Med 41:241-246.

Jones DK, Simmons A, Williams SC, Horsfield MA (1999) Non-invasive assessment of axonal fiber connectivity in the human brain via diffusion tensor MRI. Magn Reson Med 42:37-41.

Kandel ER, Schwartz, J.H., and Jessell, T.M. (2000) Principles of Neural Science, 4th Edition: McGraw-Hill Inc.

Kao YH, Guo WY, Liou AJ, Hsiao YH, Chou CC (2008) The respiratory modulation of intracranial cerebrospinal fluid pulsation observed on dynamic echo planar images. Magn Reson Imaging 26:198-205.

Larsen A, Kyllingsbaek S, Law I, Bundesen C (2005) Activation in the MT-complex during visual perception of apparent motion and temporal succession. Neuropsychologia 43:1060-1071.

Le Bihan D, Breton E, Lallemand D, Grenier P, Cabanis E, Laval-Jeantet M (1986) MR imaging of intravoxel incoherent motions: application to diffusion and perfusion in neurologic disorders. Radiology 161:401-407.

MacVicar BA, Feighan D, Brown A, Ransom B (2002) Intrinsic optical signals in the rat optic nerve: Role for K+ uptake via NKCC1 and swelling of astrocytes. Glia 37:114-123.

Mandl RCW, Schnack HGS, Zwiers MP, van der Schaaf A, Kahn RS, Hulshoff Pol HE (2008) Functional Diffusion Tensor Imaging: Measuring Task-Related Fractional Anisotropy Changes in the Human Brain along White Matter Tracts. PLoS ONE 3:e3631. doi:3610.1371/journal.pone.0003631.

Mesulam M (2005) Imaging connectivity in the human cerebral cortex: the next frontier? Ann Neurol 57:5-7.

Mori S, van Zijl PC (2002) Fiber tracking: principles and strategies - a technical review. NMR Biomed 15:468-480.

Mori S, Crain BJ, Chacko VP, van Zijl PC (1999) Three-dimensional tracking of axonal projections in the brain by magnetic resonance imaging. Ann Neurol 45:265-269.

Prichard JW, Zhong J, Petroff OA, Gore JC (1995) Diffusion-weighted NMR imaging changes caused by electrical activation of the brain. NMR Biomed 8:359-364.

Ransom BR, Yamate CL, Connors BW (1985) Activity-dependent shrinkage of extracellular space in rat optic nerve: a developmental study. J Neurosci 5:532-535.

Stroman PW, Lee AS, Pitchers KK, Andrew RD (2008) Magnetic Resonance Imaging of Neuronal and Glial Swelling as an Indicatior of Function in Cerebral Tissue Slices. Magnetic Resonance in Medicine 59:700-706.

Sykova E (2004) Extrasynaptic volume transmission and diffusion parameters of the extracellular space. Neuroscience 129:861-876.

Sykova E, Vargova L, Kubinova S, Jendelova P, Chvatal A (2003) The relationship between changes in intrinsic optical signals and cell swelling in rat spinal cord slices. Neuroimage 18:214-230.

van den Heuvel M, Mandl R, Luigjes J, Hulshoff Pol H (2008) Microstructural organization of the cingulum tract and the level of default mode functional connectivity. J Neurosci 28:10844-10851.

Windischberger C, Langenberger H, Sycha T, Tschernko EM, Fuchsjager-Mayerl G, Schmetterer L, Moser E (2002) On the origin of respiratory artifacts in BOLD-EPI of the human brain. Magn Reson Imaging 20:575-582.

Chapter 5

Chapter 6

Summary and general discussion

Diffusion tensor imaging not only provides directional information of the white matter's microstructure itself but also enables the reconstruction of complete white matter tracts using fiber tracking algorithms. With tract-based analysis this tract information can be used to automatically delineate fiber bundles and to study different aspects of the fiber bundle's underlying white matter tissue along the complete tracts. These white matter tissue characteristics are not limited to characteristics that can directly be computed from the DTI data itself (such as FA values), but may involve virtually any type of measurements (provided that these measurements can be brought into alignment with the reconstructed fiber tracts). With tract-based analysis the detection of very subtle differences between groups is possible because the signal is averaged over a region of interest (i.e. the fiber tract) that is structurally/functionally distinct from other regions. In this thesis, tract-based analysis was used to study both structural and functional characteristics of white matter fiber tracts.

In Chapter 2 we used tract-based analysis to study fronto and fronto-temporal connections in schizophrenia (Mandl et al., 2008b). Fractional anisotropy (FA) (Basser and Pierpaoli, 1996) and magnetization transfer ratio (MTR) (Wolff and Balaban, 1994) were measured along the left and right uncinate fasciculus and the genu of the corpus callosum, after which these measures were compared between patients with schizophrenia and healthy participants. The combination of FA and MTR was used to answer the question whether previously reported differences in correlations between FA and age for patients with schizophrenia and healthy participants can actually be attributed to differences in myelin concentrations (Jones et al., 2006; Kanaan et al., 2006; Mori et al., 2007; Rosenberger et al., 2008). Although the presence of myelin does moderate the diffusion profile of water molecules and therefore the measured FA value, the FA is for the major part determined by the level of alignment of the underlying axons (Beaulieu, 2002; Madler et al., 2008). Therefore the interpretation of differences in FA values between groups is difficult as it is not clear whether these differences stem from differences in myelin levels or differences in levels of axonal alignment or a combination of both. MTR putatively reflects the amount of macromolecules (including myelin) in the tissue. Therefore one could expect that differences found in measured FA values that are related to differences in myelin levels would also induce differences in MTR (Laule et al., 2002). However, it should be noted that myelin makes up only approximately 50% of the white matter in the central nervous system (MacKay et al., 2006). Thus, similar to possible group differences in FA, differences found in MTR between groups cannot exclusively be ascribed to differences in myelin concentrations. We did find the previously reported differences in correlations between FA and age in the left uncinate fasciculus. However, these differences in correlations were not found between MTR and age. Hence, our MTR findings do not support the hypothesis that the negative correlation between FA and age found in patients with schizophrenia - which was not found for healthy participants - was due to reductions in myelin. These findings suggest that an explanation for these differences in correlations between FA and age should be sought in, for instance, group differences in alignment and/or density of the axons.

Another finding was a significant increase in average MTR along the right uncinate fasciculus for patients with schizophrenia. One possible explanation was that the increased MTR reflected more myelin and that the right uncinate fasciculus is part of a compensatory mechanism. However, MTR is not exclusively sensitive to concentrations of macromolecules (Laule et al., 2007). For instance, changes in the characteristics of the free water pool influences the measured MTR value as well (MacKay et al., 2006). An alternative and intriguing explanation may therefore be that not increases in myelin but reductions in glutamate/glutamine concentrations in the extra-cellular space are responsible for the measured increase in average MTR as these reductions may indirectly lead to an increased T1-relaxation time of the free water pool thereby increasing the MTR. Although speculative, this explanation is concordant with previous results showing an increase in T1-relaxation time in schizophrenia in the right prefrontal white matter (Andreasen et al., 1991) as well as with results showing reductions in MTR in white matter due to glial cell swelling that was caused by increases in glutamate/glutamine concentrations (Rovira et al., 2001; Wyckoff et al., 2003; Coles, 2005; Miese et al., 2006).

In Chapter 3 tract-based analysis was used in combination with resting-state fMRI to determine if there is a relation between the "strength" (reflected by the average FA) of the fiber tracts between regions of resting-state networks and the level of functional connectivity within these resting-state networks. In this study we focused on two regions, namely the precuneus/posterior cingulate cortex and the medial frontal cortex, which are part of the so-called default mode network and are interconnected via the cingulum tract. The main finding of this study was a significant positive correlation between the average FA value of the cingulum tract and the level of neuronal synchronization suggesting an anatomical basis for default mode functional connectivity.

In Chapters 2 and 3 tract-based analysis was used to measure structural characteristics of the white matter tracts (van den Heuvel et al., 2008; Mandl et al., 2008b). The main difference between Chapter 2 and Chapter 3 regarding the use of tract-based analysis was the way fiber bundles were selected. While in Chapter 2 fiber tracts were selected using multiple regions of interest defined in white matter, in chapter 3 gray matter regions that are part of resting-state networks were used to delineate fiber tracts. Although in Chapter 3 fMRI was used to obtain functional information from gray matter regions, no functional information was obtained from the white matter tracts themselves.

In Chapter 4 we proposed a new method that allows the noninvasive detection of white matter fiber activation (Mandl et al., 2008a). In this new method, which we dubbed functional diffusion tensor imaging (fDTI), we hypothesized that fiber activation leads to a (very small) increase in FA. We showed that tract-based analysis can be used successfully to detect these task-related changes in FA assuming that these changes occur along the complete fiber tracts. Moreover, the results of the experiments presented in Chapter 4 suggest that the response function is slowly varying and that the response function is different for tactile and visual stimuli. This information should be taken into account in the design of new fDTI experiments.

In Chapter 5 we presented a second fDTI study. In this second fDTI experiment the same types of stimuli were used as in the first fDTI experiment but on a different group

of healthy participants and at a 3 Tesla MRI scanner. The main purpose of this fDTI study was to replicate the findings of the first fDTI study using an improved MRI acquisition scheme that further increases the sensitivity of the fDTI method by excluding more possible confounding factors. In this second fDTI study we found active fiber patterns similar to the patterns found in the first fDTI study. This replication of the first fDTI results adds to our belief that fDTI may become a valuable tool to study white matter activation.

Limitations

The phrase: "A chain is only as strong as it's weakest link" is especially true in deterministic fiber tracking. Successful reconstruction of a single tract requires that in each voxel that is part of that tract sufficient directional information is available. If this information is not available in just one of these voxels then the reconstruction of the complete fiber tract fails. There are several reasons why this information may not be available. One reason is that various types of noise (e.g. subject motion, cardiac pulsation, scanner noise) may corrupt the data because DTI has a very low signal-to-noise-ratio (SNR). The effects of noise can be reduced by increasing the SNR, simply by averaging data or by using cardiac gating to eliminate the effects of cardiac pulsation (Skare and Andersson, 2001). Both solutions do however increase the total acquisition time. The influence of subject motion is limited because the DTI scans used are single shot echo planar imaging (SS-EPI) acquisitions which are known to be robust against this type of noise (Haacke et al., 1999). However, the price paid for this robustness is a limitation of the resolution of the DTI scan. Another reason for insufficient directional information relates to the fact that for the FACT fiber tracking algorithm (Mori et al., 1999) used in these studies the diffusion profile is described by a 2nd-order tensor. Second-order tensors can adequately describe the diffusion process in a single fiber bundle having one major fiber direction. However, if the fiber bundle crosses or touches (so-called 'kissing') other fiber bundles then 2nd-order tensors fall short because at these crossings there are more than one major fiber directions. As a consequence the FACT algorithm will terminate at these positions. These effects of noise and the inability of the FACT fiber tracking algorithm to deal with fiber crossing and fiber kissing should be taken into account when interpreting the results. For instance, when tract-based analysis is used to compare groups, possible group-wise differences in noise characteristics (i.e. increased heart rate) or group-wise differences in numbers of crossings may introduce a bias into the process of tract reconstruction. In Chapter 2, we applied the concept of the average fiber (Gerig et al., 2004), which allows us to determine whether there are such systematic differences in position and spread of the reconstructed tracts between the groups. For the fDTI experiments described in Chapters 4 and 5 the comparison is done between states (active versus rest) and not between groups. In that case, a failure to reconstruct complete tracts 'only' results in a reduction of sensitivity (i.e. an increase in false negatives). However, when fDTI would be used to compare different groups then possible group-wise differences in noise characteristics or group-wise differences in numbers of crossings may introduce a bias in the white matter activation

patterns found. Further research will include the application of more sophisticated fiber tracking algorithms which use more complex models to describe the diffusion profile such as higher order tensors, spherical harmonics, multiple tensors models (Alexander, 2005) to control for these possible group-wise differences.

Future directions

The findings of the study presented in Chapter 2 suggested that 1) the difference in correlations between FA and age for patients with schizophrenia and healthy participants is not related to reductions in myelin concentrations 2) there is a subtle but consistent increase in MTR in the right uncinate fasciculus. The latter may point to a compensary role for the right uncinate fasciculus but may also reflect reductions in glutamate/glutamine concentrations. One possibility to gain more insight in the underpinning of the measured increase in MTR is to combine tract-based analysis with magnetic resonance spectroscopy (MRS) to measure glutamate/glutamine concentrations along the tracts. Especially the availability of the high field 7 Tesla MRI scanner makes this a very interesting combination as MRS is one of the domains that benefits directly from an increase in main magnetic field strength. Other possible combinations are that of tract-based analysis with quantitative T1-relaxation time measurements (Haacke et al., 1999), quantitative MTR (Sled and Pike, 2001) and myelin-water measurements (MacKay et al., 1994). The latter measures the water trapped between the myelin sheaths and is believed to be a more precise estimator for myelin concentrations than MTR (Laule et al., 2007).

Only Chapter 2 describes a patient study. The studies conducted in Chapters 3, 4 and 5 only include healthy participants. However, the techniques presented in these chapters may be used to answer a number of interesting questions in particular in the study of schizophrenia. In Chapter 3 we showed that there is a correlation between the level of functional connectivity between the precuneus/posterior cingulate cortex and the medial frontal cortex, and the average FA value of the connecting cingulum tract. Previous studies have shown reductions in FA in schizophrenia. Also reductions in default mode functional connectivity in schizophrenia have been reported. Whether the correlation between FA and functional connectivity found in healthy participants is also present in patients with schizophrenia remains to be elucidated.

The fDTI method is based on task-related changes in FA that putatively reflect morphological changes in glial cells. fDTI may therefore be an interesting method to study schizophrenia as evidence from genetic (Harrison and Weinberger, 2005; Konrad and Winterer, 2008) and post-mortem (Hakak et al., 2001; Uranova et al., 2004) studies suggests disease-related structural and functional impairment of oligodendrocytes in various white matter regions. One could hypothesize that the disease-related structural and functional impairment of oligodendrocytes may lead to reduced white matter activation patterns. The main purpose of the fDTI studies presented in Chapters 4 and 5 was to assess the feasibility of the fDTI method. Although very promising, virtually every aspect of this new method will require further improvement. For instance, additional experiments are

needed to obtain more information on the response functions for different tasks with different types of repetitive stimuli. Also more information is needed on the source of the measured signal change; to what extent do the task-related FA changes actually relate to morphological changes of glial cells? Of further issue is the optimization of the echo time (TE) in such a way that the fDTI acquisition is most sensitive to changes in the diffusion profile of extracellular water. Another important issue is that of the applied correction for multiple comparisons. How do we estimate the level of dependency between measurements? When we apply a Bonferroni correction for the number of tracts tested we assume that all tract measurements are independent. However, many tracts will show partial overlap with other tracts and as a consequence this correction for multiple comparisons will be too conservative.

fDTI may help us to answer a number of questions regarding the role of fiber bundles within networks that cannot be answered with a combination of conventional DTI and fMRI. For instance, questions regarding the role of fiber bundles within resting-state networks. The results of the combined DTI-fMRI study presented in Chapter 3 do suggest that there is a relation between the level of resting-state in the default mode network and the "strength" of the fiber bundle connecting the regions of the default mode network. However, we still do not know whether the individual regions of the default mode network actually communicate during rest via these fiber bundles. With fDTI, in combination with resting-state fMRI, this could be established by determining if there is sufficient correlation between the fDTI signal of the connecting fiber during rest and the fMRI signal of the connected regions of the default mode network during rest.

Conclusion

In this thesis tract-based analysis was successfully applied to measure structural and functional characteristics of white matter tracts. The reconstruction and selection of these tracts can be done automatically and at an individual level, which makes it suitable to study large groups. This is especially important for the study of diseases for which possible white matter impairment can be expected to be subtle and detection would require a large number of subjects. This ability of tract-based analysis to detect very subtle differences in an automatic way makes it suitable to study all types of diseases for which white matter may be implicated, in particular schizophrenia.

References

Alexander DC (2005) Multiple-fiber reconstruction algorithms for diffusion MRI. Ann N Y Acad Sci 1064:113-133.

Andreasen NC, Ehrhardt JC, Swayze VW, 2nd, Tyrrell G, Cohen G, Ku JS, Arndt S (1991) T1 and T2 relaxation times in schizophrenia as measured with magnetic resonance imaging. Schizophr Res 5:223-232.

Basser PJ, Pierpaoli C (1996) Microstructural and physiological features of tissues elucidated by quantitative-diffusion-tensor MRI. J Magn Reson B 111:209-219.

Beaulieu C (2002) The basis of anisotropic water diffusion in the nervous system - a technical review. NMR Biomed 15:435-455.

Coles JA, Deitmer JW (2005) Extracellular potassium and pH: homeostasis and signaling. In: Neuroglia (Kettenmann H, Ransom BR, ed). Oxford: Oxford University Press.

Gerig G, Gouttard S, Corouge I (2004) Analysis of brain white matter via fiber tract modeling. Conf Proc IEEE Eng Med Biol Soc 6:4421-4424.

Haacke EM, Brown RW, Thompson MR, Venkatesan R (1999) Magnetic Resonance Imaging: Physical Principles and Sequence Design. New York: John Wiley & Sons, Inc.

Hakak Y, Walker JR, Li C, Wong WH, Davis KL, Buxbaum JD, Haroutunian V, Fienberg AA (2001) Genome-wide expression analysis reveals dysregulation of myelination-related genes in chronic schizophrenia. Proc Natl Acad Sci U S A 98:4746-4751.

Harrison PJ, Weinberger DR (2005) Schizophrenia genes, gene expression, and neuropathology: on the matter of their convergence. Mol Psychiatry 10:40-68; image 45.

Jones DK, Catani M, Pierpaoli C, Reeves SJC, Shergill SS, O'Sullivan M, Golesworthy P, McGuire P, Horsfield MA, Simmons A, Williams SCR, Howard RJ (2006) Age effects on diffusion tensor magnetic resonance imaging tractography measures of frontal cortex connections in schizophrenia. Human Brain Mapping 27:230-238.

Kanaan RA, Shergill SS, Barker GJ, Catani M, Ng VW, Howard R, McGuire PK, Jones DK (2006) Tract-specific anisotropy measurements in diffusion tensor imaging. Psychiatry Res 146:73-82.

Konrad A, Winterer G (2008) Disturbed structural connectivity in schizophrenia - Primary factor in pathology or epiphenomenon? Schizophrenia Bulletin 34:72-92.

Laule C, Vavasour I, Paty D, Li D, Arnold D, MacKay A (2002) Correlation between Magnetization Transfer Ratio and Myelin Water Content in Normal White Matter and MS Lesions. Proceedings of the annual meeting of the International Society of Magnetic Resonance in Medicine.

Laule C, Vavasour IM, Kolind SH, Li DKB, Traboulsee TL, Moore GRW, MacKay AL (2007) Magnetic resonance imaging of myelin. Neurotherapeutics 4:460-484.

MacKay A, Whittall K, Adler J, Li D, Paty D, Graeb D (1994) In vivo visualization of myelin water in brain by magnetic resonance. Magn Reson Med 31:673-677.

MacKay A, Laule C, Vavasour I, Bjarnason T, Kolind S, Madler B (2006) Insights into brain microstructure from the T2 distribution. Magn Reson Imaging 24:515-525.

Madler B, Drabycz SA, Kolind SH, Whittall KP, MacKay AL (2008) Is diffusion anisotropy an accurate monitor of myelination? Correlation of multicomponent T2 relaxation and diffusion tensor anisotropy in human brain. Magn Reson Imaging 26:874-888.

Mandl RCW, Schnack HG, Zwiers MP, van der Schaaf A, Kahn RS, Hulshoff Pol HE (2008a) Functional Diffusion Tensor Imaging: Measuring Task-Related Fractional Anisotropy Changes in the Human Brain along White Matter Tracts. PLos ONE 3:e3631. doi:3610.1371/journal.pone.0003631.

Mandl RCW, Schnack HG, Luigjes J, van den Heuvel MP, Cahn W, Kahn RS, Hulshoff Pol HE (2008b) Tract-based analysis of magnetization transfer ratio and diffusion tensor imaging of the frontal and fronto-temporal connections in schizophrenia. Schizophrenia Bulletin doi:10.1093/schbul/sbn161.

Miese F, Kircheis G, Wittsack HJ, Wenserski F, Hemker J, Modder U, Haussinger D, Cohnen M (2006) 1H-MR spectroscopy, magnetization transfer, and diffusion-weighted imaging in alcoholic and nonalcoholic patients with cirrhosis with hepatic encephalopathy. AJNR Am J Neuroradiol 27:1019-1026.

Mori S, Crain BJ, Chacko VP, van Zijl PC (1999) Three-dimensional tracking of axonal projections in the brain by magnetic resonance imaging. Ann Neurol 45:265-269.

Mori T, Ohnishi T, Hashimoto R, Nemoto K, Moriguchi Y, Noguchi H, Nakabayashi T, Hori H, Harada S, Saitoh O, Matsuda H, Kunugi H (2007) Progressive changes of white matter integrity in schizophrenia revealed by diffusion tensor imaging. Psychiatry Res 154:133-145.

Rosenberger G, Kubicki M, Nestor PG, Connor E, Bushell GB, Markant D, Niznikiewicz M, Westin CF, Kikinis R, A JS, McCarley RW, Shenton ME (2008) Age-related deficits in fronto-temporal connections in schizophrenia: A diffusion tensor imaging study. Schizophr Res. 102:181-188.

Rovira A, Grive E, Pedraza S, Rovira A, Alonso J (2001) Magnetization transfer ratio values and proton MR spectroscopy of normal-appearing cerebral white matter in patients with liver cirrhosis. AJNR Am J Neuroradiol 22:1137-1142.

Skare S, Andersson JL (2001) On the effects of gating in diffusion imaging of the brain using single shot EPI. Magn Reson Imaging 19:1125-1128.

Sled JG, Pike GB (2001) Quantitative imaging of magnetization transfer exchange and relaxation properties in vivo using MRI. Magn Reson Med 46:923-931.

Uranova NA, Vostrikov VM, Orlovskaya DD, Rachmanova VI (2004) Oligodendroglial density in the prefrontal cortex in schizophrenia and mood disorders: a study from the Stanley Neuropathology Consortium. Schizophrenia Research 67:269-275.

van den Heuvel M, Mandl R, Luigjes J, Hulshoff Pol H (2008) Microstructural organization of the cingulum tract and the level of default mode functional connectivity. J Neurosci 28:10844-10851.

Wolff SD, Balaban RS (1994) Magnetization transfer imaging: practical aspects and clinical applications. Radiology 192:593-599.

Wyckoff N, Kumar A, Gupta RC, Alger J, Hwang S, Thomas MA (2003) Magnetization transfer imaging and magnetic resonance spectroscopy of normal-appearing white matter in late-life major depression. Journal of Magnetic Resonance Imaging 18:537-543.

List of publications

Cahn W, Hulshoff Pol HE, Bongers M, Schnack HG, Mandl RC, Van Haren NE, Durston S, Koning H, Van Der Linden JA, Kahn RS. (2002): Brain morphology in antipsychotic-naive schizophrenia: a study of multiple brain structures. Br J Psychiatry Suppl 43:s66-72.

Ho Pian KL, van Megen HJ, Ramsey NF, Mandl R, van Rijk PP, Wynne HJ, Westenberg HG. (2005): Decreased thalamic blood flow in obsessive-compulsive disorder patients responding to fluvoxamine. Psychiatry Res 138(2):89-97.

Hulshoff Pol HE, Schnack HG, Mandl RC, Brans RG, van Haren NE, Baare WF, van Oel CJ, Collins DL, Evans AC, Kahn RS. (2006a): Gray and white matter density changes in monozygotic and same-sex dizygotic twins discordant for schizophrenia using voxel-based morphometry. Neuroimage 31(2):482-8.

Hulshoff Pol HE, Schnack HG, Mandl RC, Cahn W, Collins DL, Evans AC, Kahn RS. (2004): Focal white matter density changes in schizophrenia: reduced inter-hemispheric connectivity. Neuroimage 21(1):27-35.

Hulshoff Pol HE, Schnack HG, Mandl RC, van Haren NE, Koning H, Collins DL, Evans AC, Kahn RS. (2001): Focal gray matter density changes in schizophrenia. Arch Gen Psychiatry 58(12):1118-25.

Hulshoff Pol HE, Schnack HG, Posthuma D, Mandl RC, Baare WF, van Oel C, van Haren NE, Collins DL, Evans AC, Amunts K and others. (2006b): Genetic contributions to human brain morphology and intelligence. J Neurosci 26(40):10235-42.

Mandl RC, Schnack HG, Luigjes J, van den Heuvel MP, Cahn W, Kahn RS, Hulshoff Pol HE. (2008a): Tract-based Analysis of Magnetization Transfer Ratio and Diffusion Tensor Imaging of the Frontal and Frontotemporal Connections in Schizophrenia. Schizophr Bull. doi:10.1093/schbul/sbn161.

Mandl RC, Schnack HG, Zwiers MP, van der Schaaf A, Kahn RS, Hulshoff Pol HE. (2008b): Functional diffusion tensor imaging: measuring task-related fractional anisotropy changes in the human brain along white matter tracts. PLoS ONE 3(11):e3631.

Neggers SF, Langerak TR, Schutter DJ, Mandl RC, Ramsey NF, Lemmens PJ, Postma A. (2004): A stereotactic method for image-guided transcranial magnetic stimulation validated with fMRI and motor-evoked potentials. Neuroimage 21(4):1805-17.

Sommer IE, Oranje B, Ramsey NF, Klerk FA, Mandl RC, Westenberg HG, Kahn RS. (2006): The influence of amphetamine on language activation: an fMRI study. Psychopharmacology (Berl) 183(4):387-93.

Sommer IE, Ramsey NF, Mandl RC, Kahn RS. (2002): Language lateralization in monozygotic twin pairs concordant and discordant for handedness. Brain 125(Pt 12):2710-8.

Sommer IE, Ramsey NF, Mandl RC, Kahn RS. (2003): Language lateralization in female patients with schizophrenia: an fMRI study. Schizophr Res 60(2-3):183-90.

Sommer IE, Ramsey NF, Mandl RC, van Oel CJ, Kahn RS. (2004): Language activation in monozygotic twins discordant for schizophrenia. Br J Psychiatry 184:128-35.

van den Heuvel M, Mandl R, Hulshoff Pol H. (2008): Normalized cut group clustering of resting-state FMRI data. PLoS ONE 3(4):e2001.

van den Heuvel M, Mandl R, Luigjes J, Hulshoff Pol H. (2008): Microstructural organization of the cingulum tract and the level of default mode functional connectivity. J Neurosci 28(43):10844-51.

van den Heuvel M, Mandl R, Kahn R, Hulshoff Pol H. (2009): Functionally linked resting state networks reflect the underlying structural connectivity architecture of the human brain. Hum Brain Mapp :In press.

van der Wee NJ, Stevens H, Hardeman JA, Mandl RC, Denys DA, van Megen HJ, Kahn RS, Westenberg HM. (2004): Enhanced dopamine transporter density in psychotropic-naive patients with obsessive-compulsive disorder shown by [123I]β-CIT SPECT. Am J Psychiatry 161(12):2201-6.

van Haren NE, Hulshoff Pol HE, Schnack HG, Cahn W, Mandl RC, Collins DL, Evans AC, Kahn RS. (2007): Focal gray matter changes in schizophrenia across the course of the illness: a 5-year follow-up study. Neuropsychopharmacology 32(10):2057-66.

Nederlandse samenvatting

De witte stof in de hersenen bestaat uit dikke bundels van gemyeliniseerde axonen die de verschillende grijze-stofgebieden in de hersenen over lange afstand met elkaar verbinden om informatie uit te wisselen. Myeline is een vetachtige stof die er voor zorgt dat het signaaltransport via de axonen snel en efficiënt verloopt. De witte-stofbanen vormen als het ware de informatiesnelwegen van het brein. Al vanaf het moment dat schizofrenie voor het eerst werd beschreven (Bleuler, 1911; Kraepelin, 1919 werd de mogelijkheid geopperd dat het gerelateerd zou kunnen zijn aan afwijkingen in deze witte-stofbanen. Met moderne beeldvormende magnetische resonantie methoden (MRI) zoals diffusion tensor imaging (DTI) (Le Bihan et al., 1986; Basser et al., 1994) in combinatie met fiber tracking algoritmen (Le Bihan et al., 2001; Mori and van Zijl, 2002; Jones, 2008) is het mogelijk deze witte-stofbanen te reconstrueren. Deze gereconstrueerde witte-stofbanen (tracts) kunnen gebruikt worden in een zogenaamde tract-gebaseerde analyse waarbij groepen (of toestanden) met elkaar vergeleken worden op het niveau van complete tracts. Dit in tegenstelling tot een conventionele voxel-gebaseerde analyse (VBM) waarbij de verge-lijkingen plaatsvinden op voxel (volume element) niveau. Tract-gebaseerde analysemethoden zijn in het bijzonder geschikt om subtiele groepsverschillen in eigenschappen van witte stof te meten die voorkomen langs de gehele tract. Deze witte stof eigenschappen kunnen eigenschappen zijn die met DTI zelf gemeten kunnen worden zoals kenmerken van het diffusieprofiel van watermoleculen in de witte stof maar ook eigenschappen waarvoor additionele metingen noodzakelijk zijn. Een voorbeeld van een eigenschap die direct met DTI gemeten kan worden is de mate van anisotropie van het diffusieprofiel van de watermoleculen welke wordt beschreven door de fractionele anisotropie (FA) (Basser and Pierpaoli, 1996). In witte stof is het diffusieprofiel doorgaans anisotroop omdat water makkelijker diffundeert in de richting parallel aan de axonen dan haaks op de axonen. Een voorbeeld van een additionele meting die gecombineerd kan worden met een tract-gebaseerde analyse is de magnetization transfer ratio (MTR) (Wolff and Balaban, 1994) waarbij informatie kan worden verkregen over de concentratie macromoleculen (waaronder myeline) in de witte stof. Hoewel er verschillende typen metingen bestaan die informatie kunnen geven over structurele eigenschappen van de witte stof was het tot nu toe niet mogelijk om noninvasief functionele eigenschappen van de witte stof te meten. In dit proefschift wordt echter een nieuwe tract-gebaseerde analayse methode geïntroduceerd waarmee het mogelijk is om *in vivo* functionele activatie van witte-stofbanen te meten op een noninvasieve manier.

Het doel van dit proefschrift is om te bepalen wat de mogelijkheden zijn om met tract-gebaseerde analyse een aantal structurele en functionele eigenschappen van de witte stof te meten ten behoeve van schizofrenieonderzoek.

In hoofdstuk 2 werd tract-gebaseerde analyse gebruikt om fronto- en frontotemporale witte-stofverbindingen te vergelijken tussen patiënten met schizofrenie en gezonde vrijwilligers (Mandl et al., 2008b). Hiervoor werden zowel FA en MTR waarden gemeten langs de linker en rechter uncinate fasciculus en langs het genu van het corpus callosum. De combinatie van FA en MTR geeft de mogelijkheid om te bepalen of er aanwijzingen zijn dat eerder gerapporteerde verschillen in correlaties tussen FA en leeftijd voor schizofreniepatiënten en gezonde controles (Jones et al., 2006; Kanaan et al., 2006; Mori et al., 2007; Rosenberger et al., 2008) kunnen worden toegeschreven aan verschillen in myelineconcentraties. Hoewel de aanwezigheid van myeline in witte stof het diffusieprofiel van watermoleculen beïnvloedt (en dus ook de FA waarde) wordt de FA waarde voornamelijk bepaald door de mate waarin de axonen dezelfde richting op wijzen (directionaliteit) (Beaulieu, 2002; Madler et al., 2008). De interpretatie van groepsverschillen in FA waarden is daarom moeilijk omdat het niet duidelijk is of deze verschillen duiden op een verschil in myeline concentratie, een verschil in directionaliteit, of een combinatie hiervan. Van MTR wordt aangenomen dat het de concentratie van macromoleculen (waaronder myeline) representeert. Daarom zou men verwachten dat als de gevonden groepsverschillen in FA waarden verschillen in myelineconcentraties zouden vertegenwoordigen, deze verschillen ook (tot op zekere hoogte) teruggevonden zouden worden in de MTR waarden (Laule et al., 2002). Hierbij moet wel rekening gehouden worden met het feit dat witte stof in het centrale zenuwstelsel ten hoogste voor 50 procent uit myeline bestaat (MacKay et al., 2006). Dit betekent dus dat ook voor MTR geldt dat eventueel gevonden groepsverschillen niet automatisch aan verschillen in myelineconcentraties toegeschreven kunnen worden.

In de studie beschreven in hoofdstuk 2 hebben we de eerder gerapporteerde groepsverschillen in correlaties tussen FA en leeftijd voor patiënten met schizofrenie en gezonde controles, welke gevonden werden in de linker uncinate fasciculus, gerepliceerd. Maar omdat deze groepsverschillen in correlaties niet gevonden werden in MTR kan men zich afvragen of de gevonden groepsverschillen in FA veroorzaakt worden door verschillen in myelineconcentraties. Wellicht dat een meer plausibele verklaring voor deze groepsverschillen in correlaties tussen FA en leeftijd bijvoorbeeld gezocht moet worden in verschillen in de mate waarin de axonen in de witte-stofbanen dezelfde richting op wijzen en/of de dichtheid van deze axonen. Een verdere bevinding was een toename van de gemiddelde MTR waarde in de rechter uncinate fasciculus voor patiënten met schizofrenie. Een mogelijke verklaring hiervoor zou kunnen zijn dat de verhoogde MTR waarde veroorzaakt wordt door meer myeline bij de schizofreniepatiënten. Dit zou er dan op kunnen wijzen dat de rechter uncinate fasciculus onderdeel is van een compensatoir mechanisme omdat meer myeline duidt op een snellere en meer efficiënte communicatie. MTR is echter niet uitsluitend gevoelig voor concentraties macromoleculen (Laule et al., 2007) maar ook bijvoorbeeld voor veranderingen in eigenschappen van de vrije watermoleculen zoals de T1-relaxatietijd (MacKay et al., 2006). Een alternatieve en intrigerende verklaring voor de gemeten verhoogde MTR waarden bij patiënten met schizofrenie zou in dat geval kunnen zijn dat verlaagde glutamaat/glutamine-concentraties in de extracellulaire ruimte indirect leiden tot een verlenging van de T1-relaxatietijd van de vrije watermoleculen en daardoor tot een verhoging van de gemeten MTR waarde. Deze

alternatieve (en speculatieve) verklaring is zowel in overeenstemming met eerder gerapporteerde bevindingen betreffende verlengde T1-relaxatietijden in de rechter prefrontale witte stof bij patiënten met schizofrenie (Andreasen et al., 1991) als met vondsten van verlaagde MTR waarden in witte stof die gerelateerd waren aan het zwellen van gliacellen. Deze zwelling van glia cellen werd namelijk veroorzaakt door een toename in glutamaat/glutamine concentraties (Rovira et al., 2001; Wyckoff et al., 2003; Coles, 2005; Miese et al., 2006).

In hoofdstuk 3 werd tract-gebaseerde analyse gebruikt in combinatie met resting-state functionele MRI (resting-state fMRI) (Damoiseaux et al., 2006; Van den Heuvel et al., 2008a). Bij resting-state fMRI worden de activatiepatronen van de verschillende grijze-stofgebieden in de hersenen tijdens rust bestudeerd. De hoogte van de correlaties in het gemeten fMRI signaal tussen verschillende grijze-stofgebieden wordt beschouwd als een maat voor functionele connectiviteit. De combinatie van resting-state fMRI (in grijze stof) en tract-gebaseerde analyse (in witte stof) maakt het mogelijk om te bepalen of er een relatie bestaat tussen de mate van functionele connectiviteit van de verschillende resting-state gebieden en de 'sterkte' van witte-stofbanen (hiervoor werd de FA als maat gebruikt) die deze resting-state gebieden met elkaar verbinden. In de hier beschreven studie richtten we ons op twee specifieke grijze-stofgebieden namelijk de precuneus/posterior cingulate cortex en de mediale frontale cortex. Deze gebieden maken deel uit van het zogenaamde default-mode netwerk (Raichle et al., 2001; Greicius et al., 2003) en zijn verbonden door het cingulum tract. De belangrijkste bevinding was een significante positive correlatie tussen de sterkte van de witte-stofverbinding en de functionele connectiviteit van de twee grijze-stofgebieden. Deze bevinding suggereert dat default-mode functionele connectiviteit (deels) anatomisch verankerd is.

In hoofdstuk 2 en 3 werd tract-gebaseerde analyse gebruikt om structurele eigenschappen van de witte-stofbanen te meten (van den Heuvel et al., 2008b; Mandl et al., 2008b). Het belangrijkste verschil voor wat betreft het gebruik van tract-gebaseerde analyse tussen deze hoofdstukken was de wijze waarop de tracts werden geselecteerd. In hoofdstuk 2 werden de witte-stofbanen geselecteerd op basis van vooraf gedefinieerde witte-stofgebieden waarvan bekend is dat de te selecteren witte-stofbanen er doorheen lopen. In hoofdstuk 3 werden de witte-stofbanen echter geselecteerd door te bepalen of de uiteinden aansluiten op de twee grijze-stofgebieden van het default-mode resting-state netwerk. Hoewel in hoofdstuk 3 functionele informatie uit grijze-stofgebieden werd gebruikt werd van de witte-stofbanen alleen structurele informatie verzameld. Met standaard fMRI technieken is het namelijk niet mogelijk om activatie van witte stof te meten. In hoofdstuk 4 introduceerden we een geheel nieuwe methode waarmee het mogelijk is om activatie van de witte-stofbanen zelf te meten (Mandl et al., 2008a). Deze nieuwe methode, die we functionele diffusion tensor imaging (fDTI) genoemd hebben, gaat er van uit dat activatie van witte-stofbanen leidt tot een subtiele verhoging van de FA waarden in de baan zelf. We hebben laten zien dat met behulp van tract-gebaseerde analyse taak-gerelateerde veranderingen in FA daadwerkelijk gemeten kunnen worden. De resultaten van de experimenten suggereren verder dat de responses voor de verschillende typen stimuli (visueel en tactiel) niet alleen traag zijn maar ook nog verschillen voor de verschillende

typen stimuli. Deze informatie is belangrijk bij het ontwikkelen van nieuwe fDTI experimenten.

Hoofdstuk 5 beschrijft een tweede fDTI studie waarbij dezelfde stimuli gebruikt worden als in het eerste fDTI experiment maar bij een nieuwe groep van gezonde vrijwilligers en met behulp van een 3 Tesla scanner. Het doel van deze tweede fDTI studie was het repliceren van de resultaten van de eerste fDTI studie gebruikmakend van een verbeterd paradigma waarbij verschillende mogelijke verstorende factoren verder uitgesloten kunnen worden. De succesvolle replicatie van de eerste fDTI resultaten geeft aan dat de eerste fDTI resultaten geen toevalsbevindingen zijn en dat de kans dat de gemeten taakgerelateerde veranderingen in FA waarden veroorzaakt kunnen worden door artefacten (bijvoorbeeld beweging) minimaal is. Deze eerste bevindingen wijzen er op dat fDTI de mogelijkheid heeft om uit te groeien tot een waardevolle methode om witte-stof activatie te bestuderen.

Hoe verder

Eén van de bevindingen in hoofdstuk 2 was een subtiele maar consistente toename in gemeten MTR waarden in de rechter uncinate fasciculus voor patiënten met schizofrenie. Dit kan wijzen op een compensitoire rol van de rechter uncinate fasciculus maar het is ook mogelijk dat deze toename in MTR (indirect) gerelateerd is aan een afname van de hoeveelheid glutamaat/glutamine in de witte stof. Een van de manieren om deze mogelijke groepsverschillen in glutamaat/glutamine concentraties in witte stof verder te onderzoeken is door tract-gebaseerde analyse te gaan combineren met MR spectroscopie (MRS). De gereconstrueerde tracts kunnen hierbij dienen om te bepalen waar precies het grid van MRS samples geplaatst moet worden maar ook om binnen het grid te bepalen welke samples behoren tot de te onderzoeken tract. De beschikbaarheid van de 7 Tesla MR scanner maakt deze combinatie met MRS in het bijzonder intressant omdat MRS één van de MR technieken is die direct profiteert van de hogere veldsterkte. Andere mogelijk interresante combinaties zijn die van tract-gebaseerde analyse met T1-relaxatietijd metingen (Haacke et al., 1999), kwantitieve MTR metingen (Sled and Pike, 2001) en myeline-water metingen (MacKay et al., 1994). De laatstgenoemde meting meet de hoeveelheid water dat zich tussen de myelinewindingen bevindt en hiervan wordt aangenomen dat dit een betere maat is voor de hoeveelheid myeline dan MTR (Laule et al., 2007).

Alleen in hoofdstuk 2 wordt een patiëntenstudie beschreven. De studies beschreven in hoofdstukken 3, 4 en 5 betreffen alleen gezonde vrijwilligers. De in deze hoofdstukken gepresenteerde technieken kunnen in de toekomst echter gebruikt worden om, bijvoorbeeld voor schizofrenieonderzoek, een aantal interessante vragen te beantwoorden. In hoofdstuk 3 werd een correlatie aangetoond tussen de mate van functionele connectiviteit tussen de precuneus/posterior cingulate cortex en de mediale frontale cortex en de gemiddelde FA waarden van de cingulum tract welke deze grijze-stofgebieden met elkaar verbindt. Voorgaande studies hebben een vermindering laten zien in functionele connectiviteit voor patiënten met schizofrenie ten opzichte van gezonde

controles. Ook zijn er studies die aantonen dat er een afname is van FA waarden in het cingulum tract bij patiënten met schizofrenie ten opzichte van gezonde controles. De vraag is of de in hoofdstuk 3 gevonden correlatie tussen functionele connectiviteit en structionele connectiveit (gereflecteerd door de FA) in gezonde vrijwilligers ook gevonden wordt bij patiënten met schizofrenie. Zo niet, dan zou dit kunnen wijzen op een verstoorde communicatie tussen deze twee grijze-stofgebieden.

De fDTI methode is gebaseerd op taak-gerelateerde veranderingen in FA waarvan we aannemen dat deze morfologische veranderingen representeren in met name astrocyten en oligodendrocyten (bepaalde soorten glia cellen). fDTI is daarom potentieel intressant voor het bestuderen van schizofrenie omdat resultaten van zowel genetische (Harrison and Weinberger, 2005; Konrad and Winterer, 2008) als post-mortem (Hakak et al., 2001; Uranova et al., 2004) studies wijzen op ziekte-gerelateerde structurele en functionele afwijkingen van oligodendrocyten in verschillende witte-stofgebieden. Een intressante hypothese is dat deze ziekte-gerelateerde structurele en functionele afwijkingen van oligodendrocyten zullen leiden tot verminderde activatie in de witte-stofbanen.

Het voornaamste doel van de twee fDTI studies zoals beschreven in de hoofdstukken 4 en 5 was om te bepalen of het met fDTI in principe mogelijk is om witte-stof activatie te detecteren. Hoewel de hier gepresenteerde resultaten veelbelovend zijn is het noodzakelijk om de verschillende onderdelen van deze methode te optimaliseren. Zo zijn er verdere experimenten nodig om informatie te krijgen over de exacte vorm van de response functies voor verschillende typen van herhaalde stimuli. Verder is er onderzoek nodig naar de oorsprong van de gemeten verandering in FA waarden. De vraag is in hoeverre deze hier gemeten taak gerelateerde veranderingen in FA waarden daadwerkelijk gerelateerd zijn aan morfologische veranderingen in gliacellen. Een verdere mogelijke verbetering valt te verkrijgen door de echotijd zo zetten dat de fDTI aqcuisitie optimaal gevoelig is voor verandering in het diffusieprofiel van water in de extracellulaire ruimte. Een ander belangrijk onderdeel dat nadere bestudering verdient is op welke manier er gecorrigeerd moet worden voor meervoudig statistisch toetsen. Hierbij moet het antwoord gevonden worden op de vraag hoe de mate van afhankelijkheid van de metingen geschat moet worden. Bij het toepassen van de Bonferroni correctie voor het aantal tracts dat getoetst worden (zoals in hoofdstuk 4 en 5) wordt aangenomen dat alle tractmetingen onafhankelijk van elkaar zijn. Dit is echter niet realistisch omdat veel tracts deels met elkaar overlappen en daarom is de Bonferroni correctie voor meervoudig toetsen in dit geval te conservatief.

Met fDTI kunnen we vragen gaan beantwoorden omtrent de rol van witte-stofbanen binnen neuronale netwerken zoals bijvoorbeeld resting-state netwerken. De resultaten van het onderzoek dat beschreven is in hoofdstuk 3 laten bijvoorbeeld wel een verband zien tussen de mate van functionele connectiviteit van de resting-state gebieden en de 'sterkte' van de witte-stofverbinding die deze grijze-stofgebieden met elkaar verbindt maar dit zegt echter nog helemaal niets over of deze gebieden tijdens rust ook daadwerkelijk met elkaar communiceren via deze witte-stofbanen. Deze vraag kan nu in principe beantwoord worden door fDTI te combineren met standaard fMRI en dan te

bepalen in hoeverre het fDTI signaal gemeten tijdens rust in de witte-stofbanen correleert met het fMRI signaal gemeten tijdens rust in de grijze-stofgebieden.

Conclusie

In dit proefschift werd tract-gebaseerde analyse succesvol toegepast om zowel structurele als functionele eigenschappen te meten van witte-stofbanen. De reconstructie en selectie van deze witte-stofbanen kan volledig automatisch worden uitgevoerd waardoor deze methode geschikt is voor het bestuderen van grote groepen. Dit is in het bijzonder van belang voor het bestuderen van aandoeningen waarvoor men kan verwachten dat eventuele witte-stofafwijkingen zeer subtiel zijn en het detecteren daarvan het vergelijken vereist van grote groepen patiënten en gezonde vrijwilligers. De mogelijkheid van tract-gebaseerde analyse om automatisch zeer subtiele groepsverschillen te detecteren maakt de methode geschikt voor het bestuderen van ziektebeelden waarvoor verwacht wordt dat witte stof een rol speelt, in het bijzonder schizofrenie.

Referenties

Andreasen NC, Ehrhardt JC, Swayze VW, 2nd, Tyrrell G, Cohen G, Ku JS, Arndt S (1991) T1 and T2 relaxation times in schizophrenia as measured with magnetic resonance imaging. Schizophr Res 5:223-232.

Basser PJ, Mattiello J, LeBihan D (1994) Estimation of the effective self-diffusion tensor from the NMR spin echo. J Magn Reson B 103:247-254.

Basser PJ, Pierpaoli C (1996) Microstructural and physiological features of tissues elucidated by quantitative-diffusion-tensor MRI. J Magn Reson B 111:209-219.

Beaulieu C (2002) The basis of anisotropic water diffusion in the nervous system - a technical review. NMR Biomed 15:435-455.

Bleuler E (1911) Dementia Praecox or the Group of Schizophrenias. NewYork: International Universities Press.

Coles JA, Deitmer JW (2005) Extracellular potassium and pH: homeostasis and signaling. In: Neuroglia (Kettenmann H, Ransom BR, ed). Oxford: Oxford University Press.

Damoiseaux JS, Rombouts SA, Barkhof F, Scheltens P, Stam CJ, Smith SM, Beckmann CF (2006) Consistent resting-state networks across healthy subjects. Proc Natl Acad Sci U S A 103:13848-13853.

Greicius MD, Krasnow B, Reiss AL, Menon V (2003) Functional connectivity in the resting brain: a network analysis of the default mode hypothesis. Proc Natl Acad Sci U S A 100:253-258.

Haacke EM, Brown RW, Thompson MR, Venkatesan R (1999) Magnetic Resonance Imaging: Physical Principles and Sequence Design. New York: John Wiley & Sons, Inc.

Hakak Y, Walker JR, Li C, Wong WH, Davis KL, Buxbaum JD, Haroutunian V, Fienberg AA (2001) Genome-wide expression analysis reveals dysregulation of myelination-related genes in chronic schizophrenia. Proc Natl Acad Sci U S A 98:4746-4751.

Harrison PJ, Weinberger DR (2005) Schizophrenia genes, gene expression, and neuropathology: on the matter of their convergence. Mol Psychiatry 10:40-68; image 45.

Jones DK, Catani M, Pierpaoli C, Reeves SJC, Shergill SS, O'Sullivan M, Golesworthy P, McGuire P, Horsfield MA, Simmons A, Williams SCR, Howard RJ (2006) Age effects on diffusion tensor magnetic resonance imaging tractography measures of frontal cortex connections in schizophrenia. Human Brain Mapping 27:230-238.

Jones DK (2008) Studying connections in the living human brain with diffusion MRI. Cortex 44:936-952.

Kanaan RA, Shergill SS, Barker GJ, Catani M, Ng VW, Howard R, McGuire PK, Jones DK (2006) Tract-specific anisotropy measurements in diffusion tensor imaging. Psychiatry Res 146:73-82.

Konrad A, Winterer G (2008) Disturbed structural connectivity in schizophrenia - Primary factor in pathology or epiphenomenon? Schizophrenia Bulletin 34:72-92.

Kraepelin E (1919) Dementia Praecox and Paraphrenia., 8 Edition. Edinburgh, Livingstone.

Laule C, Vavasour IM, Kolind SH, Li DKB, Traboulsee TL, Moore GRW, MacKay AL (2007) Magnetic resonance imaging of myelin. Neurotherapeutics 4:460-484.

Le Bihan D, Breton E, Lallemand D, Grenier P, Cabanis E, Laval-Jeantet M (1986) MR imaging of intravoxel incoherent motions: application to diffusion and perfusion in neurologic disorders. Radiology 161:401-407.

Le Bihan D, Mangin JF, Poupon C, Clark CA, Pappata S, Molko N, Chabriat H (2001) Diffusion tensor imaging: concepts and applications. J Magn Reson Imaging 13:534-546.

MacKay A, Whittall K, Adler J, Li D, Paty D, Graeb D (1994) In vivo visualization of myelin water in brain by magnetic resonance. Magn Reson Med 31:673-677.

MacKay A, Laule C, Vavasour I, Bjarnason T, Kolind S, Madler B (2006) Insights into brain microstructure from the T2 distribution. Magn Reson Imaging 24:515-525.

Madler B, Drabycz SA, Kolind SH, Whittall KP, Mackay AL (2008) Is diffusion anisotropy an accurate monitor of myelination? Correlation of multicomponent T(2) relaxation and diffusion tensor anisotropy in human brain. Magn Reson Imaging 26:874-888.

Mandl RC, Schnack HG, Zwiers MP, van der Schaaf A, Kahn RS, Hulshoff Pol HE. (2008a): Functional diffusion tensor imaging: measuring task-related fractional anisotropy changes in the human brain along white matter tracts. PLoS ONE 3(11):e3631.

Mandl RC, Schnack HG, Luigjes J, van den Heuvel MP, Cahn W, Kahn RS, Hulshoff Pol HE. (2008b): Tract-based Analysis of Magnetization Transfer Ratio and Diffusion Tensor Imaging of the Frontal and Frontotemporal Connections in Schizophrenia. Schizophr Bull. doi:10.1093/schbul/sbn161.

Miese F, Kircheis G, Wittsack HJ, Wenserski F, Hemker J, Modder U, Haussinger D, Cohnen M (2006) 1H-MR spectroscopy, magnetization transfer, and diffusion-weighted imaging in alcoholic and nonalcoholic patients with cirrhosis with hepatic encephalopathy. AJNR Am J Neuroradiol 27:1019-1026.

Mori S, van Zijl PC (2002) Fiber tracking: principles and strategies - a technical review. NMR Biomed 15:468-480.

Mori T, Ohnishi T, Hashimoto R, Nemoto K, Moriguchi Y, Noguchi H, Nakabayashi T, Hori H, Harada S, Saitoh O, Matsuda H, Kunugi H (2007) Progressive changes of white matter integrity in schizophrenia revealed by diffusion tensor imaging. Psychiatry Res 154:133-145.

Raichle ME, MacLeod AM, Snyder AZ, Powers WJ, Gusnard DA, Shulman GL (2001) A default mode of brain function. Proc Natl Acad Sci U S A 98:676-682.

Rosenberger G, Kubicki M, Nestor PG, Connor E, Bushell GB, Markant D, Niznikiewicz M, Westin CF, Kikinis R, A JS, McCarley RW, Shenton ME (2008) Age-related deficits in fronto-temporal connections in schizophrenia: A diffusion tensor imaging study. Schizophr Res. 102:181-188.

Rovira A, Grive E, Pedraza S, Rovira A, Alonso J (2001) Magnetization transfer ratio values and proton MR spectroscopy of normal-appearing cerebral white matter in patients with liver cirrhosis. AJNR Am J Neuroradiol 22:1137-1142.

Sled JG, Pike GB (2001) Quantitative imaging of magnetization transfer exchange and relaxation properties in vivo using MRI. Magn Reson Med 46:923-931.

van den Heuvel M, Mandl R, Hulshoff Pol H. (2008a): Normalized cut group clustering of resting-state FMRI data. PLoS ONE 3(4):e2001.

van den Heuvel M, Mandl R, Luigjes J, Hulshoff Pol H. (2008b): Microstructural organization of the cingulum tract and the level of default mode functional connectivity. J Neurosci 28(43):10844-10851.

Uranova NA, Vostrikov VM, Orlovskaya DD, Rachmanova VI (2004) Oligodendroglial density in the prefrontal cortex in schizophrenia and mood disorders: a study from the Stanley Neuropathology Consortium. Schizophrenia Research 67:269-275.

Wolff SD, Balaban RS (1994) Magnetization transfer imaging: practical aspects and clinical applications. Radiology 192:593-599.

Wyckoff N, Kumar A, Gupta RC, Alger J, Hwang S, Thomas MA (2003) Magnetization transfer imaging and magnetic resonance spectroscopy of normal-appearing white matter in late-life major depression. Journal of Magnetic Resonance Imaging 18:537-543.

Woord van dank

Dit deel is het meest gelezen deel van een proefschrift en dat is volkomen terecht. In dit deel worden namelijk de mensen genoemd die direct of indirect hebben bijgedragen aan de totstandkoming ervan. In mijn geval is dit wat ingewikkeld omdat ik al redelijk lang voor het Universitair Medisch Centrum Utrecht (UMCU) werk en het daardoor wat lastiger is om precies aan te geven wie wat heeft bijgedragen. Het is in ieder geval wel zo dat ik in de tien jaar die ik voor het UMCU werk, niet één dag met tegenzin naar mijn werk ben gegaan en hiervoor houd ik in ieder geval een aantal mensen persoonlijk verantwoordelijk.

Mijn promotoren en co-promotor:
Hooggeleerde Professor Hulshoff Pol, beste Hilleke, dankzij jou kon ik beginnen aan dit promotietraject. Je hebt hiermee een behoorlijk risico genomen omdat het hier een nieuw onderzoeksgebied betrof. Zonder jouw zeer kundige begeleiding had ik het bijltje er al lang bij neergegooid en was het echt nooit gelukt. Als geen ander weet jij het noodzakelijke commentaar op een manuscript positief te brengen (Het is heel goed geschreven, ik zou alleen....). Wat voor problemen er zich ook voordeden, ik kon altijd bij je aankloppen. Heel erg bedankt!
Hooggeleerde Professor Kahn, beste René, ook jij bent voor een groot deel verantwoordelijk voor de goede afloop van dit promotietraject. Wat mij altijd heeft verbaasd is de ongelooflijke snelheid waarmee jij tot de kern van de zaak wist te komen en vervolgens indien nodig meteen met een oplossing kwam. Ik weet nog goed dat je in 2003, nadat ik je de resultaten van mijn eerste fDTI experiment liet zien, direct de vele mogelijkheden hiervan zag en vroeg of het mogelijk was dat het eerste fDTI artikel voor de kerst ingestuurd kon worden (acceptatie van het artikel was natuurlijk slechts een formaliteit). Ik heb niet gelogen toen ik zei dat dat zeker mogelijk was. Volgende keer zou ik er voor de zekerheid alleen ook maar even het jaartal bij vragen.
Beste Hugo, jij bent de derde 'schuldige' van het stel. Talloze malen ben ik bij je langsgekomen voor hulp als ik er niet meer uitkwam / reality checks voor (vaak onzinnige) ideeen / vreemde vragen over quantum mechanica (iets waar ik echt nooit wat van zal begrijpen). Bedankt.

Mijn paranymfen:
Beste Martijn, je beschikt naast een enorme werklust ook nog eens over een enorme dosis humor, creativiteit en intelligentie. Normaal waag ik mij niet zo snel aan voorspellingen maar ik voorspel dat jij - en terecht - voor je 35ste hoogleraar bent. Ik verheug me op de verdere samenwerking.
Beste Margriet, we zijn ongeveer tegelijk begonnen bij het UMCU en ik heb altijd jouw originaliteit en integriteit zeer bewonderd. Het was en is altijd een waar genoegen om met jou te brainstormen over de meest uiteenlopende onderwerpen. Dat onze vriendschap en samenwerking nog maar lang moge duren.

136

Collegae:

Mijn oud-kamergenoten Hans Hoogduin en Arjen van der Schaaf wil ik bedanken voor de gezellige tijd en de vele één-op-één MRI colleges (en schaakpartijen). Marcel Zwiers wil ik bedanken voor de vele waardevolle discussies en zijn gevoel voor humor. Kuan Kho en Joost Janssen wil ik bedanken voor de vele hardloopsessies en de tijdens het hardlopen gevoerde eindeloze discussies over de zin en onzin van onderzoek in het algemeen en dat van ons in het bijzonder. Never a dull moment met Sjoerd Fluitman. Niet zelden leidden de verhitte discussies tijdens de groepslunches tot boze blikken van naburige tafels en het verzoek of het niet allemaal wat stiller kon.

Ik heb ook altijd zeer prettig samengewerkt Geert-Jan Rutten. Zeer bijzonder was de reis van San Antonio naar Area 51 in Roswell. De echte aliens kwamen we trouwens tegen tijdens deze ietwat surrealistische autorit en niet in Area 51 zelf.

Zowel Iris Sommer als Neeltje van Haren ken ik al een hele tijd en buiten dat het altijd prima samenwerken is met deze onderzoeksters hebben ze ook nog eens een enorm gevoel voor humor (dwz ze lachen om mijn grapjes). Trouwens, Caroline, Jiska en Rachel behoren tot de nieuwe onderzoeksgeneratie met wie het prima samenwerken is. Verder bewaar ik zeer goede herinneringen aan de gesprekken met Bob Oranje, Wim Baaré, Jeroen Terpstra, Wouter Staal, Damiaan Denys, Bert Heesakkers en Marco Hoeksma (en voor wat betreft mijn bijdrage aan jouw proefschrift Marco; inderdaad, ik had geen idee). Verder niet te vergeten een groet aan de bengels van kinderpsychiatrie en de mensen van GROUP (in het bijzonder Wiepke Cahn); dat onze samenwerking nog maar veel goede artikelen mag opleveren.

Beste Gibby, Vincent, Yumas, zelden heb ik zulke verschillende maar allen even kundige systeembeheerders meegemaakt. Het was (en is) altijd zeer goed samenwerken met jullie.

Hoewel hij nooit direct bij dit onderzoek betrokken is geweest is dit woord van dank niet compleet zonder het noemen van de nestor van de afdeling: Ron Hijman. Veel dank ben ik verder verschuldigd aan de secretaresses Emmy, Elly en - regel ik voor je! - Tjen.

Van de fMRI groep wil ik als eerste Nick Ramsey bedanken voor alles wat ik daar heb kunnen leren. Bas Neggers, Daan Baas en de twee Mat(t)hijssen wil ik ook bedanken voor de altijd zeer prettige samenwerking. Gerry wil ik in het bijzonder bedanken omdat zij (zonder het zelf te weten) de allereerste fDTI scan gemaakt heeft.

I would like to thank David Norris for the valuable fDTI discussions. I also would like to thank Derek Jones for his advice on various aspects of DTI aqcuisition and processing as well as for the detailed comments on the final manuscript.

Vrienden en familie:

Speciale dank aan mijn gabbers Herman Alderlieste en Arjan de Rooy. Ik ken jullie beiden al een eeuwigheid en wil dat graag nog een tijdje voortzetten. Iets minder lang dan een eeuwigheid maar daarom niet minder leuk; Linda Lie en de zusjes Samuëls, altijd gezellig! Mijn studiegenoten Martijn Kaart en Frank Burgers dank ik voor de gezellige studententijd.

Mijn beide ouders wil ik bedanken voor mijn ietwat wonderlijke maar zeer fijne jeugd.

Ten slotte, mijn liefste Monique. Als er iemand heeft moeten afzien voor deze promotie dan ben jij dat wel. Maar goed, het ei is gelegd. Nu is het dan ook tijd om samen weer heel erg veel leuke dingen te gaan doen.

René

Woord van dank

Curriculum Vitae

René Christiaan William Mandl werd geboren op 17 december 1964 te Amsterdam. Na het behalen van het HAVO diploma in 1983 heeft hij voor verschillende reclamebureaus gewerkt. Na het vervullen van zijn militaire dienstplicht van 1985 tot 1987 heeft hij de opleiding tot AMBI gecertificeerd COBOL programmeur gevolgd en succesvol afgerond. In 1988 is hij begonnen (via een colloquium doctum) met de studie informatica aan de Universiteit van Amsterdam welke hij in 1996 succesvol heeft afgerond. Tijdens zijn studie informatica is hij twee-en-halve dag per week werkzaam geweest bij merkenbureau Onel B.V. waar hij programmatuur ontwierp ten behoeve van merkonderzoeken. In 1997 is hij begonnen als wetenschappelijk programmeur bij de afdeling psychiatrie van het Universitair Medisch Centrum Utrecht (UMCU). In 2002 is hij gestart met zijn promotietraject wat heeft geresulteerd in dit proefschrift.